Wind-wave interactions, density stratification and double diffusive convection in rotating flows

A THESIS SUBMITTED IN FULFILLMENT OF THE ACADEMIC REQUIREMENTS

FOR THE DEGREE OF

DOCTOR OF PHILOSOPHY

by

C T Duba

SCHOOL OF MATHEMATICAL SCIENCES
UNIVERSITY OF KWAZULU-NATAL
NOVEMBER 2015

Contents

Abstract

This thesis investigates ocean circulation which is the result of either wind-wave interactions or density variations. Part I of this study focuses on wind-wave interactions and Part II on the processes arising from density variations.

In Part I shallow water equations are used for a rotating layer of fluid to examine the propagation properties of Rossby waves arising from the latitudinal variation in the vertical component of the Coriolis force, known as the beta-effect, which is closely related to the conservation of potential vorticity. The dispersion relation and the anisotropic properties of these waves are best understood using the Longuet-Higgins wave normal curves in the wave number space at a fixed frequency. Longuet-Higgins showed that the phase velocity is a circle in $k-$space with center displaced westward along the k_x-axis with center $(k_x, k_y) = (-\beta/2\omega, 0)$ and with diameter β/ω. The group velocity is examined and it is shown that the group velocity is an ellipse, whose center is displaced westward and permits eastward and westward propagation. Furthermore it is shown that the topographic Rossby wave has wave normal diagrams that resemble the Rossby wave on a beta plane. However, in the case of the topographic Rossby wave, the phase velocity is a circle displaced northwards. The group velocity is also an ellipse rotated northwards.

The Rossby wave patterns in zonal and meridional winds are then investigated. Using the local dispersion relation in its wave normal form, the geometry thereof plays a crucial role in illuminating the radiation patterns. In the presence of a wind or current, it is shown that the Longuet-Higgins off-set circle of a Rossby wave on a beta plane is distorted by the Doppler shift frequency into an ovoid shaped curve and a blocking line with an eastward indentation. The radiation patterns generated by a compact source were calculated using the method of stationary phase and were illuminated through a series of geometric figures given by the reciprocal polar to the various types of wave number curves. Some of these radiation patterns resemble the Kelvin ship wave or arise in different forms which we have not seen in literature before.

Part II of the study focuses on cross diffusive effects on thermohaline convection in a horizontal rotating fluid in which the temperature and salinity gradients are vertically varying. In many studies these cross diffusive parameters, the Soret and Dufour parameters, are ignored due to their smaller magnitude in relation to the Fourier and Fick laws. The Soret and Dufour effects are responsible for mass and heat transport essential for ocean circulation. The linear stability theory and method of normal modes reveal that the Soret parameter delays stationary convection, the Dufour parameter has minimal effect and rotation has a stabilizing effect on stationary convection.

Oscillatory convection on the other hand is determined by the interaction of six dimensionless variables, the Prandtl number, the Lewis number, the salinity Rayleigh number, Dufour and Soret parameters and the Taylor number as we measure the critical thermal Rayleigh number for the onset of convection. Rotation and the Soret parameters have stabilizing effects on oscilla-

tory convection, whereas the Dufour parameter enhances convection. Salinity delays oscillatory convection and the Lewis number has a stabilizing effect.

A further consideration is taken into weakly nonlinear stability analysis using Fourier modes which revealed several bifurcations as the six nondimensional parameters, the Soret and Dufour parameters, the parameters measuring the Prandtl number, the Lewis number, the Rayleigh number and the Taylor number, are varied. The effect of Soret and Dufour parameters on heat and mass transports is then examined. It has been shown that the increase in the Dufour parameter enhances heat transport and the Soret parameter affects the mass transport positively.

Declaration

This is original work done by the author under the supervision of the late Prof. J. F. McKenzie and Prof. P. Sibanda, and whatever has been borrowed from other authors has been duly acknowledged. No portion of this work has been submitted in any other form for the fulfillment of another degree at any other university.

Signed

C T Duba: Student

P. Sibanda: Supervisor

In memory of Prof. James Fairley McKenzie ("Lord Jim")

I dedicate this to my mother, with gratitude!

Acknowledgements

I would like to thank Prof. James McKenzie (may his soul rest in peace) and Prof. Precious Sibanda, my supervisors, for their guidance and huge patience towards me throughout this project. A special thanks to Prof. McKenzie for introducing me to this field. Prof. Sibanda! words are not enough, THANK YOU. Much gratitude as well to Prof. Terry Doyle, Prof. Mahesha Narayana and Dr. M Shekar for collaboration.

I would also like to thank the Durban University of Technology, University of Kwazulu-Natal and my supervisors for funding; and my colleagues for taking on some extra lecturing load so I may have time to conduct research. A thank you note also to Vuyani Mayela our inter-loan librarian for the service well-rendered. Expressions of gratitude also go to Clemens Dempers for assistance with Mathematica through which most of the diagrams were produced. A special note of thanks to Sheelagh Halstead for proof reading the thesis.

This work could not have been concluded without the support of my friends, Dr. Maleafisha Tladi, Pastor Josephine Llale, Dr. Paul Mokoena, Derek and Abena Obeng, and Martin Mncedane. Thank you!

To my family, *Bakwena! Barok'a Meetse'a Pula, Baila Lehlaka!* words are not enough to express gratitude for such love and support.

My Father who art in heaven! You have been my rock and my strength. Thank you for providing me with all that I needed to complete the project. You watched over me through the valleys and the highs and guided me throughout the journey.

You remain!

Chapter 1

Background and Motivation

1.1 Introduction

Geophysical fluid dynamics emerged as a field of study when oceanographers and meteorologists began modelling complex atmospheric and oceanic flows. More recently, with heightened concerns regarding climate change and weather variability, better understanding of the physics behind global warming and cooling has become necessary. For example, ocean circulation is induced by either wind-wave interactions or mixing processes, which in turn influence atmospheric weather and climatic conditions. Problems in geophysical fluid dynamics primarily concern fluid motion with either or both of rotation and density stratification (Cushman-Roisin and Beckers, 2011). This thesis makes an attempt to model fluids associated with oceanic and atmospheric circulation. This study presents research focusing on these two main distinguishing characteristics of geophysical fluid dynamics. This study will consider types of fluid motion that are influenced by rotation, first, as various forms of wave motions and then those that arise in mixing processes.

In the remainder of this chapter, the theoretical background to the field of study is first outlined and motivation for this research is provided. The thesis objectives are then outlined and the structure of the remainder of the thesis is described.

1.2 Background and Motivation for the study

This study concerns three main effects: rotational aspects, wave motion and mixing of strata. These are described in turn below.

In a study concerning large-scale fluids, the earth's rotation cannot be ignored. Thus,

one can expect the relevant equations of motion to have two acceleration terms:- one related to the centrifugal force and another for the Coriolis acceleration. The former does not play a part in geophysical fluids, but the Coriolis acceleration is an important factor. Furthermore, rotating homogeneous fluids have a strong tendency to be vertically rigid which is especially true with rapid rotation (Cushman-Roisin and Beckers, 2011). However, in large-scale fluids such as oceans and atmospheres, where rotation is slow, the fluids tend to still maintain their vertical structure.

Another large-scale effect of stratification arises when fluids have temperature gradients or different densities. When the heavier fluid is on top and the lighter fluid is at the bottom, stratification is considered to be stable. If the fluid is subsequently disturbed, two physical responses may occur; their influences depending on the degree of perturbation. With small perturbations, the fluid will maintain horizontal motion in the form of internal waves. However, if the perturbation is large, the heavier fluid may sink due to gravitational force and so the lighter fluid will rise, thereby experiencing a vertical motion. In some cases, even with no external perturbations, the fluid will begin to rearrange itself, simply due to buoyancy effects. The sinking of the heavier fluid and a rising of a lighter fluid results in mixing and convection. This process will also be discussed in the second part of the study.

There are several wave modes found in the ocean, including sound waves, gravity waves (surface and internal) waves, Kelvin waves, inertia-gravity (or Poincaré) waves and Rossby (or planetary) waves. Kelvin waves, Poincaré waves and Rossby waves exist due to the Earth's rotation. Stratification is the cause of internal waves and it is also important for Poincaré waves. As expected, gravity waves are generated by gravitational force. In this study we will look closely at propagation of Rossby waves and consider their interaction with zonal and meridional winds.

Rossby waves were first theorized by meteorologist Carl-Gustave Rossby (1939) and are a characteristic feature of oceans and atmospheres. They are thus important in weather and climate science. For example, in the ocean, they play a critical role in the El Niño effect interacting with other forces to cause warm water masses to move back and forth across the tropical Pacific Ocean. In this way, they are one of the major ways that the El Niño signal is transmitted across the oceans (Philander, 1990). In the atmosphere, Rossby waves are responsible for the transport of momentum, energy and water vapour and so they are an integral part of global circulation. Rossby waves have westward phase propagation, but have group velocity that may be either eastward or westward depending on their wavelength. To elaborate, long wavelength Rossby waves travel faster than

those with short wavelengths, and transport energy westward, whereas those with short wavelength transport energy eastward. In the atmosphere, Rossby waves are excited in the lower troposphere and so are forced to propagate vertically. Upwardly propagating Rossby waves are believed to play an important role in phases of sudden stratospheric warming (Holton and Hakim, 2013).

Meridionally propagating Rossby waves carry angular momentum between the tropics and middle latitudes, and so are responsible for numerous climatic/weather effects (Holton and Hakim, 2013). Specifically, in the mid-latitudes, they influence much of weather by their effect on the meandering Jet Stream. Rossby waves are also important in the Western Boundaries, for example, the Gulf Stream, as the long wavelength waves propagate westward. When they reach these boundaries they are reflected eastward as short wavelength Rossby waves, which are slower (Killworth and McIntyre, 1985). There is thus a congestion at the boundaries when reflected slow short wavelength Rossby waves compete with incoming fast long wavelength ones.

Furthermore, when Rossby waves interact with winds, they may either be absorbed or reflected (Killworth and McIntyre, 1985). This is most notable when they are slow moving, and it may delay weather movements or influence weather predictability. Specifically, if the waves are absorbed, the weather condition may not happen at the predicted time because energy is not transported as expected. Alternatively, if they are reflected, the Rossby waves may change the course of weather patterns. Therefore these waves are very important in the study of weather and climate. In this thesis, the study concerns the interaction of Rossby waves with zonal and meridional winds. This is demonstrated geometrically through wave normal curves and radiation patterns.

Geophysical fluids are generally weakly stratified. In this regard, density variations are sufficient to drive or affect motion, but are nonetheless relatively small compared to the reference density of the fluid. Density variations may arise from temperature or salinity differences. Temperature differences occur because the oceans are heated from either above, by radiation, or below, due to geothermal heating. When heated from below, the fluid at the bottom will be less dense than the upper fluid. The fluid may then begin to redistribute itself but its viscosity will inhibit this rearrangement. Thus for a certain temperature distribution the system may be maintained until it reaches a critical temperature at which the system becomes unstable due to buoyancy forces becoming dominant. This process has been well established by experimental results of Bénard and theoretical work of Rayleigh, and has subsequently been explained by many authors (for example, Chandrasekhar (1961)). Hence it is often referred to as Rayleigh-Bénard

convection or simply thermal convection.

In geophysics, wave motion may arise from instability due to density variations as follows: If, due to some initial perturbation, a fluid particle is displaced upward, it will now be heavier than its surroundings, and so it experiences a downward force due to gravity. In falling it acquires a vertical velocity. Upon reaching its original level, the particle's inertia causes it to travel further downward where it will be surrounded by heavier fluid (Holton & Hakim, 2013). The fluid parcel, now buoyant, is propelled upwards and oscillations persist about the equilibrium level. The quantity

$$N^2 = \frac{g}{\rho}\frac{d\rho}{dz}, \tag{1.1}$$

where ρ is the fluid density, g is the acceleration and z is the vertical direction; is defined as the stratification frequency, commonly known as the Brunt-Väisälä frequency after the scientists who highlighted its importance in stratified fluids. If $N^2 > 0$, then we have top-heavy configuration, and the solution exhibits exponential growth, a sure sign of instability. If however, the lighter fluid lies above the heavier fluid, $N^2 < 0$, then we have stability (Holton and Hakim, 2013). If a fluid is permanently destabilized for example by heating from below or cooling from above, the fluid will remain in constant agitation, a process called convection.

In this thesis the theoretical work by Rayleigh using hydrodynamic equations is followed to study thermal convection as demonstrated in Chandrasekhar (1961). Rayleigh showed that at certain critical temperature the fluid begins to be unstable and devised a nondimensional number, called the Rayleigh number, to measure the strength of the buoyancy against the viscosity, given as

$$R = \frac{g\alpha\Delta T d^4}{\nu\kappa}, \tag{1.2}$$

where α is the thermal expansion coefficient, g is the gravitational acceleration, d is the fluid depth, ν is the fluid viscosity and κ is the thermal diffusion coefficient. He determined that if $R > R_c$ then there is instability; if $R < R_c$ then the system is stable and it is at equilibrium when $R = R_c$.

When there are two vertical gradients involved and affecting the density in opposing directions, and causing different rates of diffusion the process is called double-diffusive convection. The study of double-diffusive convection is of practical importance in many fields of study involving convective heat and mass transfer, including oceanography, astrophysics, geophysics, geology, atmospheric physics, chemical engineering. When the two vertical gradients are salt and temperature, the convection is called thermohaline

(thermo-temperature, haline- salinity) convection. We shall consider this mechanism in the latter part of the study.

Two fundamental cases of thermohaline convection were reported in the 1960's. The first study, by Stern (1960) concentrated on the case when the temperature gradient was stabilizing and the salt gradient destabilizing, in other words, when salty warm water lies above cold and salty waters, a bottom-heavy configuration. Here, Stern noted the general properties of the motion now commonly known as 'salt fingers'. These appear as a close-packed array of upwards and downwards flowing convection cells, which exchange heat laterally but diffuse little salt. The result is an advective transport of salt and, to a lesser extent, heat, in the vertical. Typical cell widths in the ocean are 2-3 cm (Schmitt, 2001).

Veronis (1965) studied the opposite situation that occurs when the temperature gradient is destabilizing and salinity is stabilizing, in other words, the top-heavy configuration. The physics thereof is different from the salt finger case. In the top-heavy case, as the cold fresh water rises, it will become cold salty water and thus more dense than when it started moving upward. Thus instead of accelerating upward as in the salt-finger case, it is actually driven back down with greater force than it took to initially displace it (Schmitt, 2001). This is termed 'over-stability' and leads to higher amplitude oscillations. In the case of double-diffusive convection the measure of instability depends on the concentration (salinity) Rayleigh number as given by

$$R_S = \frac{g\alpha_S \Delta S}{\nu \kappa_S} d^3. \tag{1.3}$$

where α_S is the haline contraction coefficient, g is the gravitational acceleration, d is the fluid depth, ν is the fluid viscosity and κ_S is the haline diffusion coefficient. There is a plethora of studies, both experimental and theoretical in many different settings, in the literature concerning double-diffusive convection, for example, Huppert and Turner (1981), Turner (1973, 1974, 1985) and the citations therein. In this study we continue with the study of thermohaline convection using linear stability and weakly nonlinear stability theory and consider both stationary convection and oscillatory convection. We consider the case when heating is from below.

Double diffusive convection in the ocean, in particular, thermohaline convection is likened to a great conveyor belt (Burroughs, 2007) as it transports heat poleward and brings nutrient-rich waters to the surface. The most vigorous conveyor belt is in the Atlantic ocean where it carries warm water through the tropics and subtropics toward the north, and the cold dense polar water is carried southward through the Atlantic (Burroughs,

2007). Hence double diffusive convection is essential in heat and mass transports. However, the linearised equations of motion are not sufficient for the analysis of heat and mass transports. We will thus use the nonlinear analysis.

A further consideration is the rotational effect on thermohaline convection. Due to large-scale motions as in oceans and atmospheres being affected by ambient rotation of the earth, these effects should be included. It is commonly known in literature (Cushman-Roisin and Beckers, 2011) that rotation induces vertical rigidity in the fluid, especially when rotation is fast. However, in large-scale fluids, such as oceans and atmospheres, rotation is slow. Nevertheless due to their large scale, oceans and atmospheres are still affected by rotation.

In the case of Rayleigh-Bénard convection, Chandrasekhar (1961) and others showed that the Rayleigh number depends on the rotation parameter, given by the Taylor number

$$Ta = \frac{4\Omega^2 d^4}{\nu^2}, \tag{1.4}$$

where Ω is the angular velocity of the Earth. Furthermore, rotation has a stabilizing effect and has a tendency to induce a component of vorticity. An extensive study on rotational effects on double-diffusive convection has been conducted by Barnejee *et al.* (1983, 1988, 1995). They showed that for the Veronis type of configuration, there will be no oscillatory convection for certain values of the salinity Rayleigh number R_S. In addition, Tagare *et al.* (2007) showed that rotation has a stabilizing effect. In contrast, there are some studies that include Sharma *et al.* (2001) and more recently, Dhiman and Goyal (2015) that showed rotation to be causing oscillatory convection and therefore destabilizing. So we consider here the rotational influence on thermohaline convection as well as stability analysis. Besides the effect of salinity Rayleigh number on convection, we also here consider the rotational influence on nonlinear stability analysis and the bifurcation patterns thereof.

In the situation above, energy flux due to temperature gradient and energy flux due to mass concentration gradient are represented by the Soret and Dufour parameters, respectively. However, in many studies, these two factors are ignored due to their smallness compared to Fick's law of diffusion. Nevertheless, it has been shown by Awad and Sibanda (2010), Awad *et al.* (2010), Rudraiah and Siddeshwar (1998), Narayana *et al.* (2013), Malashetty and Biradar (2011) that despite their relative size, cross-diffusive effects can be significant. We note in particular, the recent study by Goyal and Garg (2015) which concluded that the effect of cross-diffusive parameters on double-diffusive convection is so strong that it cannot be ignored. In another study, Dhiman and Goyal (2015) considered

the Soret effect on double-diffusive convection in a rotating layer and they found that the influence of Soret parameter is significant. However, both these studies used only linear stability analysis. We contend that the significance of cross-diffusive factors, that is, the Soret and Dufour parameters on the system, may be better studied by nonlinear analysis. Therefore, besides the use of linear stability analysis to study them, in this study we extend work on cross diffusion effects on double-diffusive convection in a rotating layer to also include weakly nonlinear stability analysis.

In addition, the effect of cross diffusive terms on heat and mass transports is considered. Thermohaline convection as seen as a conveyor belt transports heat polewards and brings nutrient-rich deep waters to the surface. It is thus relevant to explore how these cross diffusive terms act on heat and mass transports. To this end, the effect of Soret and Dufour parameters on Nusselt and Sherwood numbers which measure heat and mass transports, respectively, are investigated.

In summary, it has been shown that further investigation is needed with regard to some aspects of thermohaline convection. These are the effects of cross-diffusive terms and the rotational effects thereby when weakly nonlinear stability analysis is employed.

1.3 Thesis objectives

In response to the deficiencies in the literature identified above, this thesis will investigate the following effects:

1. Further propagation properties of Rossby waves on a beta-plane.
2. Interaction of Rossby waves with zonal and meridional winds.
3. Soret and Dufour effects on thermohaline convection in rotating fluids.

1.4 Structure of the thesis

In essence, this thesis consists of two parts. Part I (Chapters 2 to 4) deals with wind-wave interactions through the propagation properties of Rossby waves, which are important in the understanding of weather patterns. In this part the types of waves relevant to ocean circulation are investigated; particularly those resulting from the latitudinal variations of the Coriolis force, the Rossby waves. In Chapter 2, the basic principles governing the propagation properties of waves in geophysical fluid dynamics are investigated and

it is shown how they arise from the shallow water equations. In Chapter 3, by means of a published paper, further propagation properties of Rossby waves not elucidated in literature before, are shown. Chapter 4 of the study, which also consists of a published paper, explores the interaction of Rossby waves with zonal and meridional winds. Part II (Chapters 5 and 6) of the thesis focuses on double-diffusive convection, in particular thermohaline convection. In Chapter 5, the focus is on thermohaline convection and analysis of literature thereby to set a tone for the next chapter. Chapter 6, which is formulated as a third research paper, focuses on the effect of Soret and Dufour parameters on thermohaline convection in rotating winds. This third paper, has been submitted for peer review. In Chapter 7, we give our overall conclusions and make suggestions for further research.

Contributions to existing literature

This thesis consists of three papers, two already published and one submitted for peer review. All the papers are jointly written.

1. **Propagation properties of Rossby waves for latitudinal β-plane variations of f and zonal variations of the shallow water speed**
   C. T. Duba and J. F. McKenzie
   Annales Geophysicae, 2012, vol. 30, pages 849-855

2. **Rossby wave patterns in zonal and meridional winds**
   C. T. Duba, T. B. Doyle and J. F. McKenzie
   Geophysical and Astrophysical Fluid Dynamics, 2014, vol. 108 no. 3, pages 237-257

3. **Soret and Dufour Effects on the Thermohaline Convection in Rotating Fluids**
   C. T. Duba, M. Shekhar, M. Narayana, P. Sibanda
   Submitted to Journal of Geophysical and Astrophysical Fluid Dynamics

Part I

Wind-Wave Interaction

Chapter 2

Introduction

Rotating planetary atmospheres and oceans permit different types of wave modes as discussed in many geophysical literature (for example, Pedlosky, 1987; Gill, 1982; Vallis, 2006 Cushman-Roisin and Beckers, 2011). It is also important to note that waves in oceans and atmospheres do interact with each other and with the winds (Dickinson, 1968; McKenzie and Webb, 2015). It is therefore necessary to study the different types of waves, and the mechanisms that generate them, and how they propagate. Some examples of such waves are gravity waves (surface and internal), the Kelvin wave (coastal and equatorial), inertia-gravity or Poincaré waves, Rossby (topographic and equatorial) waves. These waves may have gravity, rotation or stratification, or a combination of these, providing restoring force. For example, inertia- gravity waves, Kelvin waves and Rossby waves depend on the Earth's rotation for their existence. More specifically, Rossby waves depend on the latitudinal variation of the Coriolis force. Inertia-gravity waves depend on the rotation as well as stratification.

Important wave characteristics involve the speed and direction of wave propagation. Another salient feature is their energy transport which influences how they contribute to weather and climatic conditions. Wave activity around the equator must be considered separately because of the different physics underlying waves in that region. Specific differences and similarities exist among oceanic and atmospheric waves which include their vorticity and inertial properties. In this regard, Rossby waves are characterised by the conservation of potential vorticity; inertia-gravity waves and Kelvin waves carry no potential vorticity. To be specific, where ω is the wave frequency, N the Brunt-Väisälä frequency, and f is the Coriolis parameter; inertia-gravity waves are super-inertial ($\omega > f$) but ($\omega < N$). By contrast, Kelvin waves are sub-inertial ($\omega < f$). Rossby waves are also sub-inertial but propagate at lower frequencies ($\omega \ll f$). Rossby waves arise due to the

latitudinal variation of the vertical Coriolis frequency, as will be shown in Section 2.1.1.

In the remainder of this chapter, we will first discuss what makes rotation, and specifically the Coriolis force, important in the study of ocean and atmosphere dynamics. We then focus on how rotation relates to some wave types. Finally, we explore shallow water equations relevant to wave dynamics in the ocean and atmosphere, with the intention of deriving suitable wave equations. Shallow water equations will then enable us, in later chapters, to further explore the propagation properties of the waves and hence study their effect on weather and climate. The main goal of this chapter is, thus, to set a tone for the next chapter wherein new developments in the study of propagation properties of Rossby waves are described.

Sound waves for example, depend on compressibility for existence. Other interesting characteristics involve the speed and direction of wave propagation. One other salient feature we will discuss is their energy transport and how they contribute to weather and climatic conditions. The study will not discuss wave activity around the equator, called equatorial waves, as the underlying physics is different at the equator. Sound waves due to their high speed do not contribute to geophysical fluid dynamics. Inertia-gravity waves, Kelvin and planetary waves depend on the Earth's rotation for their existence. Inertia-gravity waves also depend on stratification. Whereas planetary waves are characterised by the conservation of potential vorticity, Poincaré waves and Kelvin waves carry no potential vorticity. It is generally believed in literature (e.g. Pedlosky, 1987) that Poincaré waves or inertial waves are super-inertial ($\omega > f$) but ($\omega < N$) where ω is the wave frequency, N is the Brunt-Väisälä (buoyancy or stratification) frequency and f is the Coriolis parameter. Kelvin waves are sub-inertial ($\omega < f$). Rossby waves are sub-inertial and propagate at lower frequencies ($\omega \ll f$). They arise because of the beta-effect describing the latitudinal variation of the vertical Coriolis frequency.

Below, there is first a discussion on what makes rotation and the Coriolis force important in the study of ocean and atmosphere dynamics. The concept of stratification is however not explained here, but in the latter part of the study, even as other waves, like Poincaré and internal waves, depend on stratification for existence. Poincaré waves and internal waves are not the focus of our study. Furthermore, although the notion of vorticity is associated with the propagation properties of Rossby waves, that discussion is not entered into here as it will not be used in subsequent studies on Rossby wave propagation. Shallow water equations relevant to wave dynamics in the ocean and atmosphere are explored with the intention of deriving Rossby wave equations. These equations are useful in further exploring the propagation properties of Rossby waves and hence the effect of Rossby waves

in weather and climate studies.

The main goal of this chapter is to set a tone for the next chapter wherein new developments are discussed in the study of propagation properties of Rossby waves.

2.1 Importance of Rotation

There are many studies in fluid dynamics in which rotation can be treated as an infinitesmal disturbance and can be ignored. However, the discussion below focuses on the conditions for which rotation is important and justify its inclusion in the study of both the oceanic waves and the mixing processes such as convection.

For a fluid, the ambient rotation rate, denoted by Ω is defined in Cushman-Roisin and Beckers (2011) as

$$\Omega = \frac{2\pi \quad \text{radians}}{\text{time of one revolution}}. \tag{2.1}$$

If fluid motions evolve on a timescale comparable to or longer than the time of one rotation, then the fluid will be affected by the ambient rotation. We use the dimensionless quantity

$$\omega = \frac{\text{time of one revolution}}{\text{motion time scale}} = \frac{2\pi/\Omega}{T} = \frac{2\pi}{\Omega T}, \tag{2.2}$$

where T denotes the time scale of the flow. If ω is of the order of or less than unity ($\omega \leq 1$), rotation effects should be considered (Cushman-Roisin and Beckers, 2011). For the Earth, this occurs when $T > 24$ hours. Motions with shorter timescales $\omega \geq 1$ but sufficiently large spatial extent could also be influenced by rotation. Furthermore, if a particle travelling at the speed U covers the distance L in a time longer than or comparable to a rotating period, it is expected that the trajectory will be influenced by the ambient rotation, so it is necessary to find

$$\epsilon = \frac{\text{time of one revolution}}{\text{time taken by particle to cover distance } L \text{ at speed } U} = \frac{2\pi/\Omega}{L/U} = \frac{2\pi U}{\Omega L}. \tag{2.3}$$

If $\epsilon \leq 1$ we conclude that rotation is important.

From the analysis above, it can be seen that rotation is important in geophysical flows. This is because ocean currents have speed of about 10 cm/s and flowing over a horizontal distance of about 10 km. Furthermore, a wind blowing at 10 m/s in a 1000 km wide anticyclonic formation will be similarly important. In both these cases, the criterion $\epsilon \leq 1$ is met.

2.1.1 The Coriolis force

Relative to the rotating earth, a body experiences an inertial (or apparent) force called the Coriolis force, which was first hypothesized by the French mathematician Gustave-Gaspard Coriolis in 1835. Due to its importance, this force has been discussed in many geophysical fluid publications (Gill, 1982; Pedlosky 1987, 2010; Vallis 2006, Cushman-Roisin and Beckers 2011).

The Coriolis force, f, is equal to $2\Omega \times V$, where Ω is the earth's angular velocity and V is the relative velocity of the air (Vallis, 2006). The Coriolis force is nonzero only if the body is in motion, and is important only if the body travels for a significant period of time. Furthermore, the Coriolis force is larger for larger velocities. Thus, for winds in the atmosphere's Jet Stream, where the timescales of motion are several days to several weeks, Earth's vorticity about the local vertical and the y-component of the parameter f is equal to the component of the earth's vorticity about the local vertical and, at latitude ϕ, is $2\Omega \sin\phi$. It deflects a moving body to the right in the Northern hemisphere and to the left in the Southern hemisphere. It has its largest deflecting effect at the poles, and is least at the equator.

If the coordinate y is directed northward and is measured from a reference latitude ϕ_0 (say, a latitude somewhere in the middle of the wave under consideration) then $\phi = \phi_0 + y/a$, where a is the Earth's radius (6371 km). Considering y/a as a small perturbation, the Coriolis parameter f can be expanded around $\phi = \phi_0$ using a Taylor series

$$\begin{aligned} f &= f_0 + \frac{\partial f}{\partial \phi}|_{\phi_0}\Delta\phi + \frac{\partial^2 f}{\partial \phi^2}|_{\phi_0}\frac{\Delta\phi^2}{2} + \cdots \\ &= 2\Omega\sin\phi_0 + 2\Omega\cos\phi_0(\phi - \phi_0) + O(\Delta\phi^2). \end{aligned} \tag{2.4}$$

Retaining only the first two terms, we write

$$f = f_0 + \beta_0 y, \tag{2.5}$$

wherein

$$f_0 = 2\Omega\sin\phi_0, \quad \beta_0 = \frac{2\Omega\cos\phi_0}{a}, \quad y = a\Delta\phi, \tag{2.6}$$

where a is the radius of the Earth. This is called the beta-plane approximation. Typical mid-latitude values on earth are $f_0 = 8 \times 10^{-5}\mathrm{m}^{-1}$ and $\beta_0 = 2 \times 10^{-11}\mathrm{m}^{-1}\mathrm{s}^{-1}$. The Cartesian framework where the beta term is not retained is called the f-plane. Rigorous justification of the beta-plane can be found in Pedlosky (1987).

The beta-plane representation is validated at mid-latitudes only if the $\beta_0 y$ term is small compared with the leading f_0 term. For the motion's meridional length scale L, this implies

$$\beta = \frac{\beta_0 L}{f_0} \ll 1 \tag{2.7}$$

where the dimensionless ratio β can be called the planetary number.

At the equator $f = 0$, that is, the Coriolis force vanishes at $\phi = 0°$. Thus it is necessary to think of the equatorial beta-plane approximation $f = \beta y$. This equatorial beta-plane requires a geostrophic balance between eastward velocity and the north-south pressure gradient.

The Coriolis parameter f is a function of latitude and changes sign at the equator, and it has units of $\sec^{-1}$.

$$\begin{aligned} f &= 2\Omega \sin\phi, \\ f_* &= 2\Omega \cos\phi. \end{aligned} \tag{2.8}$$

Whereas f is called the Coriolis parameter, f_* has no traditional name is referred to as reciprocal Coriolis parameter (Cushman-Roisin and Beckers (2011)). In the Northern Hemisphere, $f > 0$, and the Coriolis force causes a moving body to appear to move to the right of its direction of motion. In The Southern Hemisphere, $f < 0$, and causes the body to move to the left. At the equator $f_0 = 0$ and we have $f = \beta y$, this is the equatorial beta-plane approximation. f_* is positive in both hemispheres and vanishes at the poles. Eastward traveling objects can be deflected upwards (feel lighter), while the westward traveling objects will be deflected downwards (feel heavier). This aspect of the Coriolis force is greatest near the equator. In addition objects travelling upwards or downwards will be deflected to the west or east respectively. This effect is also greatest near the equator.

The Coriolis force is non-zero only if the body is in motion, and is important only if the body travels for a significant period of time. The Coriolis force is larger for larger velocities as well. For winds in the atmosphere's Jet Stream, the timescales of motion is several days to several weeks, so Earth's rotation is very important and the winds do not blow from high to low pressure. The same holds true in the ocean where currents last for weeks or years and are strongly influenced by the Coriolis force.

For large-scale ocean currents, and to some extent winds, the vertical velocity is much weaker than the horizontal velocity. Certainly, the distance that a water parcel can move in the vertical direction is much more limited than in the horizontal direction because of

both the differences in depth and width of the ocean and because of the ocean's stratification. Therefore, the Coriolis effects act mostly on the horizontal velocities and not on the vertical ones.

2.2 Shallow water equations in rotating fluids

The shallow water theory has been well discussed by Gill (1982), Pedlosky (1987), Vallis (2006), McWilliams (2006) and Cushman-Roisin and Beckers (2011). Shallow water equations represent the flow in a fluid layer with uniform density, ρ_0, when the horizontal velocity is constant with depth. This is most plausible where the horizontal scale, L is far larger than the mean depth H, that is, $H/L \ll 1$. Thus they are relevant to the modelling of oceanic and atmospheric fluid motions. Below is a discussion on shallow water equations and their governing laws. Furthermore, waves in the oceans and atmospheres, such as surface gravity waves, Kelvin waves, Poincaré waves are mentioned and a discussion is carried away on Rossby waves associated with shallow water equations. Surface gravity waves, Kelvin waves and Poincaré waves are not a focus of this study but are mentioned for completeness as they surface when discussing shallow water equations. Shallow water equations were also discussed by Paldor *et al.* (2007) where they formulated a new linear theory for the three types of linear waves of the shallow water equations on the β-plane. The intention here is not to develop new theory for shallow water equations but to revisit them as they are relevant to the work on Rossby waves in the next two chapters. We first proceed with nonlinear shallow water equations through to linear, inviscid and homogeneous equations relevant to our study.

2.2.1 Nonlinear flows

Shallow water equations consists of momentum equations and the mass continuity equation. Their derivations arise from the Newton's second law

$$\vec{a} = \frac{D\vec{v}}{Dt}, \tag{2.9}$$

which is the material acceleration, and D/Dt is the advective or material derivative given by

$$\frac{D}{Dt} = \frac{\partial}{\partial t} + u\frac{\partial}{\partial x} + v\frac{\partial}{\partial y} + w\frac{\partial}{\partial z}.$$

By Newton's law applied to a material element of fluid

$$\sum \vec{F} = m\vec{a} = m\frac{D\vec{v}}{Dt} = \rho dxdydz\frac{D\vec{v}}{Dt}, \tag{2.10}$$

where ρ is the density of the fluid. From Cauchy's equation

$$\rho\frac{\partial\vec{v}}{Dt} = \rho\vec{g} + \vec{\nabla}\cdot\sigma_{ij}, \tag{2.11}$$

where

$$\vec{g} = g_x\vec{i} + g_y\vec{j} + g_z\vec{k},$$

is the gravity vector and σ_{ij} is the stress tensor.
The viscuous stress tensor is given by

$$\tau_{ij} = \begin{bmatrix} \tau_{xx} & \tau_{xy} & \tau_{xz} \\ \tau_{yx} & \tau_{yy} & \tau_{yz} \\ \tau_{zx} & \tau_{zy} & \tau_{zz} \end{bmatrix} = \begin{bmatrix} 2\mu\frac{\partial u}{\partial x} & \mu\left(\frac{\partial u}{\partial y} + \frac{\partial v}{\partial x}\right) & \mu\left(\frac{\partial u}{\partial z} + \frac{\partial w}{\partial x}\right) \\ \mu\left(\frac{\partial v}{\partial x} + \frac{\partial u}{\partial y}\right) & 2\mu\frac{\partial v}{\partial y} & \mu\left(\frac{\partial v}{\partial z} + \frac{\partial w}{\partial y}\right) \\ \mu\left(\frac{\partial w}{\partial x} + \frac{\partial u}{\partial z}\right) & \mu\left(\frac{\partial w}{\partial y} + \frac{\partial v}{\partial z}\right) & 2\mu\frac{\partial w}{\partial z} \end{bmatrix}. \tag{2.12}$$

But for moving fluids

$$\sigma_{ij} = \begin{bmatrix} \sigma_{xx} & \sigma_{xy} & \sigma_{xz} \\ \sigma_{yx} & \sigma_{yy} & \sigma_{yz} \\ \sigma_{zx} & \sigma_{zy} & \sigma_{zz} \end{bmatrix} = \begin{bmatrix} -P & 0 & 0 \\ 0 & -P & 0 \\ 0 & 0 & -P \end{bmatrix} + \begin{bmatrix} \tau_{xx} & \tau_{xy} & \tau_{xz} \\ \tau_{yx} & \tau_{yy} & \tau_{yz} \\ \tau_{zx} & \tau_{zy} & \tau_{zz} \end{bmatrix}. \tag{2.13}$$

We need to express the stress tensor σ_{ij} in terms of density, pressure and velocity. The pressure force is given by

$$\frac{D\vec{v}}{Dt} + (\vec{v}\cdot\nabla)\vec{v} = -\frac{\nabla p}{\rho} + F' \tag{2.14}$$

where F' represents viscuous and body forces per unit mass, and v is the velocity vector $\vec{v} = (u, v, w)$ in the (x, y, z) direction.
Viscosity is the force due to internal motion of molecules (Vallis, 2006). In most literature viscosity is expressed as $\mu\nabla^2\nu$ where μ is the viscosity. With this term momentum equations then become

$$\frac{D\vec{v}}{Dt} + (\vec{v}\cdot\nabla)\vec{v} = -\frac{1}{\rho}\nabla p + \nu\nabla^2\vec{v} + F_b \tag{2.15}$$

where $\nu = \mu/\rho$ is the kinematic viscosity and F_b represents body forces (per unit mass)

such as gravity $\vec{g}$. The inviscid flow assumption means that the shear and the stresses in the force field are negligible. In effect, it also means that the boundary layer is assumed to be very thin or of no significance to the geometry of the body fluid.

The vertical component, parallel to the gravitational force, $\vec{g}$, of the momentum equation is

$$\frac{Dw}{Dt} = -\frac{1}{\rho}\frac{\partial p}{\partial z} - \vec{g}, \tag{2.16}$$

where w is the vertical component of the velocity vector and $\vec{g} = -g\hat{k}$. If the fluid is static, the gravitational term is balanced by the pressure term, thus

$$\frac{\partial p}{\partial z} = -\rho g. \tag{2.17}$$

This relation is known as the hydrostatic balance and will be a good approximation provided vertical accelerations Dw/Dt are smaller compared to gravity. In the ocean Dw/Dt is small compared to gravity (Vallis, 2006).

The conservation of mass is described by the equation

$$\rho\frac{D\vec{v}}{Dt} + v\nabla\cdot\vec{v} = 0. \tag{2.18}$$

Equations (2.15) and (2.18) are both nonlinear due to the product of dynamic variables terms in the material derivative. These equations are unfortunately not sufficient to close the dynamical system. The thermodynamic equations and the equation of state need to also be included.

Shallow water equations describe motion of a homogeneous, inviscid and incompressible fluid.

2.2.2 Compressible and incompressible Flow

Incompressible flows are flows in which the density vary so little that they have a negligible effect on the mass balance

$$\frac{\delta\rho}{\rho_0} \ll 1, \tag{2.19}$$

where $\delta\rho$ is the variation in density and ρ_0 is the mean density. Therefore it becomes a good approximation to consider the density constant. Then the mass continuity equation

$$\frac{D\rho}{Dt} + \rho\nabla\cdot\vec{v} = 0, \tag{2.20}$$

reduces to

$$\nabla \cdot \vec{v} = 0, \tag{2.21}$$

preserving the volume of each material fluid element. However, this equation is not applicable to fluid flows governed by the equation of state which relates density and pressure. But for incompressible flows, density can be taken as constant. Furthermore, incompressibility does not mean that we should ignore the density variations in momentum equations, it is only in the mass continuity equation where the density is neglected.

2.2.3 Effects of rotation and stratification

Momentum equations in a rotating frame for the shallow water equations governing incompressible, inviscid, homogeneous flows are given by

$$\frac{Dv}{Dt} + 2\Omega \times v = -\frac{1}{\rho}\nabla p - \nabla\phi \tag{2.22}$$

where the centrifugal acceleration is incorporated in the velocity potential ϕ. In the f-plane momentum equations are given by

$$\frac{Du}{Dt} - f_0 v = -\frac{1}{\rho}\frac{\partial p}{\partial x} \tag{2.23}$$

$$\frac{Dv}{Dt} + f_0 u = -\frac{1}{\rho}\frac{\partial p}{\partial y} \tag{2.24}$$

$$\frac{Dw}{Dt} = -\frac{1}{\rho}\frac{\partial p}{\partial z} - g, \tag{2.25}$$

where $f_0 = 2\Omega \sin\theta_0$.

For small variations in latitude, that is, in the beta-plane, momentum equations become

$$\frac{Du}{Dt} - fv = -\frac{1}{\rho}\frac{\partial p}{\partial x} \tag{2.26}$$

$$\frac{Dv}{Dt} + fu = -\frac{1}{\rho}\frac{\partial p}{\partial y} \tag{2.27}$$

$$\frac{Dw}{Dt} = -\frac{1}{\rho}\frac{\partial p}{\partial z} - g. \tag{2.28}$$

2.2.4 Linear wave dynamics

The governing equations in the previous section are essentially nonlinear; consequently, their linearisation can proceed only by imposing restrictions on the flows under consider-

ation. We restrict ourselves to low-Rossby-number situations

$$R_0 = \frac{v}{\Omega L},$$

where L is the length scale. This is usually accomplished by restricting attention to relatively weak flows, large scale or fast rotation. The terms expressing the local time rate of change of the velocity $\partial u/\partial t$ and $\partial v/\partial t$ are linear and are retained here in order to permit the investigation of unsteady flows. Thus temporal Rossby number is assumed to be on the order of unity

$$R_{0_T} = \frac{1}{\Omega T} \sim 1,$$

also the scale for the wave speed

$$c = \frac{L}{T} \sim \Omega L \gg v,$$

where T is the timescale.

We restrict ourselves to homogeneous, incompressible, inviscid flows, for which the shallow water model is adequate. The horizontal momentum reduce to

$$\frac{\partial u}{\partial t} - fv = -g\frac{\partial \eta}{\partial x} \tag{2.29}$$

$$\frac{\partial v}{\partial t} + fu = -g\frac{\partial \eta}{\partial y}, \tag{2.30}$$

where $\eta = h - H$ is the surface displacement, with h the total depth, H mean fluid thickness. The vertical component is absent for the flow is vertically homogeneous.

Shallow water waves Shallow water equations are based on several approximations. First, incompressible approximation that relates the mass conservation to the smallness of the variations in density. Second, is the hydrostatic approximation expressed in the equation

$$\frac{\partial p}{\partial z} = -g\rho,$$

where p is the pressure, ρ is the fluid density and g is the gravitational acceleration.

Under the influence of rotation, the equations governing the linear, inviscid and homogeneous fluid are the shallow water equations which have been discussed in many geophysical fluid dynamics literature, including a publication by Paldor *et al.* (2007). The governing equations on the f-plane about a state of rest are given by the following conservation of

momentum and mass continuity equations:

$$x-\text{momentum}: \qquad \frac{\partial u}{\partial t} - fv = -g\frac{\partial \eta}{\partial x}, \tag{2.31a}$$

$$y-\text{momentum}: \qquad \frac{\partial v}{\partial t} + fu = -g\frac{\partial \eta}{\partial y}, \tag{2.31b}$$

$$\text{continuity}: \qquad \frac{\partial \eta}{\partial t} + H\left(\frac{\partial u}{\partial x} + \frac{\partial v}{\partial y}\right) = 0, \tag{2.31c}$$

where $f > 0$ is the Coriolis parameter, g is the gravitational acceleration, u and v are the velocity components in the $x-$ and $y-$ directions, and η is the surface displacement equal to $\eta = h - H$ the total depth h minus the mean fluid thickness H. The z momentum component is absent as the fluid is vertically homogeneous.

The operations $\frac{\partial}{\partial t}$ **div** on the momentum equations plus f times the z component of the curl of the horizontal momentum, and the use of the continuity equation to eliminate **div** $\vec{v}$ in favour of $-\frac{\partial \eta}{\partial t}$, and the horizontal momentum to eliminate $\vec{v}$ in terms of $\nabla\eta$, immediately lead to the following wave equation for the displacement η

$$\frac{\partial}{\partial t}\left[\left(\frac{\partial^2}{\partial t^2} + f^2\right)\eta - \mathbf{div}(c^2\nabla\eta)\right] = (\nabla(c^2 f) \times \nabla\eta)_z \tag{2.32}$$

in which f and c may be functions of x and y.This is the combined system of Poincaré-Rossby waves (Pedlosky, 1987).

In the low-frequency approximation ($\partial/\partial t \ll f$), this equation reduces to the Rossby wave equations

$$\frac{\partial}{\partial t}\left[\frac{f^2}{c^2} - \left(\frac{\partial^2}{\partial x^2} + \frac{\partial^2}{\partial y^2}\right)\right]\eta = (\beta \times \nabla\eta)_z, \tag{2.33}$$

in which $\beta = \partial f/\partial y$, and $c^2 = gH$ is the shallow water speed.

We shall here not discuss the propagation properties of Rossby waves as it is a focus of our study in the next chapter.

To obtain a dispersion relationship we look for solutions of the form

$$(u, v, \eta) = Re(u_0, v_0, \eta_0)e^{i(\mathbf{k}\cdot\mathbf{x}-\omega t)},$$

where $k = k\hat{i} + l\hat{j}$, ω is the nondimensional frequency. Substituting in the above system yields the dispersion relation

$$\omega(\omega^2 - (f^2 + c^2k^2)) = 0, \tag{2.34}$$

relating the propagation behaviour for waves. In the limit $\omega = 0$, the wave does not have phase or energy propagation (McWilliams, 2006). This gives a stationary wave solution. The second set of solutions satisfies the equation

$$\omega^2 = f^2 + c^2 k^2.$$

The corresponding waves are the Poincaré waves.

In the long wave limit, $k \to 0$, and $k^2 \ll f^2/gH$, the rotation effect dominates, yielding $\omega \simeq f$ (McWilliams(2006) and Vallis (2006)). For intermediate wavenumbers, the frequency $\omega > f$ always, and the waves exhibit a mixed behaviour between gravity waves and inertial oscillations, they are often called inertia-gravity waves. In the short wave limit $k^2 \gg f^2/c^2$, the dispersion relation reduces to that of non-rotational case (McWilliams(2006), Vallis(2006))

$$\omega = \pm c|k| \to \infty. \tag{2.35}$$

This condition is equivalent to requiring that the wavelength be much shorter than the deformation radius $L_d = \sqrt{gh}/f$ but still be longer than the depth of the fluid, otherwise the shallow water condition is not met (Vallis, 2006). The waves are non-dispersive and will preserve their shape.

Kelvin waves exist in the presence of both rotation and a lateral boundary. Supposing there is a solid boundary $y = 0$ then solutions in the y-direction are not allowable. Then in the governing equations (2.31c) we set $v = 0$ everywhere (Vallis, 2006), to obtain

$$\frac{\partial u}{\partial xt} = -g\frac{\partial \eta}{\partial x}, \quad fu = -g\frac{\partial \eta}{\partial y} \quad \frac{\partial \eta}{\partial t} + H\frac{\partial u}{\partial x} = 0. \tag{2.36}$$

The first and last equations giving

$$\frac{\partial^2 u}{\partial t^2} = c^2 \frac{\partial^2 u}{\partial x^2}, \tag{2.37}$$

where $c = \sqrt{gH}$ is the wave speed of shallow water waves. The solution thereof being a superposition of two waves, one traveling to the positive x-direction and the other to the negative x direction:

$$u = F_1(x + ct, y) + F_2(x - ct, y), \tag{2.38}$$

with the corresponding surface displacement

$$\eta = \sqrt{H/g}[-F_1(x+ct,y) + F_2(x-ct,y)]. \tag{2.39}$$

It is shown in Vallis (2006) that

$$F_1 = F(x+ct)e^{y/L_d}, \quad F_2 = G(x-ct)e^{-y/L_d},$$

where $L_d = \sqrt{gH}/f$ is the radius of deformation. If $y > 0$, then F_1 must be eliminated as it grows without bound, leaving F_2 to ensure boundedness at the boundary. Kelvin waves propagate with the coast to the right (anticlockwise) in the Northern Hemisphere ($f > 0$) and to the left (clockwise) in the Southern Hemisphere, ($f < 0$), and the direction is cyclonic in both Northern and Southern Hemispheres. Wang (2003) discuss these waves in greater detail.

Below we briefly discuss the contribution of the shallow water waves to weather and climate conditions. Rossby waves are known for their westward phase propagation whereas the group velocity can be in either direction depending on the wavelength, as we shall see in the next chapter. Their importance in weather and climate change lies in the impact on western boundaries. The westward propagating Rossby waves when they reach the Western Boundaries will be reflected. Unlike surface gravity waves the reflected waves do not simply become the mirror image of the incident waves. The reflected waves which were travelling westward must now have an eastward component of the group velocity and so must be of short zonal wavelength. Moreover, they will propagate relatively slower than the incoming waves. Thus there will be some kind of congestion at the western boundary. And this is what causes Western Boundary intensification as at the boundary there will be waves of short wavelength accumulating propagating against fast incoming long wavelength (Pedlosky, 1987).

Poincaré waves play a substantial role in the circulation of the atmosphere and oceans and they transport energy and momentum as they propagate either vertically or horizontally thereby causing a transfer of energy and momentum to their sink where they dissipate. This dissipation of energy and momentum when the waves break is also important as it may cause mixing. They are known to contribute to the generation of turbulence and to influence the thermal structure of the middle atmosphere, and in the oceans they contribute to mixing and are a possible energy source for the thermohaline circulation.

Kelvin waves are of particular importance on eastern boundaries (as opposed to Rossby waves) since they transfer information poleward from the equator. They are also central

to how the equatorial ocean adjusts to changes in wind forcing, such as during an El Niño.

2.3 Conclusion

In this chapter one of the most important concept in geophysical fluids, namely, rotation, has been revisited. Stratification will be discussed in more detail in Part II of the study. Some of the waves generated under the influence of these two factors, their propagation and their contribution to weather and climate conditions have been discussed. It is shown here how the shallow water equations are relevant to model rotating fluid motions like, Poincaré waves, Kelvin waves and Rossby waves. In particular, some of the propagation properties of Rossby waves were highlighted because they will be the focus of our next two chapters. In the next chapter further propagation properties of Rossby waves are discussed, which were to the best of my knowledge not discussed before in the literature.

Chapter 3

Propagation Properties of Rossby waves

In this chapter, shallow water equations already introduced in section 2.2 are employed, to first develop the general equation of motion governing the Poincaré-Rossby wave and the low frequency Rossby wave on the β-plane. The wave normal diagram is used to further explore Rossby wave propagation properties using the dispersion equation. Some propagation properties of Rossby waves have already been discussed in the previous chapter. The discussion here emanates from work by Longuet-Higgins (1964), who observed that the wave normal diagrams showed the phase velocity of the Rossby waves as a displaced circle. However, the group velocity was not explored further than its parametric form as shown in equations (18) and (19) of this chapter. Here, the group velocity is shown to be, instead, an ellipse, in so doing, reveal the anisotropic nature of Rossby waves.

Propagation properties are further discussed where the Rossby waves arise from the shallow water equations in the meridional, y, direction wherein $\beta_x = 0$ on the (k_x, k_y) plane using a parameter m which depends on the Mach number (or Froude number), which is, a measure of the equatorial rotation speed ΩR. It is also discussed here the Rossby wave propagation in the limiting case of infinite Rossby deformation radius ($m \to \infty$).

Furthermore the propagation properties of topographical Rossby waves are developed; phase velocity and group velocity diagrams, where the shallow water speed varies in the zonal direction ($\beta_y = 0$). In this case it is found that the phase velocity is also a displaced circle in the northward direction, whereas the group velocity is also an ellipse with northward and southward components as will be shown later in Figure 8. It is as if the westward propagating Rossby wave has been rotated ninety degrees. These discussions are carried out through a published paper that follows.

Ann. Geophys., 30, 849–855, 2012
www.ann-geophys.net/30/849/2012/
doi:10.5194/angeo-30-849-2012

Annales Geophysicae

Propagation properties of Rossby waves for latitudinal β-plane variations of f and zonal variations of the shallow water speed

C. T. Duba[1] **and J. F. McKenzie**[1,2]

[1]Department of Mathematics, Statistics and Physics, Durban University of Technology, P.O. Box 1134, Durban, South Africa
[2]School of Mathematical Sciences, University of Kwazulu Natal, Private Bag X54001, Durban, 4000, South Africa

Correspondence to: C. T. Duba (thamadub@dut.ac.za)

Received: 4 December 2011 – Revised: 7 April 2012 – Accepted: 17 April 2012 – Published: 15 May 2012

Abstract. Using the shallow water equations for a rotating layer of fluid, the wave and dispersion equations for Rossby waves are developed for the cases of both the standard β-plane approximation for the latitudinal variation of the Coriolis parameter f and a zonal variation of the shallow water speed. It is well known that the wave normal diagram for the standard (mid-latitude) Rossby wave on a β-plane is a circle in wave number (k_y, k_x) space, whose centre is displaced $-\beta/2\omega$ units along the negative k_x axis, and whose radius is less than this displacement, which means that phase propagation is entirely westward. This form of anisotropy (arising from the latitudinal y variation of f), combined with the highly dispersive nature of the wave, gives rise to a group velocity diagram which permits eastward as well as westward propagation. It is shown that the group velocity diagram is an ellipse, whose centre is displaced westward, and whose major and minor axes give the maximum westward, eastward and northward (southward) group speeds as functions of the frequency and a parameter m which measures the ratio of the low frequency-long wavelength Rossby wave speed to the shallow water speed. We believe these properties of group velocity diagram have not been elucidated in this way before. We present a similar derivation of the wave normal diagram and its associated group velocity curve for the case of a zonal (x) variation of the shallow water speed, which may arise when the depth of an ocean varies zonally from a continental shelf.

Keywords. Electromagnetics (Wave propagation)

1 Introduction

The propagation properties of mid-latitude Rossby waves on a β-plane are well known (Gill, 1982; Pedlosky, 1987). The dispersion equation in either its diagnostic form, (ω, k) plots, or wave normal form (Longuet-Higgins, 1964) shows that phase propagation is purely westward and that the waves cannot propagate above a critical frequency, at which the zonal group velocity becomes zero for a wave number equal to the inverse Rossby radius. This implies that for wavelengths less (greater) than the Rossby radius, the zonal group velocity is eastward (westward), while the phase velocity remains westward. This "backward" property, i.e. phase and group velocities in opposite directions, also manifests itself at a general angle of phase propagation, in that poleward directed rays (energy flux direction) correspond to equatorward wave normal (or phase) directions.

In this paper we highlight these anisotropic and dispersive properties through the use of the phase and group velocity diagrams, in which the former takes the well known form of a circle, whose centre is displaced westward and the latter, the less well known form, is an ellipse, whose centre is also displaced westward. The important parameters are the wave frequency ω (suitably normalized) and a parameter m, which is the ratio of the Rossby wave zonal speed (at low frequencies and long wavelengths) to the shallow water speed.

In the next section we use the shallow water equations to derive the wave equation for the system, which reduces to the classical Rossby wave equation in the low frequency approximation. This leads to the well-known dispersion equation at mid-latitudes and is generalized to include not only the usual β-effect arising from the latitudinal variation of the

Coriolis force, but also a topographic β-effect arising from background variations in the shallow water speed.

In Sect. 3 we outline the propagation properties of the mid-latitude Rossby wave in terms not only of its well-known wave normal diagram (Longuet-Higgins, 1964), but also its phase and group velocity diagrams. Of particular interest is the latter, which is normally given as expressions for the zonal and latitudinal group speeds in terms of the wave number vectors, which can be reduced to the zonal wave normal as the generating parameter. At a given frequency we show that the group velocity, (V_{gy}, V_{gx}), curve is in fact an ellipse, with centre displaced westward by an amount that depends on the "m" of the planet and the ratio of the wave frequency to the critical frequency, above which Rossby waves are evanescent. The major and minor axes yield the maximum zonal, westward, eastward and northward speeds as functions of frequency and m. The corresponding phase velocity diagram is a circle, with centre displaced westward. In the limiting case of $m \to \infty$ (or infinite Rossby radius), the group velocity curve becomes a parabola, and the phase velocity curve becomes a line indicating constant zonal phase velocity for all directions of propagation (limited of course to the 2nd and 3rd quadrants). These results are supplemented by the relation between the ray direction χ and the wave normal angle ϕ. It is well known that the latitudinal components of the phase and group velocities are anti-parallel. Interestingly, this "backward" property of the Rossby wave has been invoked to explain the dipole-like formation of equatorial easterly jets resulting from localized equatorial heating and at higher latitudes westerly jets (Diamond et al., 2008).

In Sect. 4 we carry out similar calculations for a topographic β-effect arising from zonal variations of the shallow water speed. In this case, it is as if the properties described in Sect. 3 were rotated through $\pi/2$ from west to north.

2 The general Poincaré-Rossby wave equation and the low frequency Rossby wave

The linearised shallow water equations in a rotating layer of fluid of depth $H(x, y)$ may be written (Gill, 1982; Pedlosky, 1987)

$$\frac{\partial \underline{Q}}{\partial t} + \underline{f} \times \underline{Q} = -c^2 \nabla \eta \tag{1}$$

$$\frac{\partial \eta}{\partial t} + \mathrm{div}\underline{Q} = 0 \tag{2}$$

in which $\underline{Q} = (Q_x, Q_y) = H(u, v)$ is the perturbation horizontal momentum vector, (u, v) the horizontal velocity, η the displacement of the surface from its equilibrium depth H, $f = 2\Omega(\sin\theta)\hat{z}$ is the Coriolis parameter (Ω rotation frequency) and $c = \sqrt{gH}$ the shallow water speed. The operations $\frac{\partial}{\partial t}$div on Eq. (1) plus f times the z component of the curl of Eq. (1), and the use of Eq. (2) to eliminate div$\underline{Q}$ in favour of $-\partial\eta/\partial t$, and Eq. (1) to eliminate $\underline{Q}$ in terms of $\nabla\eta$ immediately lead to the following wave equation for the displacement η:

$$\frac{\partial}{\partial t}\left[\left(\frac{\partial^2}{\partial t^2} + f^2\right)\eta - \mathrm{div}\left(c^2\nabla\eta\right)\right] = \left(\nabla\left(c^2 f\right) \times \nabla\eta\right)_z, \tag{3}$$

in which f and c may be functions of x and y. Equation (3) is the general equation for the combined system of Poincaré-Rossby waves (Pedlosky, 1987). In the "low-frequency" approximation ($\frac{\partial}{\partial t} << f$), this equation reduces to the classical Rossby wave equation:

$$\frac{\partial}{\partial t}\left[\frac{f^2}{c^2} - \left(\frac{\partial^2}{\partial x^2} + \frac{\partial^2}{\partial y^2}\right)\right]\eta = \left(\underline{\beta} \times \nabla\eta\right)_z, \tag{4}$$

in which

$$\underline{\beta} \equiv \left(\beta_x, \beta_y\right) = c^{-2}\nabla\left(c^2 f\right) \tag{5}$$

since $\nabla f = (0, \beta, 0)$. Equation (4) is a generalization of the usual Rossby wave equation (see Pedlosky, 1987) to include the topographic "β" effect through spatial variations (in x and y) of the shallow water speed c as well as the y variation of $f(= f_0 + \beta y)$ in the classical β-plane approximation of the latitudinal variation of the vertical component $f\hat{z}$ on a spherical planet of radius R where

$$f = f_0 + \beta_0 y, \quad \beta_0 = \frac{2\Omega\cos\theta_0}{R}, \quad f_0 = 2\Omega\sin\theta_0. \tag{6}$$

Here θ_0 is the latitude at which the β-plane is constructed tangent to the surface at θ_0, and therefore y measures distance northward whilst x is directed eastward.

If the background variations of $c^2(x, y)$ and $f(y)$ are assumed "slow" over a wavelength, the wave Eq. (4) admits a local dispersion relation for plane waves, varying as $\exp i(\omega t - k_x x - k_y y)$ namely

$$\omega = \frac{-\beta_y k_x + \beta_x k_y}{\left(k_x^2 + k_y^2 + f_0^2/c^2\right)} \tag{7}$$

or

$$\left(k_y - \frac{\beta_x}{2\omega}\right)^2 + \left(k_x + \frac{\beta_y}{2\omega}\right)^2 = \frac{{\beta_x}^2 + {\beta_y}^2}{4\omega^2} - \frac{{f_0}^2}{c^2}. \tag{8}$$

For a given ω the latter wave normal form is a circle centred at $(-\beta_y/2\omega, \beta_x/2\omega)$ of radius given by the square root of the RHS of Eq. (8). The presence of an inhomogeneity in x (zonal eastward), dc^2/dx, gives rise to a displacement of the usual Rossby wave, representing purely westward propagation ($k_x < 0$), northward so as to permit eastward phase

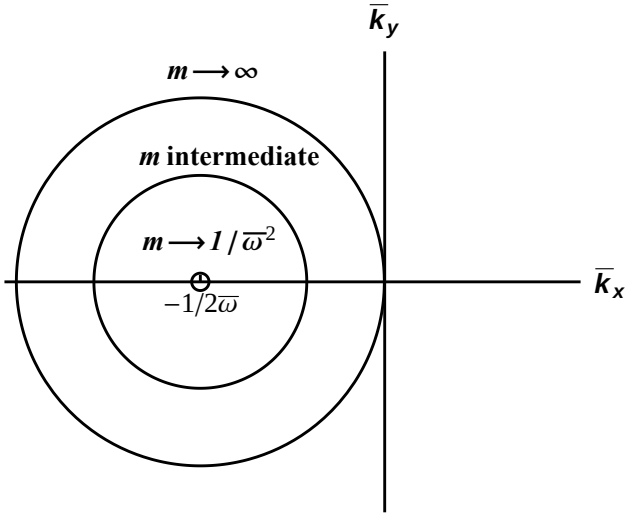

Fig. 1. The wave normal circle for various values of m.

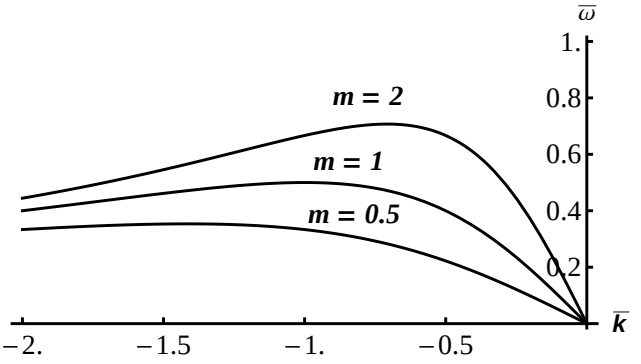

Fig. 2. The diagnostic diagram $(\bar{\omega}, \bar{k})$ plot for various values of m.

propagation ($k_x > 0$), as represented by any $\underline{k}$ pointing northeast with a corresponding ray directed southwest. Thus, a northwest propagation vector $\underline{k}$ gives rise to a ray directed southwest. Such are the rather peculiar propagation properties of the Rossby wave, which follow from the theorem that the group velocity vector points along the normal to the wave normal curve in the direction of increasing ω (Lighthill, 1978). We shall now explore these properties in greater detail through the use of figures representing the wave normal diagram and the phase and group velocity diagrams at given frequencies for different values of m.

3 Propagation properties of the mid-latitude Rossby wave: wave normal, phase and group velocity curves for $\beta_y \neq 0$ ($\beta_x = 0$)

The propagation properties of the Rossby wave have been discussed extensively, for example, in the texts by Gill (1982) and Pedlosky (1987). Here we develop the group velocity diagram at a fixed ω, which provides the counterpart to the wave normal diagram. In the case where the Rossby wave arises from inhomogeneity only in the y-direction ($\beta_x = 0$), the diagnostic $(\bar{\omega}, \bar{k})$ plot and the wave normal curves are given by

$$\bar{\omega} = \frac{-\bar{k}_x}{\bar{k}^2 + 1/m}, \tag{9}$$

and Eq. (8) may be written

$$\bar{k}_y^2 + \left(\bar{k}_x + \frac{1}{2\bar{\omega}}\right)^2 = \frac{1}{4\bar{\omega}^2} - \frac{1}{m}, \tag{10}$$

in which $\bar{\omega}$ is the normalized frequency, $\omega/\sqrt{\beta_y c}$, $\underline{\bar{k}}$, the normalized wave number vector $\underline{k}\left(c/\beta_y\right)^{1/2}$ and m is given by

$$m \equiv \beta_y c/f_0^2 = \frac{\cos\theta_0}{\sin^2\theta_0}\frac{1}{2M}, \tag{11}$$

$$M = \Omega R/c. \tag{12}$$

Here we have assumed that there is no latitudinal variation of c^2, and therefore the β effect arises solely from the variation of f as in Eq. (6); M is a Mach (or Froude) number measuring the equatorial rotation speed ΩR in units of the shallow water speed c, and m is in fact the ratio of the Rossby zonal phase speed (at low frequencies and long wavelengths) to c. Equation (10) is a circle in $(\bar{k}_y, \bar{k}_x)$ space of radius $\sqrt{1/4\bar{\omega}^2 - 1/m}$, whose centre is displaced along the negative $\bar{k}_x$ axis by $-1/2\bar{\omega}$ units (Longuet-Higgins, 1964), as shown in Fig. 1 along with the $(\bar{\omega}, \bar{k})$ plot in Fig. 2. Note that the phase propagation is entirely westward and propagation requires $\bar{\omega} < \sqrt{m}/2$. Figure 3 demonstrates the geometrical relation between the ray direction χ and the wave normal angle ϕ, both measured from $\bar{k}_x$-axis, which shows the two values of χ for any given ϕ. The relationship between χ and ϕ is found by expressing χ as normal to the slope of the $(\bar{k}_y, \bar{k}_x)$ curve, i.e. $\tan\chi = -1/(\partial\bar{k}_y/\partial\bar{k}_x)$, which yields

$$\tan\chi = (\sin\phi\cos\phi)/\left(\cos^2\phi + \frac{1}{-1 \pm \sqrt{1 - 4\omega^2/m\cos^2\phi}}\right). \tag{13}$$

For a given ϕ there are two values of χ, as shown in Fig. 4. We also show the limiting case $m \to \infty$, which yields $\chi = 2\phi$ (lower sign m in Eq. 13) and $\chi = \pi$ (upper sign). In this limit ${f_0}^2/c^2 \to 0$, and the Rossby wave Eq. (4) reduces to the classic form (see e.g. Yagamata, 1976)

$$\frac{\partial}{\partial t}\nabla^2\psi = -\beta\frac{\partial\psi}{\partial x} \tag{14}$$

where ψ is the stream function corresponding to strict 2-D compressibility. It is for this reason we include a discussion in the limit $m \to \infty$.

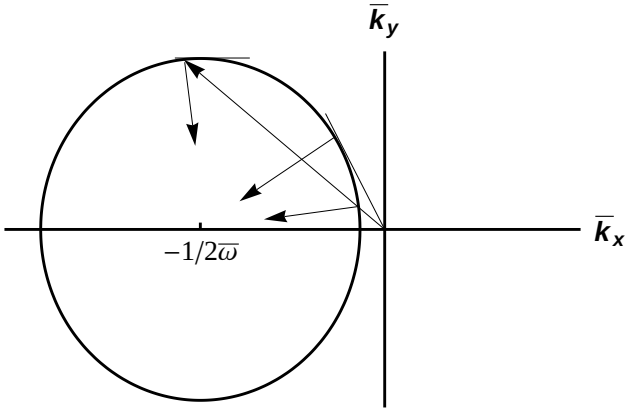

Fig. 3. The wave normal displaced circle showing the relation between the ray direction χ (given by the arrows pointing towards the centre measured from $\bar{k}_x$) and the wave normal angle ϕ between $\underline{\bar{k}}$ and $\bar{k}_x$.

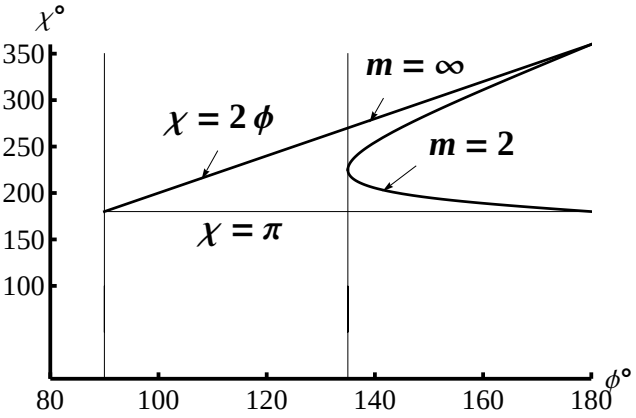

Fig. 4. The variation of χ (two values) with ϕ for $m = 2$.

The phase velocity $V_p = \omega/k$, which follows immediately from Eq. (7), may be written in the normalized form

$$\bar{V}_{py}^2 + \left(\bar{V}_{px} + \frac{m}{2}\right)^2 = \frac{m^2}{4}\left(1 - \frac{4\bar{\omega}^2}{m}\right), \tag{15}$$

in which V_p has been normalized with respect to the shallow water speed c. Thus, the phase velocity diagram is a circle of radius $\frac{m}{2}\sqrt{1-4\bar{\omega}^2/m}$, whose origin is displaced westward by $-m/2$ units and therefore lies entirely in the regime of westward propagation. The smallest value of the westward $\bar{V}_{px}$ (in which $\bar{V}_{py} = 0$ in Eq. 15) is

$$\bar{V}_{pxmin} = \frac{-m}{2} + \frac{m}{2}\sqrt{1 - \frac{4\bar{\omega}^2}{m}}, \tag{16}$$

which approaches $-\bar{\omega}^2$ as $m \to \infty$. Thus, in the limit $m \to \infty$ (which corresponds to infinite Rossby radius or Rossby wave speed greatly in excess of the shallow water speed)

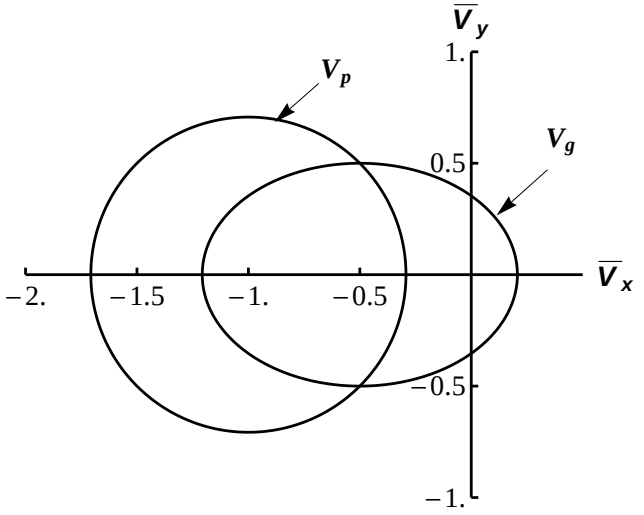

Fig. 5. The phase velocity V_p (a circle) and group velocity V_g (an ellipse) diagrams for a fixed $\bar{\omega}$ and $m = 2$.

the phase velocity diagram reduces to the line $\bar{V}_{px} = -\bar{\omega}^2$ in $(\bar{V}_{py}, \bar{V}_{px})$ space.

The group velocity $\underline{V}_g = \partial\omega/\partial\underline{k}$ follows from Eq. (7) (in which we put $\beta_x = 0$) in the form

$$V_{gx} = \frac{\beta\left(k_x{}^2 - \left(k_y{}^2 + f_0{}^2/c^2\right)\right)}{\left(k_x{}^2 + k_y{}^2 + f_0{}^2/c^2\right)^2}, \tag{17}$$

$$V_{gy} = \frac{2\beta k_y k_x}{\left(k_x{}^2 + k_y{}^2 + f_0{}^2/c^2\right)^2}. \tag{18}$$

In the classic texts (Pedlosky, 1987; Gill, 1972) the group velocity is left in this less than perspicacious parametric form, in which the $\bar{k}_x$ is the generating parameter, with $\bar{k}_y$ given in terms of $\bar{k}_x$ from the dispersion equation. Here we show that the group velocity diagram is in fact an ellipse. This simple result follows from a few algebraic steps by eliminating the denominator from Eqs. (17) and (18) using the dispersion equation, so that in normalized form, Eqs. (17) and (18) become

$$\bar{V}_{gx} = \bar{\omega}^2\left(2 + 1/\bar{\omega}k_x\right), \tag{19}$$

$$\bar{V}_{gy} = 2\bar{\omega}^2\left(\bar{k}_y/\bar{k}_x\right). \tag{20}$$

It is now straightforward to eliminate $\bar{k}_x$ in favour of $\bar{V}_{gx}$ from Eq. (19), which on substitution into the square of Eq. (20) gives directly the group velocity $(\bar{V}_{gx}, \bar{V}_{gy})$ curve in the form

$$\bar{V}_{gy}^2 = 4\bar{\omega}^4\left[\left(1 - \frac{\bar{V}_{gx}}{\bar{\omega}^2}\right) - \frac{\bar{\omega}^2}{m}\left(\frac{\bar{V}_{gx}}{\bar{\omega}^2} - 2\right)^2\right], \tag{21}$$

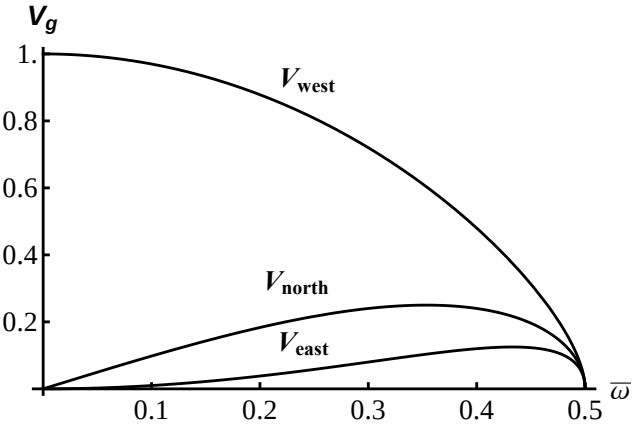

Fig. 6. The maximum westward, northward and eastward group speeds as a function of frequency $\bar{\omega}$ for $m = 1$.

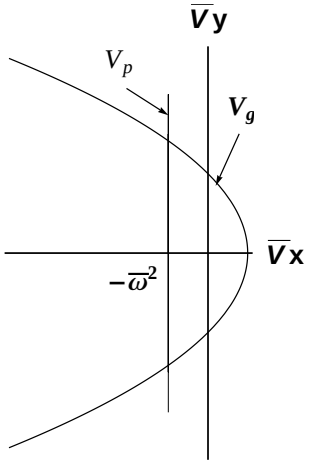

Fig. 7. The group velocity (a parabola) and phase velocity (a line) diagrams for the case $m \to \infty$.

which may also be written as

$$\frac{m\bar{V}_{\mathrm{gy}}^2}{4\bar{\omega}^2} + \left[\bar{V}_{\mathrm{gx}} + \frac{m}{2}\left(1 - \frac{4\bar{\omega}^2}{m}\right)\right]^2 = \frac{m^2}{4}\left(1 - \frac{4\bar{\omega}^2}{m}\right). \quad (22)$$

The group velocity curve is an ellipse, whose centre is displaced $\frac{-m}{2}\left(1 - 4\bar{\omega}^2/m\right)$ units along the $\bar{V}_{\mathrm{gx}}$ axis. The phase and group velocity curves are shown in Fig. 5. The southward group velocity is simply a reflection of the northward group velocity in the x-axis. The maximum eastward and westward group speeds are given by

$$\bar{V}_{\mathrm{gx}}^{\pm} = \frac{m}{2}\left(1 - \frac{4\bar{\omega}^2}{m}\right)^{1/2}\left[\pm 1 - \left(1 - \frac{4\bar{\omega}^2}{m}\right)^{1/2}\right], \quad (23)$$

and the maximum northward (southward) group speed also follows as

$$\bar{V}_{\mathrm{gymax}} = \pm\bar{\omega}m^{1/2}\left(1 - \frac{4\bar{\omega}^2}{m}\right)^{1/2}. \quad (24)$$

Examples of the behaviour of extremal group velocities $\bar{V}_{\mathrm{pxmin}}$, $\bar{V}_{\mathrm{pxmax}}$ and $\bar{V}_{\mathrm{pymax}}$ are shown in Fig. 6. Note that the ellipse collapses to the origin as $m \to 4\bar{\omega}^2$, at which the wave normal collapses to the point $k_{\mathrm{x}} = -1/2\bar{\omega}$. In the limiting case in which $m >> 1$, which can prevail quite near the equator ($\theta_0 \to 0$), Eq. (21) tends to the parabola

$$\bar{V}_{\mathrm{gy}} = \pm 2\bar{\omega}^2\left(1 - \frac{\bar{V}_{\mathrm{gx}}}{\bar{\omega}^2}\right)^{1/2}, \quad (25)$$

which is shown in Fig. 7 together with the phase velocity diagram, which is simply the line $V_{\mathrm{px}} = -\bar{\omega}^2$. It is of some interest to emphasize that Rossby waves are "backward" in the sense that the latitudinal components of their phase and group velocities are always in opposite directions. This property can be invoked to describe the formation of a dipole pair of jets in the following way: Northward (away from the equator) wave energy flux is associated with southward, towards the equator, wave momentum flux; and the opposite in the case of southward directed energy flux, away from the equator, corresponds to northward (towards the equator) momentum flux. In other words, a poleward energy flux from the equator is associated with an equatorward flux of momentum. Hence, Rossby wave dynamics implies that localized equatorial heating gives rise to equatorial easterly zonal jets. This "convergence" of equatorial momentum implies a deficit at higher latitudes such that a westerly jet must necessarily form there (Diamond et al., 2008).

4 Propagation properties of the topographic Rossby wave: wave normal, phase and group velocity curves for $\beta_{\mathrm{x}} \neq 0$ ($\beta_{\mathrm{y}} = 0$)

In this case a zonal inhomogeneity (c a function of x) dispersion and wave normal curves given by putting $\beta_{\mathrm{y}} = 0$ in Eqs. (7) and (8), are

$$\bar{\omega} = \frac{\bar{k}_{\mathrm{y}}}{\bar{k}_{\mathrm{x}}^2 + \bar{k}_{\mathrm{y}}^2 + 1/m}, \quad (26)$$

$$\bar{k}_{\mathrm{x}}^2 + \left(\bar{k}_{\mathrm{y}} - \frac{1}{2\bar{\omega}}\right)^2 = \frac{1}{4\bar{\omega}^2} - \frac{1}{m}, \quad (27)$$

in which ω and k have been normalized to $\sqrt{\beta_{\mathrm{x}}c}$ and $(c/\beta_{\mathrm{x}})^{1/2}$, respectively and m is now given by

$$m = \beta_{\mathrm{x}}\frac{c}{f_0^2}, \quad (28)$$

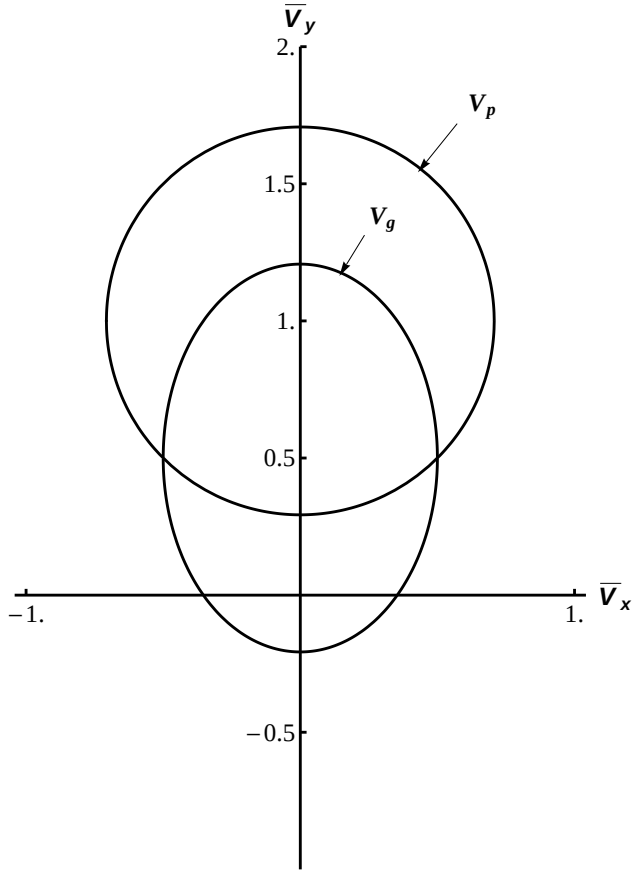

Fig. 8. The phase and group velocity diagrams for topographic Rossby waves where shallow water speed varies zonally for fixed $\bar{\omega}$ and $m = 2$.

$$\beta_x = \frac{f_0}{c^2}\frac{dc^2}{dx}. \tag{29}$$

The wave normal diagram is again a circle, but now its centre is displaced $1/2\bar{\omega}$ units along the positive $\bar{k}_y$ axis. The corresponding phase velocity diagram is given by

$$\left(\bar{V}_{py} - \frac{m}{2}\right)^2 + \bar{V}_{px}^2 = \frac{m^2}{4}\left(1 - \frac{4\bar{\omega}^2}{m}\right), \tag{30}$$

which is a circle of radius $\frac{m}{2}\left(1 - 4\bar{\omega}^2/m\right)^{1/2}$ with centre displaced $m/2$ units along the $\bar{V}_{py}$ axis. Hence, phase propagation is always northward, although as we can now anticipate, there are both northward and southward components of the group velocity. It is as if the classical westward Rossby wave phase were rotated through ninety degrees. The calculation of the group velocity follows similar lines but now with

$$\bar{V}_{gy} = \bar{\omega}^2\left(-2 + \frac{1}{\bar{\omega}\bar{k}_y}\right), \tag{31}$$

$$\bar{V}_{gx} = -2\bar{\omega}^2\bar{k}_x/\bar{k}_y. \tag{32}$$

Hence, the group velocity curve is now given by the ellipse

$$\bar{V}_{gx}^2 = 4\bar{\omega}^4\left[\left(\frac{\bar{V}_{gy}}{\bar{\omega}^2} + 1\right) - \frac{\bar{\omega}^2}{m}\left(\frac{\bar{V}_{gy}}{\bar{\omega}^2} + 2\right)^2\right], \tag{33}$$

or

$$\frac{m\bar{V}_{gx}^2}{4\bar{\omega}^2} + \left[\bar{V}_{gy} - \frac{m}{2}\left(1 - \frac{4\bar{\omega}^2}{m}\right)\right]^2 = \frac{m^2}{4}\left(1 - \frac{4\bar{\omega}^2}{m}\right), \tag{34}$$

which is shown in Fig. 8. This curve can be obtained by rotating the curve given by Eq. (22) and Fig. 5 through ninety degrees. Thus, the maximum northward, southward and zonal (east or west) speeds are given by Eqs. (23) and (24) in which the labels x and y are interchanged.

5 Summary

The propagation properties of mid-latitude Rossby waves are illustrated through the local dispersion equation either in its diagnostic form ((ω, k) plot) or as a wave normal curve for given values of ω, both of which descriptions highlight the dispersive and anisotropic nature of the wave. Here we develop this further by showing that the group velocity diagram is an ellipse, whose centre is displaced westward (Fig. 5) and whose major and minor axis yield the maximum westward, eastward and northward (southward) group speeds as a function of frequency and the parameter m (Fig. 6). This elegant construction replaces the earlier (somewhat cumbersome) expressions for the group velocity, which are usually given in terms of the zonal and northward wave numbers acting as generating parameters as in Eqs. (17) and (18). Similar diagrams exist for the case of topographic Rossby waves, in which shallow water speed varies zonally (Fig. 8). We emphasize that the "backward" property of the Rossby wave has been invoked to explain dipole-like formation of equatorial easterly jets and at higher latitudes westerly jets, as discussed by Diamond et al. (2008).

Acknowledgements. The authors would like to thank the reviewers for the most useful and constructive comments towards the finalization of this paper. This work was supported by the National Research Foundation of South Africa. A thank you note to Clemens Dempers of BlueStallion Technologies who provided technical assistance with the graphics.

Topical Editor C. Jacobi thanks L. Debnath and two other anonymous referees for their help in evaluating this paper.

References

Diamond, P. H., Gurcan, D. D., Hahn, T. S., Miki, K., and Garbet, X.: Momentum theorems and the structure of atmospheric jets

and zonal flows in plasmas, Plasma Phys. Control. Fusion, 50, 124018, doi:10.1088/0741-3335/50/12/124018, 2008.
Gill, A. E.: Atmosphere and Ocean Dynamics, Academic Press, London, 662 pp., 1982.
Lighthill, J.: Waves in Fluids, Cambridge University Press, 504 pp., 1978.
Longuet-Higgins, M. S.: On Group Velocity and Energy Flux in Planetary Wave Motions, Deep-Sea Research and Oceanographic Abstracts, 11, pp. 35–42, 1964.
Pedlosky, J.: Geophysical Fluid Dynamics, 2nd Edition, Springer-Verlag, New York, 710 pp., 1987.
Yagamata, T.: On trajectories of Rossby Wave-packets Released in a Lateral Shear Flow, J. Oceanogr. Soc. Japan, 32, 162–168, 1976.

Chapter 4

Rossby waves in Winds

In the previous chapters, I alluded to Rossby waves having westward propagation and being low frequency waves which means that they travel for days in the westward direction. Furthermore, the energy transport can be directed westward through long wavelength Rossby waves or eastward via the short wavelength Rossby waves. The question that arose was what happens when Rossby waves travel westward? In other words, what happens if Rossby waves encounter zonally propagating easterly or westerly winds in their path? A further and similar question for meridional winds is relevant. The answer to these questions lies in the interaction of the frequency of the Rossby wave propagation and the frequency of the wind, that is, the Doppler shift frequency, as it now has a consequence for the dispersion relation.

The results are demonstrated through wave number curves, as was done in the previous chapter. The conclusion here, with respect to the westerly zonal flow, is that the displaced Longuet-Higgins circle is distorted into an ovoid-shaped curve and a new branch consisting of an eastward indentation develops. This indentation corresponds to the limit where the Rossby wave frequency and the Doppler shift frequency coincide. On the other hand, in the case of the eastward zonal flow, the indentation is entirely westward. The radiation patterns are determined through the method of stationary phase as used by Lighthill (1978). Some of these patterns resemble the Kelvin-ship wave and others I have not seen before in literature. Interaction with meridional winds is more complicated and the associated radiation patterns are remarkable.

Another intriguing result is that radiation patterns associated with the stationary wave resemble the radiation patterns for the gravity wave as shown by Lighthill (1978). Further results are elucidated in the following published paper.

Geophysical and Astrophysical Fluid Dynamics, 2014
Vol. 108, No. 3, 237–257, http://dx.doi.org/10.1080/03091929.2013.867604

Rossby wave patterns in zonal and meridional winds

C.T. DUBA*†, T.B. DOYLE‡§ and J.F. MCKENZIE†

†Department of Mathematics Statistics and Physics, Durban University of Technology, P.O. Box 1334, Durban 4001, South Africa
‡iThemba Laboratory for Accelerator Based Sciences, Somerset West 7129, South Africa
§School of Chemistry and Physics, University of KwaZulu-Natal, Westville, South Africa

(*Received 15 July 2013; in final form 15 November 2013; first published online 31 March 2014*)

The propagation properties of Rossby waves in zonal and meridional winds are analyzed using the local dispersion relation in its wave number form, the geometry of which plays a crucial role in illuminating radiation patterns and ray trajectories. In the presence of a wind/current, the classical Rossby wave number curve, an offset circle, is distorted by the Doppler shift in frequency and a new branch, consisting of a blocking line with an eastward facing indentation, arises from waves convected with or against the flow. The radiation patterns generated by a time harmonic compact source in the laboratory frame are calculated using the method of stationary phase and are illustrated through a series of figures given by the reciprocal polars to the various types of wave number curves. We believe these results are new. Some of these wave patterns are reminiscent of a "reversed" ship wave pattern in which cusps (caustics) arise from the points of inflection of the wave number curves; whilst others bear a resemblance to the parabolic like curves characteristic of the capillary wave pattern formed around an obstacle in a stream. The Rossby stationary wave in a westerly is similar to the gravity wave pattern in a wind, whereas its counterpart in a meridional wind exhibits caustics, again arising from points of inflection in the wavenumber curve.

Keywords: Rossby waves; β-plane; Radiation pattern

1. Introduction

Rossby waves play a pivotal role in the transport of energy and momentum in the geophysical fluid dynamics of quasi-geostrophic flows in atmospheres and oceans. The particular wave dynamics arise from the latitudinal variation of the Coriolis acceleration (through the Coriolis parameter f) and the near balance achieved between it and the pressure gradient. This quasi-geostrophic balance is described within the framework of the β-plane approximation which retains the essential dynamics, whilst the spherical geometry is replaced with a Cartesian β-plane constructed tangential to the surface at a given latitude. These features have all been extensively discussed in the texts of Gill (1982), Pedlosky (1987), Vallis (2006), and elsewhere. Some of the latter will be referenced to in the following.

In this well-researched field it may be expected that there is nothing new or interesting to reveal about the linear behavior of Rossby waves. However, recently it has been shown

*Corresponding author. Email: thamadub@dut.ac.za

that the group velocity diagram, at a given wave frequency, is in fact an ellipse whose focus lies at the origin (Duba and McKenzie 2012, McKenzie under review). This elegant feature complements the wave number curve, namely an offset circle in wave number space (Longuet-Higgins 1964), in revealing the propagation properties of Rossby waves. Furthermore, it has been shown (Rhines 2003, McKenzie under review) that the radiation pattern of Rossby waves (in the wind-free case) consists of two sets of hyperbolae, confined to westward pointing Mach–Froude like lines, in a fashion analogous to the gravity-capillary waves generated by an obstacle in uniform motion on deep water (see Doyle and McKenzie (2013) for a recent treatment of this classical ship wave problem). These features of the radiation pattern generated by some time harmonic spatially compact source are illuminated by the use of the method of stationary phase in calculating the far field disturbance. This method demonstrates that the radiation pattern is in fact given by the reciprocal polar to the wave normal curve (Lighthill 1978, 1960, p. 372–373) and this simple geometrical construction provides not only the mathematical expressions for, but also a means of visualizing, the radiation pattern which, in zonal and meridional winds reveals new and interesting patterns.

In this paper, we extend the above analysis to include the effects of zonal and meridional winds which give rise to new and interesting features of the wave number curves resulting from the Doppler shift in frequency. In a recent paper, Gerkema *et al.* (2013) call this effect a "quasi-Doppler shift" referring to the difference between the frequency ω measured by an observer at rest (the laboratory frame) and the frequency $\hat{\omega}$ measured by an observer moving with the mean flow. This shift has a profound effect on wave propagation in a moving medium, particularly if the medium is both dispersive and anisotropic, as is indeed the case for Rossby waves. The wave number diagrams therefore are important in revealing the propagation properties of Rossby waves, in much the same way as the Appleton–Hartree refractive index (Ratcliffe 1972, p. 18, section 2.5) is crucial to the understanding of electromagnetic waves in a magneto-ionic medium, and of the slowness ($\boldsymbol{k}$) surfaces in MHD (Lighthill 1960).

In section 2, we develop the standard equations of motion on a β-plane and derive the wave energy equation. Although the Coriolis term makes no contribution to this equation, it nevertheless has an indirect effect through shaping the propagation properties of the natural modes (inertial and planetary) of the system. In section 3, we derive the coupled equations for the northward and eastward mass flux perturbations and the excess pressure (all of which are shown to be equivalent to the shallow water equations with an appropriate definition of the Kelvin speed). In the case of Fourier type zonal wave modes, the coupled equations reduce to a single second-order differential equation for the latitudinal structure of the northward mass flux.

In section 4, we examine the wave propagation properties revealed by the dispersion equation in the form of wave number curves at a given frequency ω in the laboratory frame for different values of the zonal and meridional wind speeds. These diagrams enable the calculation of the radiation pattern generated by a time harmonic spatially compact source in a steady, uniform wind, through the reciprocal polar to the appropriate wave number curve. For example, in the case of a westerly zonal wind, its effect is to distort the Longuet-Higgins circle into an ovoid-shaped curve, and importantly, to introduce a new branch, due to the Doppler shift, consisting essentially of a blocking line with an indentation to the right (i.e. eastward) of this line, and corresponds to propagation arising from waves convected with or against the zonal flow. The reciprocal polar of the (closed) ovoid curve is a parabolic like curve corresponding to both eastward and westward energy propagation; whilst that for the line with an indentation we have an eastward facing deltoid, reminiscent of an inverted or "reversed" Kelvin ship wave. In this case, the radiation pattern is confined to a Kelvin-like angle (given by a line drawn from the

origin to the cusp point which arises from the point of inflection in the wave number curve). The analysis for westward zonal flow (an easterly) reveals similar features with a parabolic like curve for the reciprocal polar within which is embedded a Kelvin-like ship wave deltoid facing the "correct" way (i.e. eastward) associated with the indented line. An analysis of the effects of a meridional wind, including the stationary wave patterns (obtained as the limit in which the frequency ω tends to zero) yields similar interesting features but with the presence of a north-south symmetry.

2. Linearized equations of motion in a zonal wind shear

The linearized continuity equation is given by

$$\frac{\mathrm{D}\rho_e}{\mathrm{D}t} + \nabla \cdot \boldsymbol{q} = 0, \tag{1}$$

in which $\mathrm{D}/\mathrm{D}t = \partial/\partial t + U_x(y)\partial/\partial x$ is the convective derivative, $\boldsymbol{q} = \rho_0 \boldsymbol{u}$ is the mass flux perturbation, where ρ_0 is the background density, $\boldsymbol{u}$ is the velocity perturbation, ρ_e is the density perturbation, and $U_x(y)$ is a given zonal flow sheared in the y (north) direction. The x (east), y (north), and z (vertical) components of the momentum equation are

$$\frac{\mathrm{D}q_x}{\mathrm{D}t} - (f - U')q_y = -\frac{\partial p_e}{\partial x}, \tag{2a}$$

$$\frac{\mathrm{D}q_y}{\mathrm{D}t} + f q_x = -\frac{\partial p_e}{\partial y}, \tag{2b}$$

$$\frac{\mathrm{D}q_z}{\mathrm{D}t} = -\frac{\partial p_e}{\partial z} - \rho_e g, \tag{2c}$$

respectively, in which p_e is the pressure perturbation and U' is the derivative of $U_x(y)$ with respect to y. We have assumed a β-plane approximation, at a given latitude θ_0 on a planet with radius R. Ω is the earth's rotation frequency, so that the Coriolis parameter f is given by

$$f = f_0 + \beta y, \qquad \beta_0 = \frac{2\Omega}{R}\cos\theta_0. \tag{3a,b}$$

The equation for adiabatic flow (which, in the dissipationless case, is equivalent to the energy equation) takes the form (Lighthill 1978, p. 292, section 4.2)

$$g\frac{\mathrm{D}\rho_e}{\mathrm{D}t} = N^2 q_z + \frac{g}{c_0^2}\frac{\mathrm{D}p_e}{\mathrm{D}t}, \tag{4}$$

in which the square of the Brunt–Väisälä frequency N is given by

$$N^2 = g\left(-\frac{1}{\rho_0}\frac{\mathrm{d}\rho_0}{\mathrm{d}z} - \frac{g}{c^2}\right) = (g/H)(1 - \gamma^{-1}), \tag{5}$$

where H is the density scale height, γ is the ratio of the specific heats, and c_0 is the speed of sound given by $\sqrt{\gamma p_0/\rho_0}$. The background state is described by hydrostatic equilibrium and geostrophic balance, namely

$$\frac{\partial p_0}{\partial z} = -\rho_0 g, \qquad \frac{\partial p_0}{\partial y} = -\rho_0 f U_x(y). \tag{6a,b}$$

In general, these equations must be supplemented by a background energy equation which includes heating, cooling, and dissipation processes such as those resulting from viscous and heat conduction effects, in order to completely determine the background state (ρ_0, p_0, U_x).

The perturbation equations (1), (2), and (4) can be somewhat simplified by using the Boussinesq approximation which filters out high frequency acoustic waves. This is accomplished by neglecting $\mathrm{D}\rho_e/\mathrm{D}t$ in (1) which becomes

$$\nabla \cdot \boldsymbol{q} = 0, \tag{7}$$

and also by letting $c_0 \to \infty$ in the second term on the right-hand side of (4) which becomes

$$g\frac{\mathrm{D}\rho_e}{\mathrm{D}t} = N^2 q_z. \tag{8}$$

We note that in this approximation the continuity equation no longer evolves the density in time which is now evolved by the incompressible form, equation (8), for adiabatic flow, with the implication that there is now no equation which evolves the pressure. However, we note that, if we do the operation $\mathrm{D}/\mathrm{D}t$ on (2c), we obtain

$$\frac{\mathrm{D}}{\mathrm{D}t}\left(\frac{\partial p_e}{\partial z}\right) = -\frac{\mathrm{D}^2}{\mathrm{D}t^2}q_z - g\frac{\mathrm{D}\rho_e}{\mathrm{D}t}, \tag{9a}$$

$$= -\left(\frac{\mathrm{D}^2}{\mathrm{D}t^2} + N^2\right)q_z. \tag{9b}$$

The last result follows from the use of (8) to eliminate ρ_e. Furthermore, if we do the operation $\partial/\partial z$ on (9b) and use continuity in its incompressible form (7) to eliminate $\partial q_z/\partial z$, we obtain

$$\frac{\mathrm{D}}{\mathrm{D}t}\left(\frac{\partial^2 p_e}{\partial z^2}\right) = \left(\frac{\mathrm{D}^2}{\mathrm{D}t^2} + N^2\right)\left(\frac{\partial q_x}{\partial x} + \frac{\partial q_y}{\partial y}\right). \tag{10}$$

In what follows we will use the low frequency approximation $\mathrm{D}^2/\mathrm{D}t^2 \ll N^2$ (which filters out higher frequency internal gravity waves with $\omega \sim N$) and assume waves of the form $\exp(-\mathrm{i}k_z z)$ in the vertical direction, so that (10) may be written

$$\frac{\mathrm{D}p_e}{\mathrm{D}t} = -c^2\left(\frac{\partial q_x}{\partial x} + \frac{\partial q_y}{\partial y}\right), \qquad c^2 \equiv N^2/k_z^2. \tag{11a,b}$$

Here, c may be called the effective Kelvin speed which, in shallow water theory, is $\sqrt{gH}$, where H is the depth. In this rather circuitous route, we now have an equation (11a) which evolves the perturbation pressure p_e. Hence, the system has been reduced to three "evolutionary" equations, namely equations (2a,b) which evolve the horizontal components of the mass flux (or velocity) in time and (11a) which evolves p_e. These are equivalent to the shallow water equations in which the speed $c(\equiv N/k_z)$ replaces $\sqrt{gH}$, as already noted.

The system of equations, (1), (2), (4), and (8), possesses a wave energy equation which follows by taking the scalar product of the momentum equation with $\boldsymbol{q}$ to obtain

$$\frac{\mathrm{D}}{\mathrm{D}t}\left[\frac{1}{2}\left({q_x}^2 + {q_y}^2 + {q_z}^2\right)\right] + U' q_x q_y = -\boldsymbol{q} \cdot \nabla p_e - q_z \rho_e g. \tag{12}$$

The terms on the right-hand side may be written in the form

$$-\boldsymbol{q} \cdot \nabla p_e = -\nabla \cdot (p_e \boldsymbol{q}), \tag{13}$$

on using $\nabla \cdot \boldsymbol{q} = 0$, and

$$-g q_z \rho_e = -\frac{g^2}{N^2}\frac{\mathrm{D}}{\mathrm{D}t}({\rho_e}^2/2), \tag{14}$$

on using (8). Hence (12), after division through by ρ_0, assumes the "conservation form" with "sources"

$$\frac{\mathrm{D}}{\mathrm{D}t}\left[\frac{1}{2}\rho_0 u^2 + \frac{1}{2}\frac{g^2}{N^2}\frac{{\rho_e}^2}{\rho_0}\right] + \boldsymbol{\nabla}\cdot(p_e\boldsymbol{u}) = -p_e u_z\left(\frac{1}{\rho_0}\frac{\mathrm{d}\rho_0}{\mathrm{d}z}\right) - \frac{\mathrm{d}U_x}{\mathrm{d}y}u_x u_y. \tag{15}$$

On the left-hand side, the first term is the rate of change of the energy density consisting of the kinetic energy and the thermobaric potential energy (Eckart 1960), and the second term is the divergence of wave energy flux. The "source" terms on the right-hand side represent wave interaction with the background state through buoyancy (the first term) and shear flow (the second term). The latter term can lead to Kelvin-Helmholtz, baroclinic type, instability, whereas the former can generate convective instability if the atmosphere is unstably stratified, $N^2 < 0$. Here we assume $N^2 > 0$.

3. The latitudinal structure equation

In this section we derive the second-order differential equation for the northward mass flux to which the zonal mass flux and pressure are related through equations (see below). Its hydromagnetic version including magnetic as well as velocity shear has been discussed by Eltayeb and McKenzie (1977) and Mekki and McKenzie (1977). Here, we examine in detail the effects of the wind, through the Doppler shift, on the propagation properties.

For Fourier wave modes of the form

$$(q_x, q_y, p_e) = (Q_x(y), Q_y(y), P_e(y))\exp\left[\mathrm{i}(\omega t - k_x x - k_z z)\right],$$

equations (2a,b) become

$$\mathrm{i}\hat{\omega}Q_x - (f - U')Q_y = \mathrm{i}k_x P_e, \tag{16a}$$

and

$$\mathrm{i}\hat{\omega}Q_y + fQ_x = -\frac{\partial P_e}{\partial y}, \tag{16b}$$

whilst (11a) reduces to

$$P_e = \frac{c^2}{\hat{\omega}}\left(k_x Q_x + \mathrm{i}\frac{\mathrm{d}Q_y}{\mathrm{d}y}\right). \tag{17}$$

Here $\hat{\omega}$ is the Doppler shifted frequency given by

$$\hat{\omega} = \omega - k_x U. \tag{18}$$

Eliminating P_e from equations (16a,b) using (17) yields the coupled system for Q_x and Q_y:

$$(\hat{\omega}^2 - {k_x}^2 c^2)Q_x = \mathrm{i}\left[k_x c^2\frac{\mathrm{d}Q_y}{\mathrm{d}y} - (f - U')\hat{\omega}Q_y\right], \tag{19a}$$

$$\hat{\omega}^2 Q_y + \hat{\omega}\frac{\mathrm{d}}{\mathrm{d}y}\left(\frac{c^2}{\hat{\omega}}\frac{\mathrm{d}Q_y}{\mathrm{d}y}\right) = \mathrm{i}\left[\hat{\omega}k_x c^2\frac{\mathrm{d}}{\mathrm{d}y}\left(\frac{Q_x}{\hat{\omega}}\right) + f\hat{\omega}Q_x\right]. \tag{19b}$$

Elimination of Q_x in (19b), using (19a), gives the second order differential equation for the latitudinal structure of $Q_y(y)$:

$$\frac{\mathrm{d}^2 Q_y}{\mathrm{d}y^2} - \left[\frac{\mathrm{d}}{\mathrm{d}y}\ln\left(\hat{\omega}^2 - c^2 k_x^2\right)\right]\frac{\mathrm{d}Q_y}{\mathrm{d}y} + \kappa^2 Q_y = 0, \tag{20a}$$

$$\kappa^2 \equiv \frac{\hat{\omega}^2 - f\left(f - U^{'}\right)}{c^2} + k_x(f - U')\frac{\mathrm{d}}{\mathrm{d}y}\ln\left(\hat{\omega}^2 - c^2k_x^2\right) - {k_x}^2 - \frac{\left(\beta - U^{''}\right)k_x}{\hat{\omega}}, \quad (20b)$$

in which we have used $\mathrm{d}f/\mathrm{d}y = \beta$, $\mathrm{d}\hat{\omega}/\mathrm{d}y = -k_x U^{'}$. At this stage the latitudinal wave number κ^2 (given by (20b)) describes gravity-inertial waves (the first term of left-hand side of (20b) and Rossby waves (the last two terms) in the presence of a zonal shear (the middle term). Equation (20) yields an invariant (related to the Wronskian) by multiplying it by ${Q_y}^*$, and its complex conjugate form by Q_y, to obtain

$$\mathrm{Im}\left\{\frac{\left({Q_y}^*\mathrm{d}Q_y/\mathrm{d}y - Q_y\mathrm{d}{Q_y}^*/\mathrm{d}y\right)}{\left(\hat{\omega}^2 - {k_x}^2c^2\right)}\right\} = \text{const.} \quad (21)$$

From the viewpoint of wave dynamics this quantity is related to the conservation of wave action except at critical points where it undergoes a discontinuous jump (Booker and Bretherton 1967, Dickinson 1968).

The connection to the classical Rossby wave latitudinal structure equation is obtained in the limit $c \to \infty$ in which (20a) reduces to

$$\frac{\mathrm{d}^2Q_y}{\mathrm{d}y^2} + \left(-{k_x}^2 - \frac{(\beta - U^{''})k_x}{\hat{\omega}}\right)Q_y = 0. \quad (22)$$

In the slowly varying (JWKB) approximation, this yields the local Rossby wave dispersion equation for k_y, namely

$${k_y}^2 + {k_x}^2 = -\beta_e\frac{k_x}{\hat{\omega}}, \quad (23a)$$

where

$$\beta_e \equiv \beta - U^{''} = \frac{\mathrm{d}}{\mathrm{d}y}\left(f - U^{'}\right). \quad (23b)$$

These results follow directly from equations (2a,b), the z component of the curl of which yields

$$\frac{\mathrm{D}}{\mathrm{D}t}\left(\frac{\partial q_y}{\partial x} - \frac{\partial q_x}{\partial y}\right) + \left(\beta - U^{''}\right)q_y = 0, \quad (24)$$

since as $c \to \infty$ we have the 2-D incompressibility equation

$$\frac{\partial q_y}{\partial y} + \frac{\partial q_x}{\partial x} = 0. \quad (25)$$

The operation $\partial/\partial x$ of (24) and the use of 2-D incompressibility condition (25) to eliminate q_x, yield the classical Rossby wave equation (for infinite Rossby radius), namely

$$\frac{\mathrm{D}}{\mathrm{D}t}\left(\frac{\partial^2 q_y}{\partial x^2} + \frac{\partial^2 q_y}{\partial y^2}\right) + (\beta - U^{''})\frac{\partial q_y}{\partial x} = 0. \quad (26)$$

For Fourier wave modes $\propto Q_y(y)\exp\mathrm{i}(\omega t - k_x x)$ this yields (22) for the latitudinal structure, in agreement with the limit obtained from our more general analysis in which $c \neq \infty$.

This last result (26) and (24) essentially express conservation of total (planetary plus zonal shear plus wave) vorticity. At the outset one could choose a derivation with the idea of using conservation of potential vorticity for a shallow layer, which would involve taking the curl of the horizontal components of the equation of motion (to give $(\nabla \times \boldsymbol{u})_z$), but this would still be coupled to an equation for the horizontal divergence, and together with suitable approximations as given above, would lead to the Potential-Vorticity equation (Rhines 2003).

4. Radiation pattern in a wind

In this section, the radiation pattern generated by a time harmonic spatially compact source in a uniform wind is analyzed. This is equivalent to calculating wave generation by traveling forcing effects (Lighthill 1960). The effects of the frequency Doppler shift play an important role in wave propagation in a moving medium. This is revealed through the geometry of the wave number curves in the laboratory frame, which in turn determine the radiation pattern using the method of stationary phase. For uniform winds, $\boldsymbol{U}$, the local dispersion equation is given by (20b), which, with derivatives of $\boldsymbol{U}$ put to zero and $\hat{\omega} \ll f$, simplifies to

$$k_y^2 + k_x^2 + f^2/c^2 = -\frac{\beta k_x}{\omega - \boldsymbol{k}\cdot\boldsymbol{U}}. \tag{27}$$

The quantity $\hat{\omega} = \omega - \boldsymbol{k}\cdot\boldsymbol{U}$ is sometimes referred to as the "intrinsic" frequency (Bretherton and Garrett 1968, Dickinson 1968, Lighthill 1978), and where it is zero the wave is said to exhibit critical level behavior (Booker and Bretherton 1967). At such a level the wave action undergoes a discontinuous jump.

4.1. *Method of stationary phase*

Asymptotic approximations to Fourier integrals, representing the solution of linear wave problems, can be evaluated by the method of stationary phase (for a detailed account, see for example, Lighthill's classical book "Waves in Fluids" 1978, p. 351–361). In the far, or radiation, field the dominant contribution to a Fourier integral, representing the solution of the problem, comes from those portions of the rapidly oscillating phase which are stationary with respect to the component of the wave number over which the integration is being carried out. For example, in the case of a two-dimensional problem such as on a β-plane, the phase $\Phi(\boldsymbol{x}, \boldsymbol{k})$ may be written, in Cartesian co-ordinates, in the form

$$\Phi = \omega t - k_x x - k_y y, \tag{28}$$

in which ω is the (given) angular frequency of the source, and $\boldsymbol{k} = (k_x, k_y)$ is the two-dimensional wave number vector. These quantities are related through a dispersion relation (for example (27) above) arising from the Fourier image of the wave operator which appears as a simple pole, thus through the calculus of residues, reducing the two-dimensional Fourier integral to a single integral over either (k_x, k_y) space (using the residue theorem), and is given by some relation

$$D(\omega - \boldsymbol{k}\cdot\boldsymbol{U}, k_x, k_y) = 0. \tag{29}$$

Here D is an algebraic function representing the Fourier image of the wave operator in which the Doppler shifted frequency $\hat{\omega} = \omega - \boldsymbol{k}\cdot\boldsymbol{U}$ arises from winds or flows of velocity $\boldsymbol{U}$ relative to the laboratory frame. This relation can be written in the polar form

$$D(\omega - kU\cos(\theta - \alpha), k, \theta) = 0 \tag{30}$$

in which $\boldsymbol{k} = k(\cos\theta, \sin\theta)$, $\boldsymbol{U} = U(\cos\alpha, \sin\alpha)$, and may have solutions

$$k(\theta) = k_i(\theta, \omega, \alpha, U), \tag{31}$$

where $i = 1, 2, \ldots, n$ represents the possible n roots of the dispersion equation representing different modes of propagation. We refer to the solutions $k_i(\theta)$ as the polar form of the wave

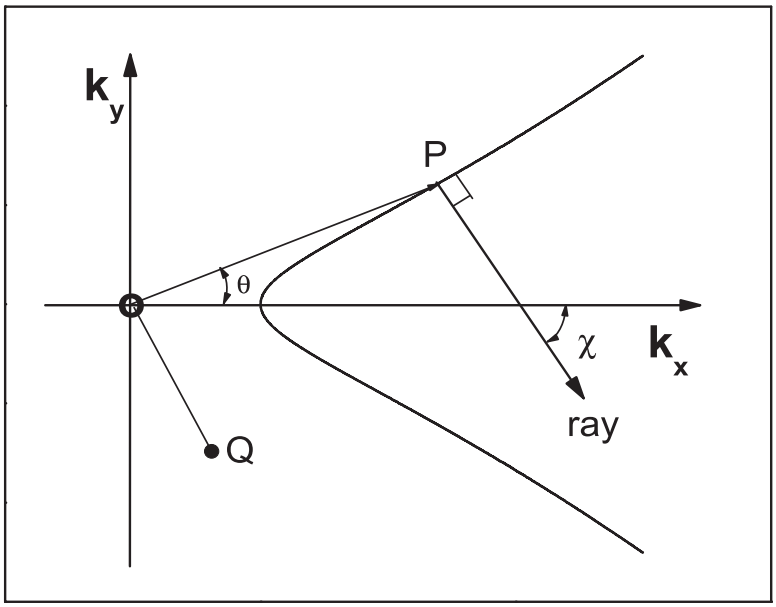

Figure 1. The geometrical interpretation of the reciprocal polar of the wave number curve. The example shown is actually appropriate to the wave number $k(\theta)$ for stationary waves on deep water ($k(\theta) \sim 1/\cos^2\theta$) generated by a uniformly moving source (ship).

number diagrams at given values of (ω, α, U) in the laboratory frame. Writing the space coordinates (x, y) in polar form $r(\cos\chi, \sin\chi)$, the phase given by (28) of the ith mode may be written

$$\Phi_i = r(\chi)k_i(\theta)\cos(\theta - \chi), \tag{32}$$

where we now regard θ, the wave number angle, as the variable over which the Fourier integral is taken. For large r (i.e. the far field) the phase Φ_i is stationary with respect to θ if

$$\frac{\partial \Phi_i}{\partial \theta} = 0, \tag{33}$$

which implies

$$\frac{k_i'(\theta)}{k_i(\theta)} = \tan(\theta - \chi), \tag{34}$$

or

$$\tan\chi = \frac{\tan\theta - (k'/k)_i}{1 + \tan\theta(k'/k)_i} = -\frac{1}{\partial k_y/\partial k_x}, \tag{35}$$

which defines the ray direction χ in terms of θ.

The radiation pattern is given by (32) which for a given phase Φ_i may be written as

$$r(\chi) = \frac{\Phi_i}{k_i(\theta)\cos(\theta - \chi)}, \tag{36}$$

in which θ may be regarded as a generating parameter for χ through (34), which shows that the ray direction χ is perpendicular to the wave number diagram at a given θ. The curve given by (36) is therefore the reciprocal polar of the wave number curve and lends itself to the geometrical interpretation shown in figure 1 in which OP represents the wave number vector and OQ is the radius vector of the reciprocal polar to the curve (see also Lighthill 1978, p. 372-373).

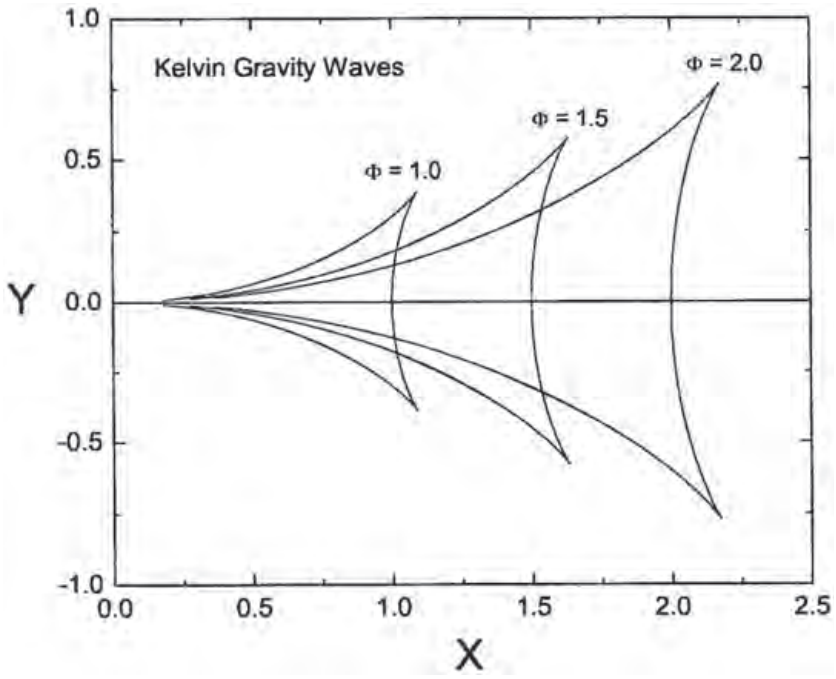

Figure 2. The family of deltoids (reciprocal polars) for the classic ship wave pattern. The semi-angle of the Kelvin wedge is $\sin^{-1}(1/3) \sim 19.5°$) and arises from the point of inflection of the wave number curve.

This particular figure is, in fact, appropriate to the stationary wave number diagram for surface gravity waves generated by a uniformly moving source, and gives rise to the deltoid shape characteristic of the classic ship wave pattern exhibiting a Kelvin-wedge cusp associated with the point of inflection of the wave number curve (as shown in figure 2).

4.2. *Rossby radiation pattern in a zonal wind*

Here, we extend the work of McKenzie (under review) on the radiation pattern of Rossby waves to include the effects of winds or flows. In the case of a constant zonal flow $U\hat{\boldsymbol{x}}$ the Rossby wave dispersion relation (27) becomes

$$k^2 + f^2/c^2 = \frac{-\beta k \cos\theta}{(\omega - Uk\cos\theta)}, \tag{37}$$

which is a cubic for $k(\theta)$. In the classic case of $f^2/c^2 = 0$ (corresponding to infinite Rossby radius) this equation reduces to a quadratic with solutions

$$k_{\pm}(\theta) = \frac{\omega}{2U\cos\theta}\left(1 \pm \sqrt{1 + 4M_r\cos^2\theta}\right), \qquad M_r \equiv \beta U/\omega^2. \tag{38a,b}$$

M_r is a "Rossby" Mach number measuring the flow speed in units of the speed ω^2/β characteristic of the Rossby zonal wave speed. At mid-latitudes this speed ranges from $80\,\mathrm{ms}^{-1}$ for two day wave periods to $20\,\mathrm{ms}^{-1}$ for four day periods. Therefore, M_r may take a wide range of values from the very small to of the order of or greater than unity depending upon the wind speed and the wave period.

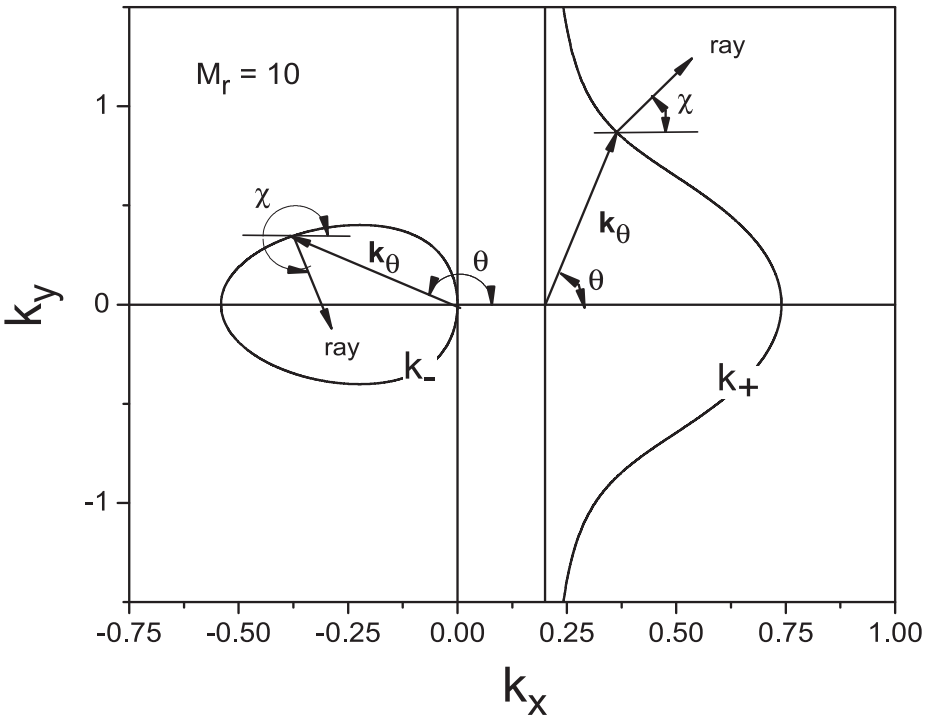

Figure 3. The wave number curves $k_{\pm}(\theta)$ for Rossby waves in a westerly zonal wind ($U > 0$), illustrating the relation between the ray direction χ and the wave number angle θ for each curve.

4.2.1. *Westerly wind*

In the case of a westerly wind ($U > 0$, $M_r = 10$), the wave number curves given by (38a) are shown in figure 3.

The $k_{-}(\theta)$ is the closed ovoid-like curve lying in $k_x < 0$ (corresponding to westward phase propagation) modified slightly by the flow so that it extends to $k_x = k_{-}(\theta = \pi)$ rather than $-\beta/\omega$, whereas the $k_{+}(\theta)$ is a new mode arising from the zonal flow, consisting of the line $k_x = \omega/U$ with the forward facing indentation at $k_x = k_{+}(\theta = 0)$.

The relation between the ray angle χ and the wave number angle θ follows from (35) in which we use (38a) for $k(\theta)$ yielding

$$k'(\theta) = \frac{\omega}{2U}\frac{\sin\theta}{\cos^2\theta}\,(A \pm 1)\,, \tag{39}$$

and hence

$$\tan\chi = \frac{t\,(1 \mp 1/A)}{\left(1 \pm t^2/A\right)}, \qquad t \equiv \tan\theta \tag{40a,b}$$

with

$$A = \sqrt{1 + 4M_r\cos^2\theta}\,. \tag{40c}$$

The variation of χ for $k_{\pm}(\theta)$ wave number curves at $M_r > 1$ are shown in figures 4(a),(b). The $k_{\pm}(\theta)$ curves for various M_r are shown in figure 5.

The radiation pattern for the closed Rossby wave normal diagram $k_{-}(\theta)$ yields a family of parabolic like curves as shown in figure 6(a) for the case $M_r = 10$. These are similar to the case of no flow (Rhines 2003, McKenzie under review), which consists of two families of hyperbolas, these being the reciprocal polars of the Longuet-Higgins offset circle. On the other

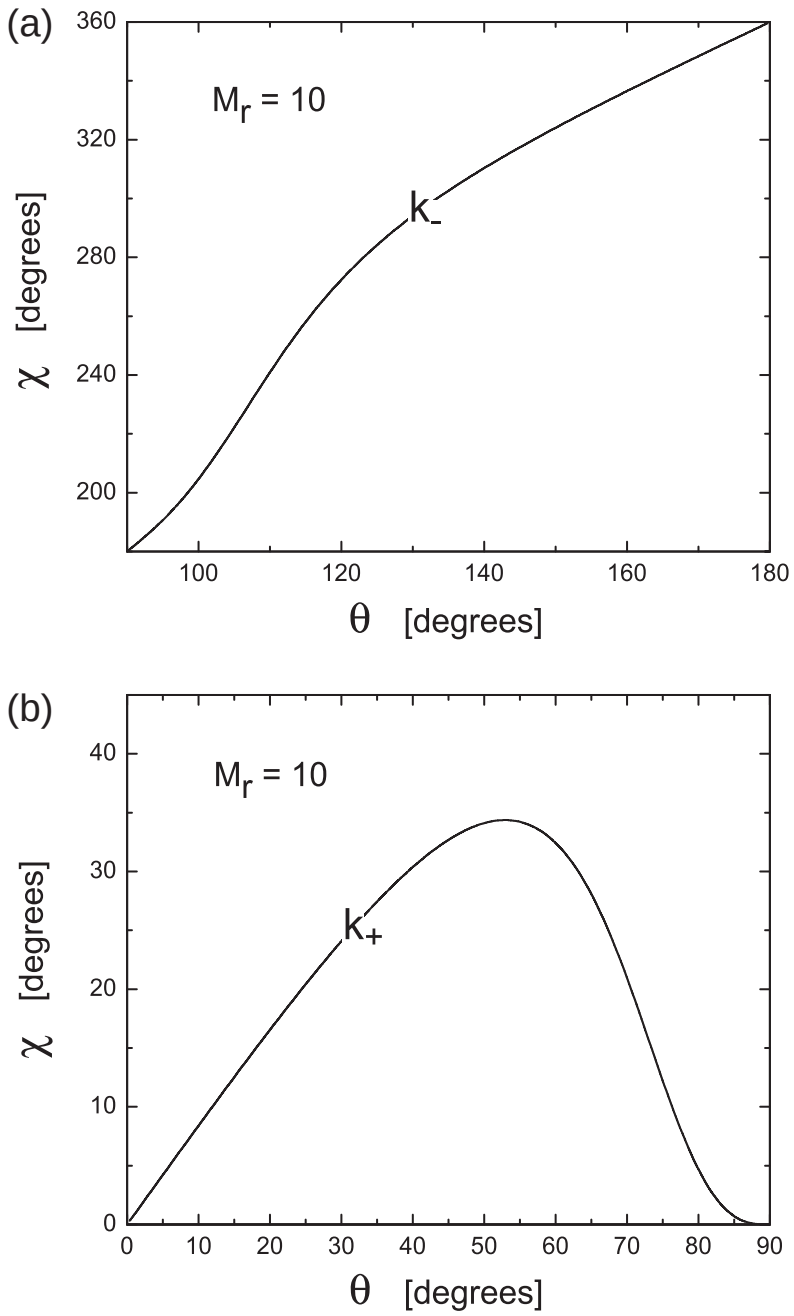

Figure 4. (a) The (χ, θ) curve for the $k_+(\theta)$. The maximum deviation (χ_m) of the ray from the east arises from the point of inflection in the $k_+(\theta)$. Note $\exists$ two values of θ for any given $\chi(<\chi_m)$. (b) The (χ, θ) curve for the $k_-(\theta)$ wave number curve.

hand the reciprocal polar of the westward branch $(k_+(\theta))$, namely the "indented line", yields the radiation pattern as the family of deltoid-like curves shown in figure 6(b) for $M_r = 10$.

These curves resemble a "reverse" ship wave with the disturbance confined to a Kelvin-like wedge angle which is given by the ray direction at the point of inflection of the $k_+(\theta)$ in figure 3. To a good approximation this critical wedge-angle χ_I is given by

$$\tan \chi_I = \left(\frac{3}{4}\right)^{3/2} \frac{\left(\sqrt{1+4M_r}-1\right)}{2}, \tag{41}$$

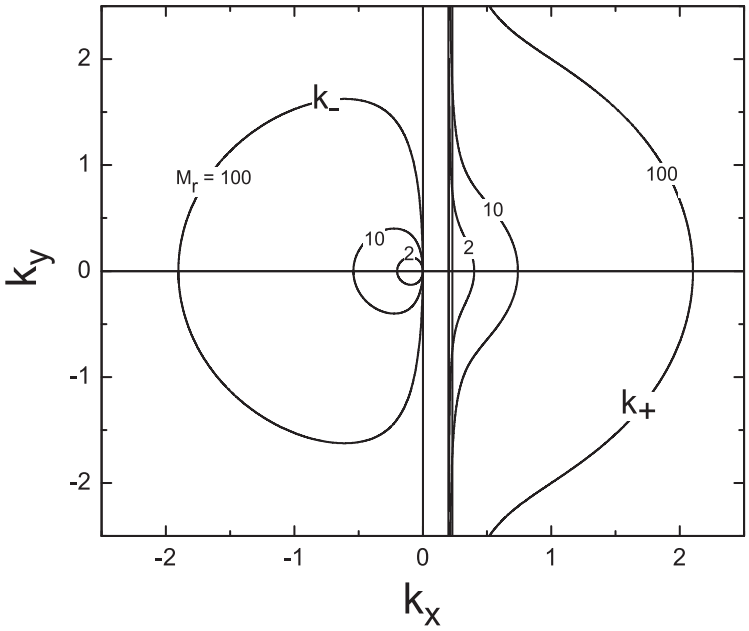

Figure 5. The $k_{+,-}(\theta)$ wave number curves for various values of M_r.

which shows that $\chi_I \to 0$ as $M_r \to 0$, $\chi_\pm \simeq 22°$ for $M_r = 1$, and $\chi_- \to 90°$ as $M_r \to \infty$. The "reversed" ship wave pattern (figure 6(b) arises from the shape of the $k_+(\theta)$ (figure 3) exhibiting the indentation to the right (i.e. $k(\theta)\cos\theta$ increases with θ).

4.2.2. *Easterly wind*

For $U < 0$ the wave number curves, for various values of $M_r < 0$ are shown in figure 7.

The open branch with the asymptote $k_x = \omega/U$ and the indentation at $k_x = k_+(\theta = \pi)$ now lie entirely westward ($k_x < 0$). We note that as $M_r \to -1/4$ the open and closed branches coalesce and for $|M_r| > 1/4$ are joined as shown in figure 7 for $M_r = -0.3$ and -0.275. The associated radiation patterns are shown in figures 8 and 9.

In figure 8, we observe that the family of deltoids lie entirely to the west (in the direction of the wind) and, in contrast to the case of a westerly, the deltoids face the same way as would a Kelvin ship wave. This is because in the corresponding wave number curves (labeled $M_r = -0.225$), the line with the indentation lies to the right of the asymptote (i.e. to the west). In the latter, the deltoid "interacts" with the parabolic-like curves.

4.2.3. *Stationary wave*

For the case of stationary waves in the laboratory frame, in which we let $\omega = 0$ and consider the case $f^2/c^2 \neq 0$ so that equation (37) becomes

$$k^2 = (\beta/U) - (f^2/c^2), \qquad k_x = 0. \tag{42a,b}$$

Hence, the wave normal diagram becomes a circle of radius $\sqrt{(\beta/U) - (f^2/c^2)}$ if U is westerly and less than $\beta c^2/f^2$, which is the long wavelength zonal phase speed of the Rossby wave, but is otherwise evanescent when $U < 0$. However, the line $k_x = 0$ is also part of the wave number diagram, whose complete form is shown in figure 10(a).

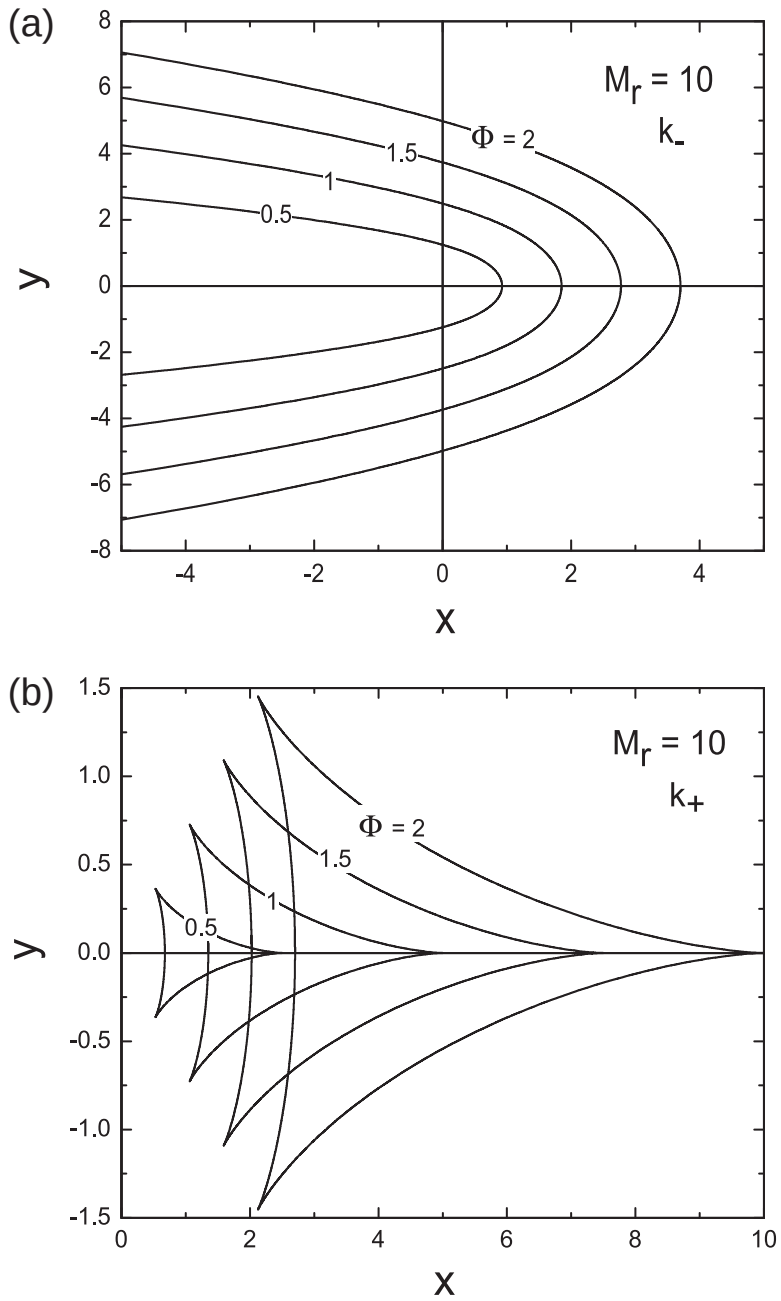

Figure 6. (a) The radiation pattern corresponding to the $k_-(\theta)$ wave normal is a family of parabolic-like curves, which is reminiscent of the capillary waves generated by an object in a stream. (b) The radiation pattern (family of reciprocal polars- deltoids) for the $k_+(\theta)$ wave number for $M_r = 10$. The pattern looks like an "reversed" ship wave pattern. The cusps result from the point of inflection in the $k_+(\theta)$ curve and confine the pattern to a semi-wedge angle χ_m.

The direction of the arrows (rays) are obtained from the limiting form of the general wave normal diagram as $\omega \to 0$ ($M_r \to \infty$) as shown in figure 5. This case is similar to the two-dimensional internal gravity wave pattern generated in a horizontal flow (Lighthill 1978 p. 415, 416 figures 108(a),(b)). The reciprocal polar is shown in figure 10(b) and consists of the semi-circle (taken twice), the double line $k_y = 0$ (for $k_x >$ radius of circle) and the two lines extending westwards.

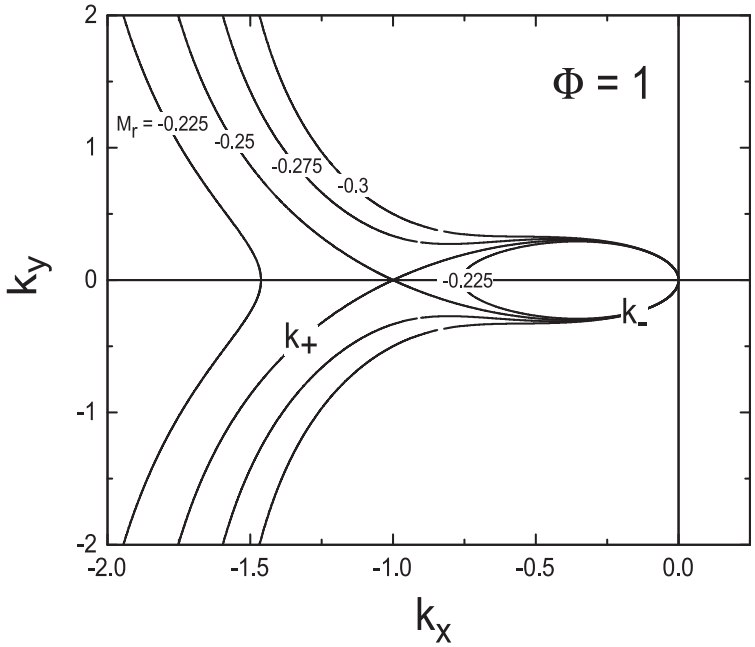

Figure 7. The $k_{+,-}(\theta)$ curves in an easterly wind ($U < 0$) for various values of M_r. For $|M_r| > 1/4$ the curves coalesce as shown.

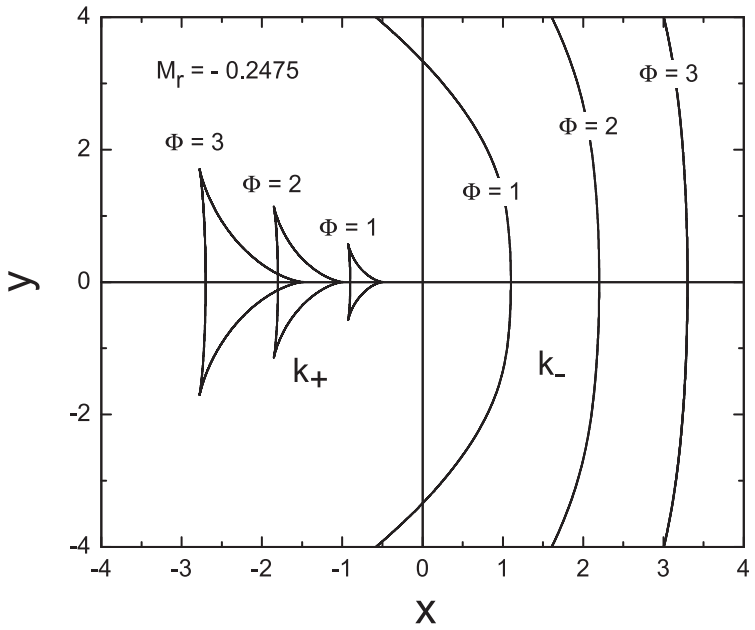

Figure 8. The corresponding radiation pattern for $|M_r| < 1/4$. The deltoids lying entirely to the west correspond to the open branch (plane with an indented line), whereas the parabolic like curves are associated with the closed ovoid, and lie both ahead (east) and behind (west).

4.3. *Radiation patterns in a meridional wind*

In the case of a constant meridional wind/flow, $U\hat{\boldsymbol{y}}$, the Rossby wave dispersion relation (27) becomes

$$k^2 + f^2/c^2 = -\frac{\beta k \cos\theta}{\omega - kU\sin\theta}. \tag{43}$$

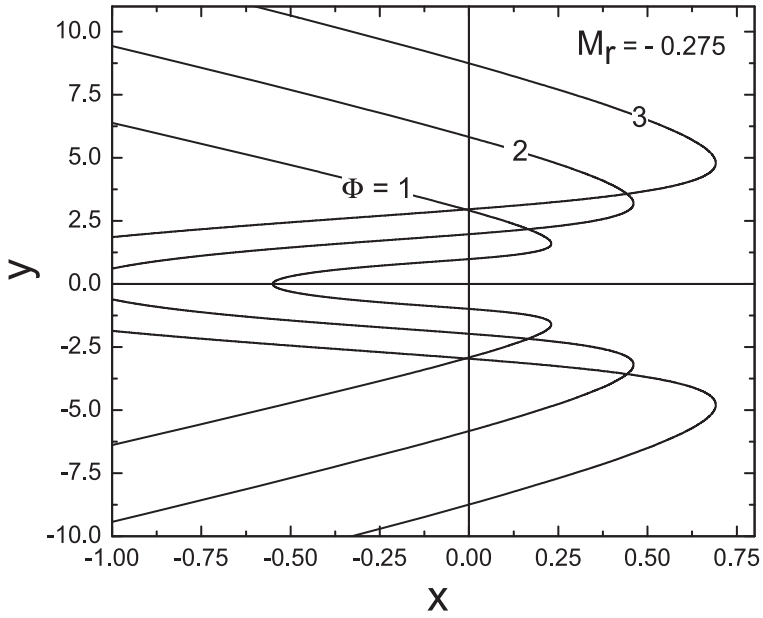

Figure 9. The radiation pattern, for $|M_r| > 1/4$ and various Φ, which involves an "interaction" between the deltoids and paraboloids.

We consider the classic case $c \to \infty$ (but return to c finite in the case of stationary waves, given at the end of this section). Equation (43) becomes a quadratic for $k(\theta)$ with solutions (after factoring out $k = 0$)

$$k_\pm = \frac{\omega}{2U \sin\theta}\left(1 \pm \sqrt{1 + 4M_r \sin\theta \cos\theta}\right). \tag{44}$$

The $k_+(\theta)$ and $k_-(\theta)$ wave number curves for various M_r are shown in figure 11. Note that for $(M_r > 1/2)$ the open and closed curves (for k_+ and k_-, respectively) coalesce.

The radiation patterns (reciprocal polars) are calculated using equations (36) with (35) and the wave number curves $k_\pm(\theta)$ given by (44). We obtain from (35) and (44) the relation between the ray angle χ and the wave number angle θ:

$$\tan\chi = \tan\theta\left(1 \pm \frac{B}{A\tan^2\theta}\right)\Big/\left(1 \mp \frac{B}{\tan^2\theta}\right) \tag{45a}$$

with

$$A \equiv \sqrt{1 + 2M_r \sin 2\theta}, \qquad B \equiv (1 + 2M_r \tan\theta)/(1 \pm A)\,. \tag{45b,c}$$

The corresponding radiation patterns for $M_r \le 0.5$ are shown in figure 12 (for $k_+(\theta)$) and figure 13 (for $k_-(\theta)$). The cusps in the radiation pattern shown in figure 12 arise from the points of inflection in the wave number curve $k_+(\theta)$ for $M_r = 0.4$.

In the case of $M_r > 1/2$, the open and closed curves "interact", or coalesce, as already noted and illustrated in figure 11. The reciprocal polars for $M_r = 0.45$, 0.5, and 0.55 are shown in figure 14. In this case, the $k(\theta)$ curve given by (44) is complex in the angular range $\theta_- > \theta > \theta_+$, where

$$\sin\theta_\pm = \sqrt{\frac{1 \pm \sqrt{1 - (1/4)M_r^2}}{2}}. \tag{46}$$

The angles $\theta_{+,-}$ lie in the second quadrant.

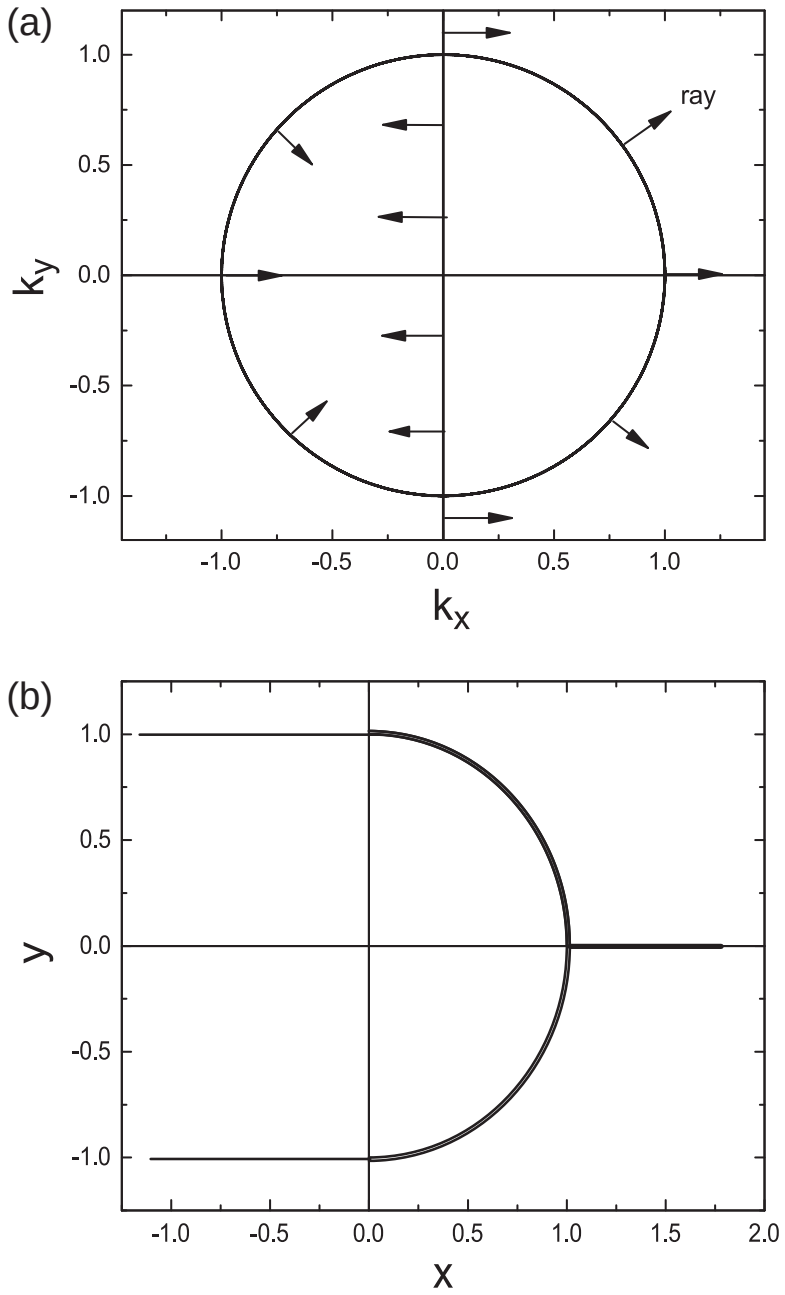

Figure 10. (a) The stationary wave number in a westerly wind. The arrows indicate the ray directions which can be deduced from figure 6 for the case of $M_r = 100$ (ω small). (b) The corresponding reciprocal polar.

In the case of stationary waves ($\omega = 0$), the dispersion equation becomes

$$k^2 = \frac{\beta}{U}\cot\theta - \frac{f^2}{c^2} = \frac{\beta}{U}\left(\cot\theta - \cot\theta_c\right), \tag{47}$$

where

$$\cot\theta_c = \frac{U}{\beta}\frac{c^2}{f^2}. \tag{48}$$

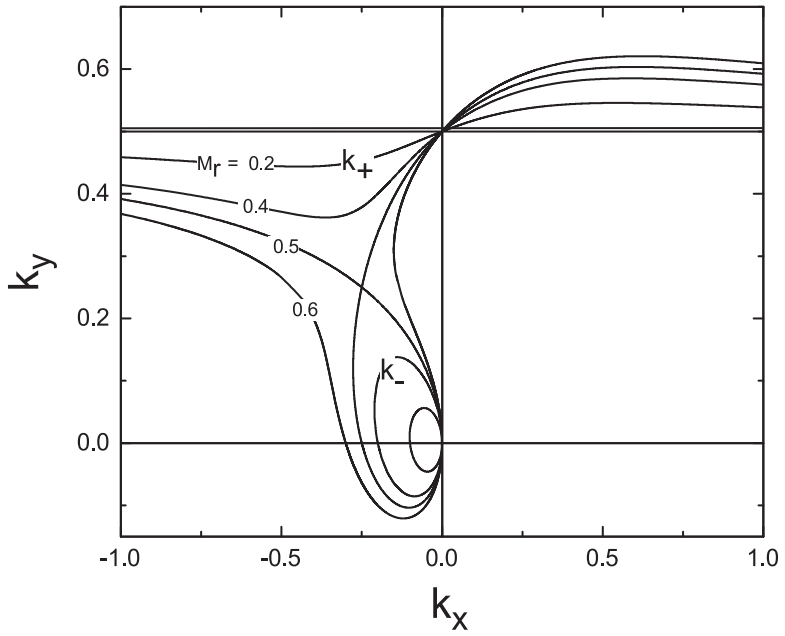

Figure 11. The wave number curves $k_+(\theta)$ and $k_-(\theta)$ in a meridional wind for various values of M_r. The curves coalesce for $M_r \geq 1/2$.

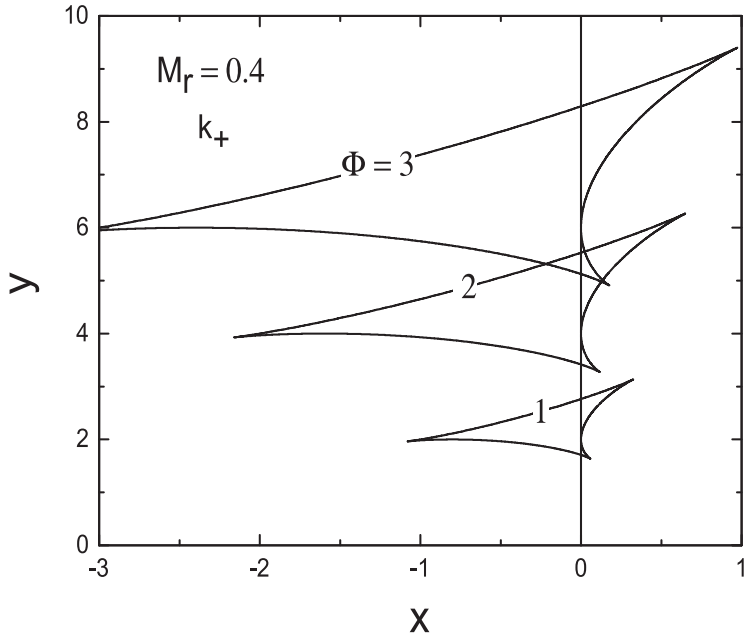

Figure 12. The radiation pattern for the wave number $k_+(\theta)$ for various Φ with $M_r = 0.4$.

cot θ_c is therefore another Rossby "Mach" number where the flow speed is measured in units of the long wavelength Rossby speed which, at mid-latitudes, takes values from about 120 ms^{-1} in an ocean of depth 4 km to around 200 ms^{-1} in the atmosphere.

The wave number diagrams and their associated reciprocal polars are shown, respectively, in figures 15 and 16 for various values of θ_c. The radiation patterns for various Φ are shown in figure 17 for the case $\theta_c = 90°$.

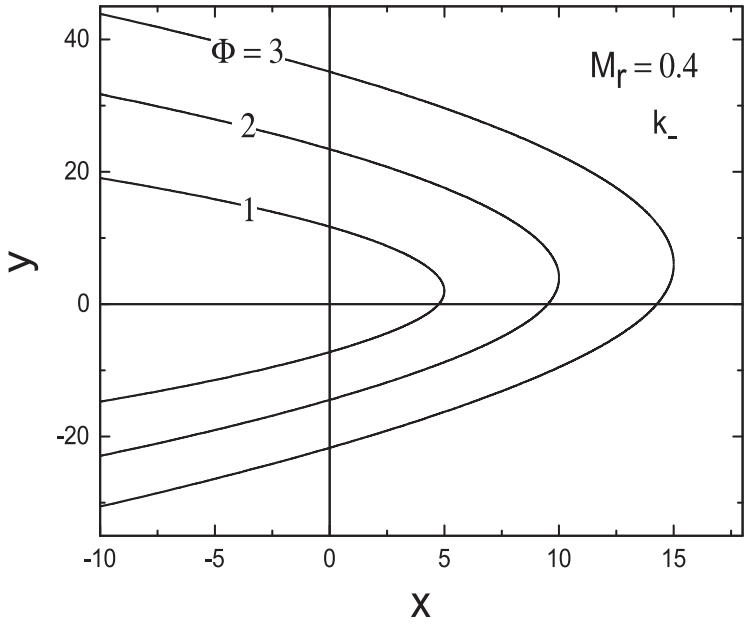

Figure 13. The radiation pattern for $k_{-}(\theta)$ wave number for various Φ at $M_r = 0.4$, exhibiting the parabolic-type curves similar to capillary waves.

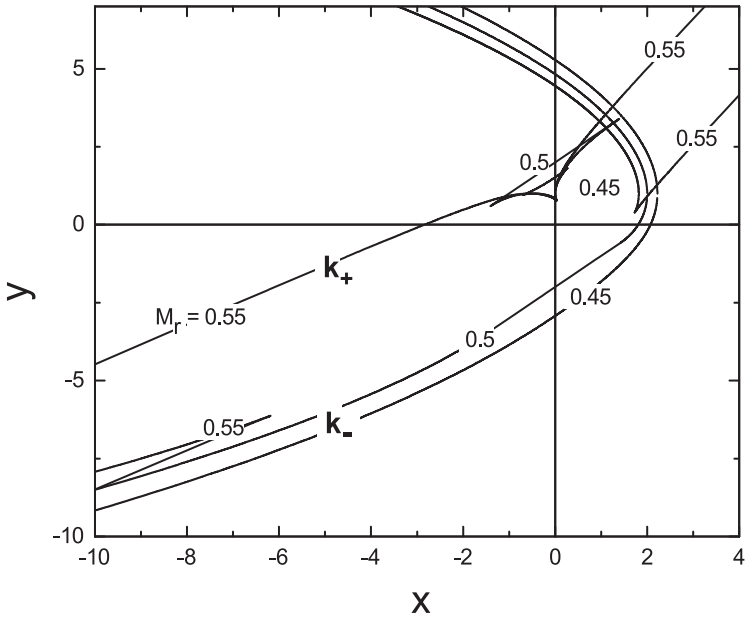

Figure 14. Reciprocal polar curves for the wave number curves for a meridional wind (as shown in figure 11) for $M_r = 0.45$, 0.5, and 0.55. Note the two "Mach"-like lines, which appear for $M_r = 0.55$ on the k-curve, and which are associated, in the wave number curves of figure 11, with the asymptote tangent lines drawn from k_x, k_y origin to the two points where the rays are normal to the wave number curve.

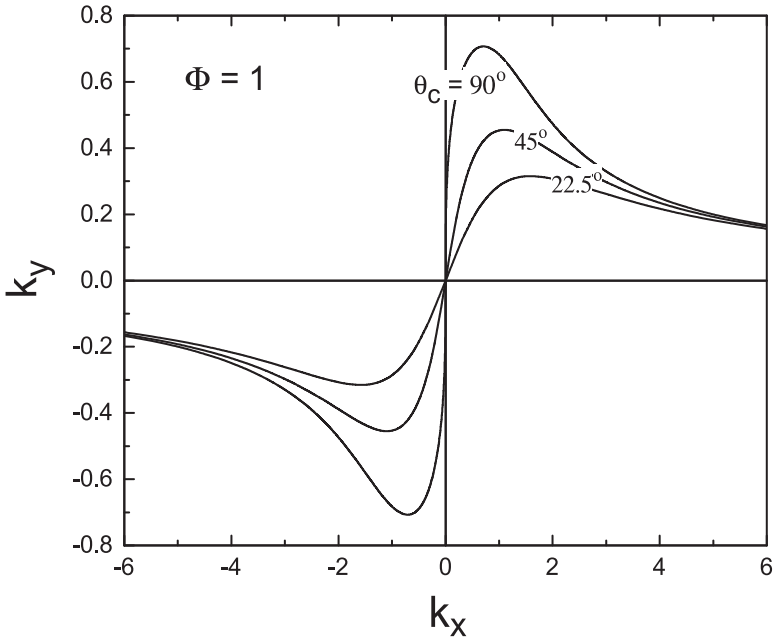

Figure 15. Stationary wave number curve in meridional wind for various θ_c.

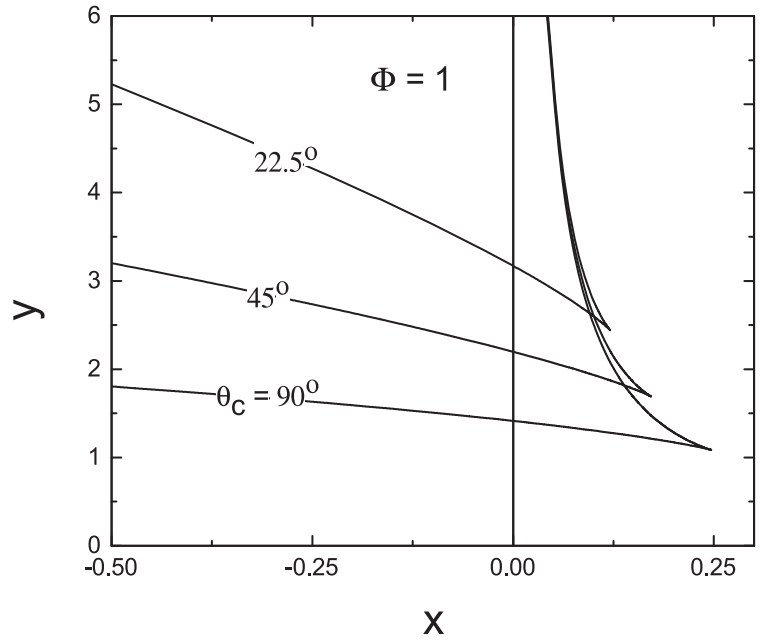

Figure 16. Reciprocal polar curve corresponding to stationary wave normal forms (taken twice) for a meridional wind (figure 15).

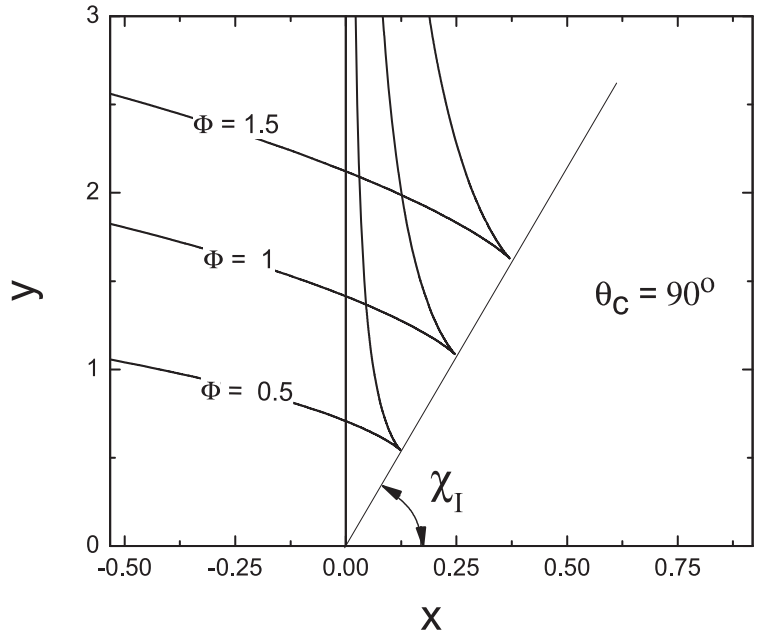

Figure 17. The stationary radiation pattern in a meridional wind.

5. Summary

For Fourier type zonal plane wave modes, we derive a second-order differential equation describing the latitudinal structure of Rossby type wave perturbations on a β-plane in zonal (and meridional) winds.

We have followed Lighthill (1978) to show how the local dispersion equation, when interpreted as a wave number diagram in $\boldsymbol{k}$ space at a given frequency ω, can be used to construct the radiation pattern generated by a time harmonic compact source in a laboratory frame relative to which zonal and meridional winds flow/blow. The effect of the Doppler shift in frequency, due to the mean flow, on the wave number curve (the Longuet-Higgins offset circle in the rest frame) is quite dramatic and is highlighted by a series of figures 3–8. The most important effect is the appearance of a new branch in $\boldsymbol{k}$-space caused by the background wind consisting of a blocking line with an indentation. In the case of a zonal wind, the new branch consists essentially of the line $(k_x = \omega/U)$ with the indentation facing to the right. In the case of a westerly flow, the radiation pattern associated with this branch is a family of deltoids which resemble a reverse ship wave pattern (see figure 6(b)). On the other hand, the radiation pattern associated with the distorted Longuet-Higgins circle is a family of parabolic-like curves rather similar to the wind-free case (e.g. see figure 6(a)). In the case of a westward wind (an easterly flow), the radiation pattern is shown in figure 8 with the family of deltoids lying entirely to the west and embedded in the parabolic like patterns associated with the closed wave number curve. However, if $|M_r| > 1/4$ an interaction between the deltoids and the parabolic curves as depicted in figure 9 arises. The case of a meridional wind is slightly more complicated but again these diagrams (figures 11–17) depict the diversity of the radiation patterns. In the case of stationary waves in the laboratory frame, we obtain the interesting figures 12 and 14 for the zonal and meridional cases, respectively. The new results here have the wave number curves in zonal and meridional flows and their reciprocal polars which provide the various Rossby

radiation patterns. These provide the Rossby wave problem equivalent to the classic ship wave problem (involving both gravity and capillary waves) and internal gravity waves in a wind.

Acknowledgements

The authors wish to thank the National Research Foundation of South Africa and TBD (Under NRF grant number: 2053776) for support and express a heartfelt appreciation for the most useful and constructive work of the anonymous reviewers toward the finalization of this paper.

References

Booker, J.R. and Bretherton, F.P., The critical layer for internal gravity waves in a shear flow. *J. Fluid Mech.* 1967, **27**, 513–539.

Bretherton, F.P. and Garrett, C.J.R., Wave trains in inhomogeneous moving media. *Proc. R. Soc. Lond. A* 1968, **302**, 529–554.

Dickinson, R.E., Planetary Rossby waves propagating vertically through weak westerly wind wave guides. *J. Atmos. Sci.* 1968, **25**, 984–1002.

Doyle, T.B. and McKenzie, J.F., Stationary wave patterns in deep water. *Quest. Math.* 2013, **36**, 1–14.

Duba, C.T. and McKenzie, J.F., Propagation properties of Rossby waves for latitudinal β-plane variations of f and zonal variations of the shallow water speed. *Ann. Geophys.* 2012, **30**, 1–7.

Eckart, C., *Hydrodynamics of Oceans and Atmospheres*, 1960 (Cambridge: Pergamon Press).

Eltayeb, A. and McKenzie, J.F., Propagation of hydromagnetic planetary waves on a beta-plane through magnetic and velocity shear. *J. Fluid Mech.* 1977, **81**, 1–12.

Gerkema, T., Maas, L.R.M. and van Haren, H., A note on the role of mean flows in Doppler-shifted frequencies. *J. Phys. Oceanogr.* 2013, **43**, 432–441.

Gill, A.E., *Atmosphere and Ocean Dynamics*, 1982 (London: Academic Press).

Lighthill, J., Studies on magneto-hydrodynamical waves and their anisotropic wave motions. *Proc. R. Soc. Lond. A* 1960, **252**, 397–430.

Lighthill, J., *Waves in Fluids*, 1978 (Cambridge: Cambridge University Press).

Longuet-Higgins, M.S., Planetary waves on a rotating sphere. *Proc. R. Soc. Lond. A* 1964, **279**, 446–473.

McKenzie, J.F., The group velocity and radiation patterns of Rossby waves. Sub judice 2013.

Mekki, O.M. and McKenzie, J.F., The propagation of atmospheric Rossby-gravity waves in latitudinally sheared zonal flows. *Phil. Trans. R. Soc. Lond. A* 1977, **287**, 115–143.

Pedlosky, J., *Geophysical Fluid Dynamics*, 1987 (New York: Springer-Verlag).

Ratcliffe, C., *An Introduction to the Ionosphere and Magnetosphere*, 1972 (Cambridge: Cambridge University Press).

Rhines, P.B., Rossby waves. In *Encyclopaedia of Atmospheric Sciences*, edited by J.R. Holton, J.A. Curry and J.A. Pyle, pp. 1–37, 2003 (Academic Press: Oxford).

Vallis, G., *Atmospheric and Oceanic Fluid Dynamics: Fundamentals and Large-scale Circulation*, 2006 (Cambridge: Cambridge University Press).

4.1 Addendum

This small section here attempts to give an interpretation of the results in the previous paper using the JWKB method.

JWKB Solutions and Ray paths in wind shear

A qualitative idea of the wave behaviour in a wind shear is revealed through the JWKB approximation, in which the variations over a wavelength are assumed small, so that to "zeroth" order, equation (22) possesses approximate solutions of the form

$$\Delta Q_y(y) \sim \frac{1}{{k_y}^{1/2}} \exp\left(\pm i \int^y k_y(y^{'})\, dy^{'}\right), \tag{4.1}$$

where, in the low frequency approximation $\omega^{'} \ll f$, the local wave number k_y is given by equation (23a)

$${k_y}^2 = -f^2/c^2 - {k_x}^2 - \beta_e k_x/\omega^{'}. \tag{4.2}$$

This is the mid-latitude Rossby wave dispersion equation with the effect of the wind shear included through the Doppler shifted frequency $\omega^{'} = \omega - k_x U$. As we have seen in the paper, Duba *et al.* (2014), this Doppler shift has a profound effect on the geometry of the local wave normal curves in (k_y, k_x) space. The effect of the zonal wind on the wave normal diagram has already been described in the previous paper and is shown in figure 7 (for westerly $U > 0$), and figure 3 (for an easterly, $U < 0$).

We will analyze the ray paths in both westerly and easterly jets, using the geometry of the wave normal curves. The ray direction χ, drawn normal to the wave normal curve is given by equation (35) which may be written as

$$\tan\chi = \frac{dy}{dx} = -\frac{1}{\partial k_y/\partial k_x}, \tag{4.3}$$

in which

$$k_y^2 = \frac{k_x\,(k_x - k_+)\,(k_x - k_-) - (f^2/c^2)\,(\omega/U - k_x)}{(\omega/U - k_x)}, \tag{4.4a}$$

$$k_{+,-} = \frac{\omega}{2U}\left(1 \pm \sqrt{1 + 4\beta U/\omega^2}\right). \tag{4.4b}$$

As we have already noted equation (18) lends itself to the geometric interpretation that

the ray direction is perpendicular to the wave normal curve at any given wave normal angle θ. Thus a ray path in a zonal wind shear $U_x(y)$ may be determined by constructing the wave normal curves in (k_y, k_x) space at successive latitudes and following the direction of the arrows (direction of the ray) drawn normal to the wave normal curve where it is intersected by a line k_x = constant at each latitude. Note that in the course of the ray trajectory ω and k_x are conserved whilst k_y changes according to the local dispersion equation as a result of the Doppler shift introduced by the wind shear $U_x(y)$. This elegant construction has been used to examine ray paths, for example, by Lighthill (1967) in the case of travelling forcing effects and and others, for example, Mekki and McKenzie (1977) for Rossby waves. Here we reproduce and correct the latter's conclusions which supplement some related and recent work on Rossby ray paths.

First, however, we briefly discuss the reflection and critical level points associated with the differential equation (20a) or its reduced form equation (22). A point denoted by y_r, at which the local wave number k_y goes to zero corresponds to a reflection point. The differential equation approximates to the classical Airy form (e.g., Lighthill, 1978, p.385) which describes incident and reflected waves on one side (say $y < y_r$), accompanied by an evanescent disturbance on the other side. On the other hand a "resonance" arises at points where $k_y \to \infty$. This occurs where the Doppler shifted frequency goes to zero, or equivalently where the zonal phase speed equals the local zonal flow speed, and this is called a critical level (Booker and Bretherton (1967) (for the case of gravity waves in a wind shear), and Dickinson (1968) for Rossby waves). At such a critical level the wave (in linear theory) is neither reflected nor transmitted but is absorbed, with the wave action undergoing a discontinuous jump, and therefore the JWKB approximation breaks down. In fact, the nonlinear evolution near such a level is more complicated in which it can evolve from an absorber, to a reflector and back to an over-reflector (see Killworth and McIntyre (1985) and references therein for a detailed discussion).

Lighthill's construction for the ray path in a jet stream is shown in figure 4.1, and by joining together the arrows (at different latitudes) for given values of ω and k_x we obtain the various types of ray paths shown in figure 4.1 (b), figure 4.2 (c) and (d). For example the ray path labelled 1 is reflected before reaching the centre of the jet and is eventually captured at a critical latitude in the west. The ray paths 3, 4, 5 and 6 correspond to westward phase propagation ($k_x < 0$), with paths 3 and 4 being reflected before reaching the jet centre, whereas those labelled 5 and 6 penetrate through the jet. Similarly, we can construct the various ray paths for an easterly jet stream as shown in figure 4.3 with the corresponding ray paths shown in figures 4.4 b, c d, e, and f. Rays labelled 3 (figure 4.4 c and 4.3 are trapped in a waveguide type path around the jet centre. The rays

labelled 4 and 5 (figure 4.4 d exhibit critical latitude behaviour in which that latitude acts as an absorber, whereas the rays labelled $1'$ and $2'$ (figure 4.4 e) the critical latitude appears as an emitter, in the sense that rays emerge from the critical latitude, rather than asymptotic approach. These results supplement the original work of Yagamata (1976) and more recent work by Lu and Boyd (2008), Shaman *et al.* (2012), Karoly and Hoskins (1982), and Farrell and Watterson (1985). El Mekke (1980) in his work on hydromagnetic planetary waves propagating through a zonal flow and transverse magnetic field, showed that some planetary waves are known to be blown eastwards by zonal flows at critical levels or latitudes; westward propagation remains a characteristic of trapped planetary modes.

For waves propagating through meridional winds, the radiation patterns are complicated and it is not easy to follow the ray paths. Indeed, such a study would give a full description of critical wave behaviour at critical latitude.

References

Booker, J. R. and Bretherton, F. B. (1967) The critical layer for internal gravity waves in a shear flow. *J Fluid Mech.*, **27**, 513-539

Dickinson, R. E., (1968) Planetary Rossby waves propagating vertically through weak westerly wind wave guides. *J Atmos. Sc.*, **25**, 984-1002

El Mekki, O. M. (1980) Hydromagnetic Planetary Waves in vertically sheared zonal flow and transverse magnetic field. *Solar Physics*, **68** 3-15

El Mekki, O. M. and McKenzie, J. F. (1977) The propagation of atmospheric Rossby-gravity waves in latitudinally sheared zonal flows *Phil. Trans. Roy. Soc.*, **287**, 115-143

Farrell, B. and Watterson, I. (1985) Rossby waves in opposing currents. *J. Atmos. Sc.*, **42**(16), 1746-1756

Karoly, D. and Hoskins, B. J. (1982) Three dimensional propagation of planetary waves. *J. Meteor. Soc. Japan* **60**(1), 109-122

Killworth, P. D. and McIntyre, M. E. (1985) Do Rossby-wave critical layers absorb, reflect or over-reflect? *J. Fluid Mech.* **161**, 449-492

Lighthill, J. (1960) Studies on magneto-hydrodynamical waves and their anisotropic wave motions. *Proc. Roy. Soc.* **A 252**, 397-430

Lu, E. and Boyd, J. D. (2008) Rossby wave ray traveling in a barotropic-divergent atmosphere. *J. Atmos. Sci.*, **65**, 1679-1691

Shaman, J. Samelson, R. M., Tziperman, E. (2012) Complex number Rossby ray triangle.

J. Atmos. Sci. **69**, 2112-2133
Yagamata, T. (1976) On trajectories of Rossby wave packets released in a lateral shear flow. *J. Oceanogr. Soc. Japan*, **32**, 162-168

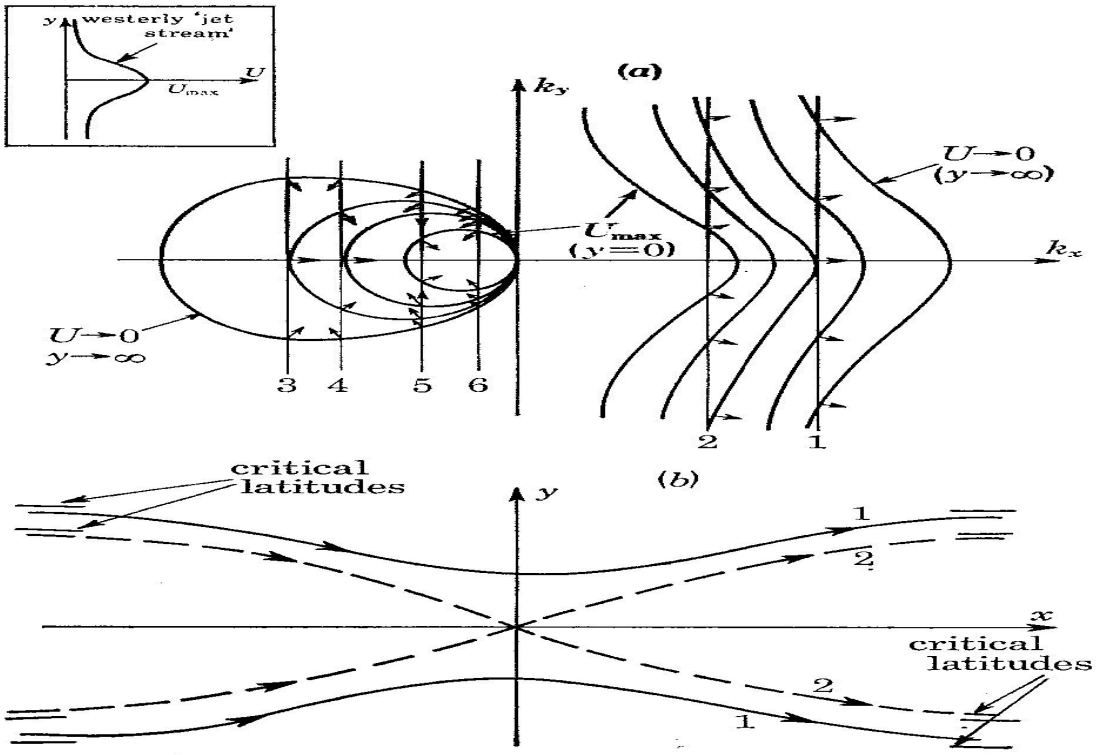

Figure 4.1: *(a) Geometric construction of ray paths through westerly jet (b) The ray path labelled 1 is reflected northward before reaching the centre of the jet and is eventually trapped at a critical latitude in the west. Ray path labelled 2 penetrates through the centre of the jet.*

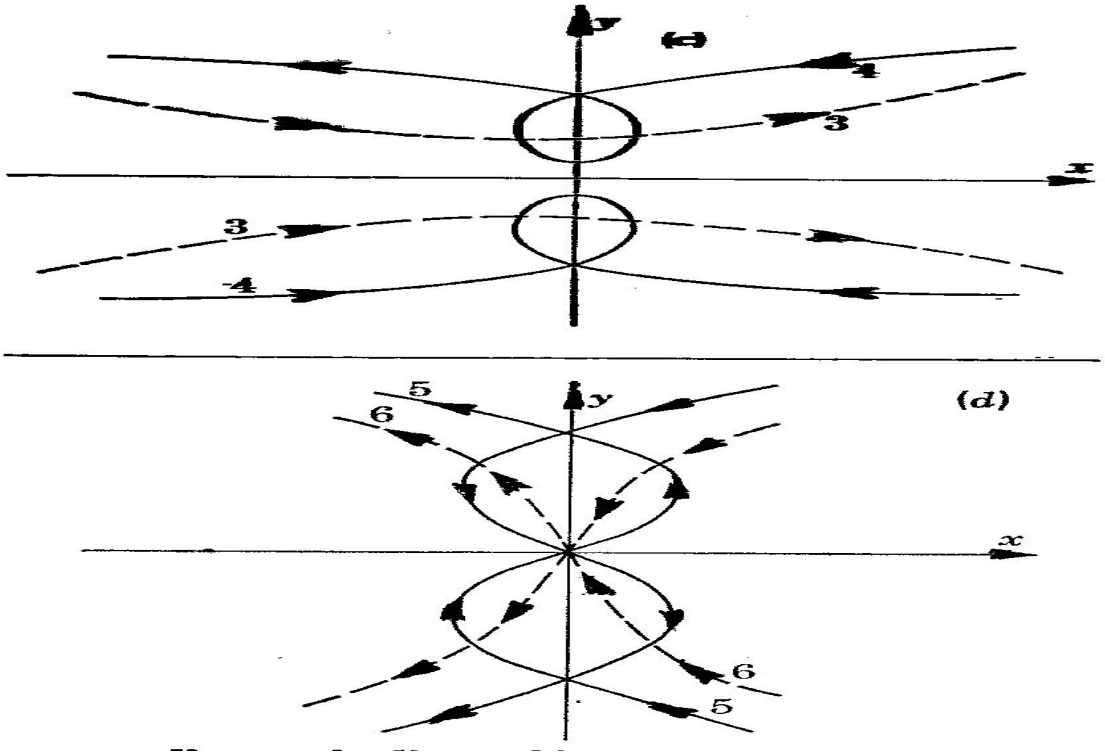

Figure 4.2: *Ray paths 3, 4, 5 and 6 correspond to westward phase propagation. (c) Ray path 3 and 4 are being reflected before reaching the jet centre. Ray path 3 corresponds to eastward energy propagation and ray 4 to westward energy propagation. (d) Ray paths labelled 5 and 6 penetrate the jet.*

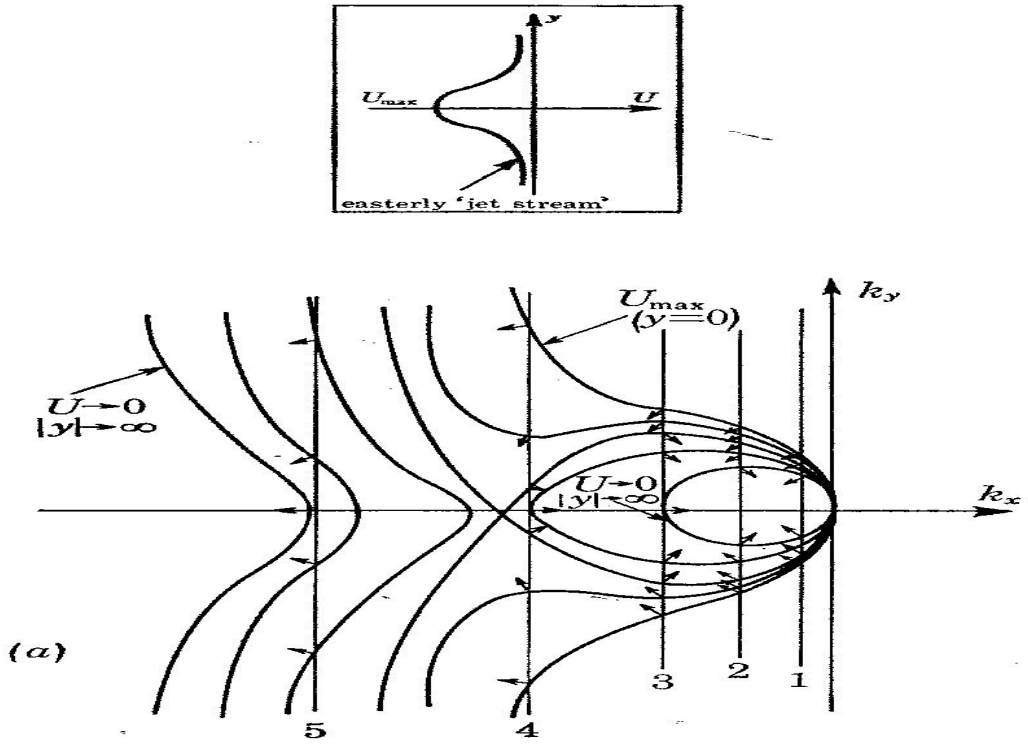

Figure 4.3: *Geometric construction of various ray paths in easterly jet.*

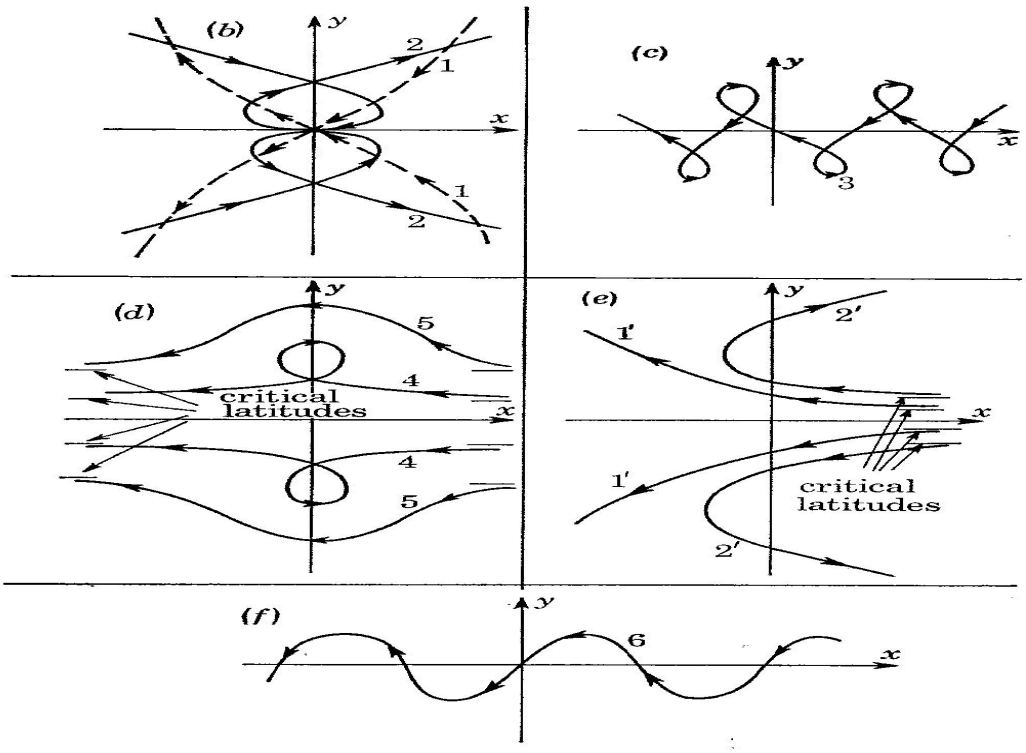

Figure 4.4: *(b) Rays 1 passes through the jet whereas ray 2 is reflected at the centre of a jet. (c) Rays labelled 3 are trapped in the jet. (d) Rays 4 and 5 exhibit critical latitude behaviour. (e) The critical latitude acts an emitter of rays labelled* $1^{'}$ *and* $2^{'}$*. (f) Ray 6 is trapped in the jet.*

Part II

Effects of Density Stratification and Double Diffusive Convection

Chapter 5

Introduction

Geophysical fluids typically consist of fluid masses of different densities, which under gravity tend to arrange themselves in vertical stacks corresponding to a state of minimal potential energy (Cushman-Roisin and Beckers, 2011). At the air-water interface, it is possible to have convection due to differing temperatures. The phenomenon of convection occurs in different fields of study, and is thus not confined to geophysics. For instance, besides convection in the Earth's mantle and in the atmosphere it is also relevant in chemical engineering where stratification is an important component of the system.

5.1 Stratification

The sun is the major source that heats up the oceans and atmosphere, thereby creating variations in densities. An important result for this stability is that motion parallel to gravity is inhibited and this tends to produce large-scale horizontal motions. Furthermore, due to this stability, there is a disparity between vertical and horizontal motions. The depth of the ocean is about 10 km whereas the horizontal distance is about tens of thousands of kilometers. So in general, these large scale motions take place within a very thin layer of fluid. The relation between the depth H and the horizontal scale L will determine how these motions can be modelled. For the scale $\delta = (H/L) \ll 1$ is the shallow-water limit.

Furthermore, due to stratification, if the fluid is displaced upward, and the fluid parcel is heavier than its surroundings, the fluid will experience the downward tendency due to gravity and falls down and in the process acquires a vertical velocity; upon reaching its original level, the particle's inertia causes the particle to go further downward and to be

surrounded by heavier fluid. The parcel now buoyant is propelled upward and oscillations persist about the equilibrium level. In such cases we can measure stability using the Brunt-Väisälä frequency. As we mentioned before if $N^2 > 0$, then we have instability and the system is stable when $N^2 < 0$. If a fluid is permanently destabilized for example by heating from below or cooling from above, the fluid will remain in constant agitation, a process called convection. In a compressible fluid, density can change in one of two ways: by pressure changes or by internal energy changes.

In many of the traditional fluid dynamics literature (e.g. Chandrasekhar (1961), Drazin and Reid (2004)), convection is described using the critical Rayleigh number for which the onset of convection is observed. We shall adopt this in Part II of this thesis when studying double-diffusive convection. McKenzie (2011) made an observation during the celebration of the life and work of Chandrasekhar, that "Chandrasekhar: The all rounder" had omitted the use of the Brunt-Väisäilä frequency in his study of thermal instability, and it was the atmospheric physicists who describe instability using the buoyancy frequency.

If a free surface liquid interacts with air, buoyancy and surface tension both play a role in developing convection patterns. Buoyancy effects occur when a free surface liquid is heated from either below or above. In this situation, the temperature differences induce buoyancy so that the liquid experiences an overturning as colder (heavier) water sinks and warmer (lighter) water rises. This effect is called Rayleigh-Bénard convection, or simply thermal convection of Bénard convection. With regard to surface tension, liquid will migrate from places of lower surface tension to places of higher surface tension; called the Marangoni effect. Furthermore, if the liquid is heated from below, there will be a temperature gradient through the liquid. Furthermore, as temperature increases, surface tension drops, thus also causing liquid to flow upwards from warmer areas to cooler areas. Again, in order to maintain the horizontal flow patterns, cooler waters will then sink and create a downwelling. This type of convection is called Bénard-Marangoni convection or thermo-capillary convection. So in this case the two effects of thermal convection and thermo-capillary convection (driven, respectively, by buoyancy and surface tension) work in concert.

A different situation arises when two opposing gradients (such as temperature and concentration) are involved, due to different rates of diffusion. The process is called double-diffusive convection. In the ocean, where heat and salt diffuse at different rates, in fact, with the rate of salt diffusion being 100 times slower, this convection is called thermohaline convection (thermo-temperature, haline- salt). In other fields, such as engineering, that involve a non-haline solute, the corresponding convection is called thermosolutal con-

vection. Thermohaline convection is important in ocean circulation because it transports heat poleward and brings nutrient-rich deep water to the surface.

In the work below the study will consider Rayleigh-Bénard convection leading to double-diffusive convection; specifically thermohaline convection. Because rotation contributes to the fluid's vertical rigidity it is a notable factor in modeling the phenomenon of convection in the ocean where rotation cannot be ignored. To address this factor, rotational effects are added to the mix and discuss the implications thereof. Chandrasekhar (1961) and others discussed rotational influences in the case of Rayleigh-Bénard convection. It is from this basis that the study considers rotational influences in thermohaline convection.

When there are two opposing gradients in the system, they often interfere with each other. As such it is possible to have heat flux due to the concentration gradient and the mass flux due to temperature gradient. These are called cross-diffusive factors.

The remainder of this chapter will first discuss Rayleigh-Bénard convection. The study then focuses attention on rotational effects on Rayleigh-Bénard convection. Furthermore, salt is included into the mix to discuss thermohaline convection. In addition, rotation effects on thermohaline convection are considered. The chapter concludes with cross diffusive effects. In the next chapter the study considers thermohaline convection under rotatory influences and cross-diffusive effects and it employs linear and nonlinear stability analysis to extend the work already undertaken in literature.

5.2 Rayleigh-Bénard Convection

Unlike the shallow water equations already discussed in Part I, which are governed by inviscid theory, the hydrodynamic equations governing thermal convection have viscosity as an important factor. Nevertheless, as with shallow water motion, the equations that describe the motion with thermal convection are based on the Navier-Stokes equations.

The phenomenon of thermal convection in fluids was discovered by Rumford in 1870. This was followed by the first quantitative experiment on the onset of thermal instability and the recognition of the role of viscosity in the phenomenon conducted by Bénard in the 1900s which led to his recognition of the role of viscosity in the phenomenon. In this experiment the height of the layer was taken to be small compared to the horizontal dimension, which is similar to the description of ocean and atmospheric flows. In 1961 Lord Rayleigh conducted a theoretical study and developed a mathematical theory for this problem. Rayleigh asserted that instability occurs as a result of the buoyancy effect due to heating from below. Convection due to buoyancy and its role in instability is important

in many physical systems, especially oceanography. Instability theory is discussed in the classical book by Chandrasekhar (1961) and in Drazin and Reid (2004). We base the ensuing discussion on these publications.

In a fluid mass where initially there was equilibrium, when the heating is from below, the fluid at the bottom will be lighter than the fluid at the top. As a result, the fluid will redistribute itself, but its viscosity will also inhibit this rearrangement. Thus for a a while the temperature at the top is the same as temperature at the bottom, and there is equilibrium. Then the temperature at the bottom will slightly increase. The fluid will redistribute itself but its viscosity will begin to inhibit this rearrangement. Thus for a certain temperature distribution the system may be unchanged until it reaches a critical temperature, at which the system becomes unstable. The subsequent fluid motion will result in a cellular arrangement called Bénard cells. If the temperature is increased further, turbulent flow will result, leading to chaos.

The theoretical foundations for modelling the phenomenon, as put forward by Lord Rayleigh is a system of three dimensional equations that is based on the Boussinesq approximation. In this approximation the fluid density ρ is considered to be independent of the pressure (i.e., assuming incompressibility) and to depend linearly on the temperature T:

$$\rho = \rho_0[1 - \alpha(T - T_0)], \tag{5.1}$$

where ρ_0 is the reference density and T_0 is the reference temperature, and α is volume of expansion coefficient. This is called the equation of state. What this equation means is that density variations can be ignored everywhere except in the buoyancy term they should include the factor of gravitational acceleration g. Rayleigh's system is based on the conservation of momentum and mass, and includes internal energy and the equation of state. Using a Cartesian system of coordinates (x, y, z) where x and y are horizontal coordinates and z is the vertical coordinate:

$$\rho \frac{D\mathbf{u}}{Dt} = -\nabla p + \mu \nabla^2 \mathbf{u} + F, \tag{5.2}$$

where $\mathbf{u} = (u, v, w)$ is the fluid velocity, ρ is the density, μ is the molecular viscosity, p is the pressure, and F is the external force for example, gravity and rotational effects. Here

$$\frac{D\mathbf{u}}{Dt} = \frac{\partial \mathbf{u}}{\partial t} + (\mathbf{u} \cdot \nabla)\mathbf{u}, \tag{5.3}$$

is the material derivative or convective derivative. Together with the momentum equation,

there is also the continuity equation

$$\nabla \cdot \mathbf{u} = \frac{\partial u}{\partial x} + \frac{\partial v}{\partial y} + \frac{\partial w}{\partial z} = 0 \tag{5.4}$$

under the Boussinesq approximation and the equation for the temperature gradient

$$\frac{\partial T}{\partial t} + \mathbf{u}\nabla T = \kappa_T \nabla^2 T \tag{5.5}$$

where T is the temperature and κ_T is a (constant) thermal diffusivity.

If a fluid parcel is located at position z_1, it has a temperature $T_1 = T_{z_1}$ and hence density $\rho = \rho(z_1)$. In this case the system is in equilibrium or in hydrostatic balance. Instability will arise if there is any disturbance, small or large. Instability can be determined from the density variations. In this regard, an incompressible fluid is unstable if density varies with height in the absence of viscous and diffusive effects. If $d\rho/dz > 0$ then the system is positively buoyant, if $d\rho/dz = 0$ then the system is in equilibrium, and when $d\rho/dz < 0$ then the system is negatively buoyant (Holton & Hakim, 2013). This is the same as using the buoyancy frequency, N, which was previously introduced in Section 5.1.

In some other literature, where density only depends on temperature, the vertical variation in temperature is used. In this case stability conditions are: if $dT/dz > 0$ the system is stable, $dT/dz = 0$ implies a neutral state, but $dT/dz < 0$ implies an unsteady state. In other publications, stability analysis is performed using the conservation of energy. However, these shall not be used in the work below.

In Rayleigh-Bénard instability, Rayleigh derived a quantity now called the Rayleigh number as the measure of stability, which is given by

$$R = \frac{g\alpha\Delta T d^3}{\nu\kappa} \tag{5.6}$$

where κ is the contraction coefficient, and ν is the viscosity.

Using linear stability analysis and the method of normal modes, assume that the equations of motion are linearised with respect to small perturbations, a Rayleigh number for a free-free surface, free-rigid, rigid-rigid surface can be derived as

$$R = \frac{(\pi^2 + a^2)^3}{a^2}. \tag{5.7}$$

The critical Rayleigh number for the onset of stationary convection is determined by the

condition

$$\frac{\partial R}{\partial a^2} = 0 \tag{5.8}$$

which gives $a^2 = \pi^2/2$, where a is the wave number. At this wave number, the corresponding Rayleigh number is

$$R_c = \frac{27\pi^4}{4} = 657.5. \tag{5.9}$$

The critical Rayleigh number depends on the boundary conditions. Chandrasekhar (1961) gives the critical Rayleigh numbers for free-rigid as $R_c = 1100.657$ and that for rigid-rigid conditions as 1707.762.

As can be seen, the conditions for Rayleigh-Bénard instability are such that if $R = R_c$ then the system is in equilibrium; if $R < R_c$ then the system is marginally stable, and if $R > R_c$ then the system is unstable. We follow Rayleigh's stability analysis in subsequent work to be considered in the next chapter.

When temperature is increased, as the system rearranges itself, the result is a pattern formation called Bénard cells in the case of free-free surface. These Bénard cells have introduced to convection patterns to the theory of convection. Chandrasekhar (1961) represents Bénard cells pictorially.

5.2.1 Rotational Effects

Many flows in nature are modulated by rotational effects. Therefore, rotational influences are relevant in many geophysical, astrophysical, geological studies. To be specific, tropical cyclones are typical examples of geophysical flows under rotation.

It has already been noted in this regard that rotation forces the fluid to be vertically rigid (Cushman-Roisin and Beckers, 2011). The effect of rotation on the onset of thermal instability has been investigated theoretically by Chandrasekhar (1961) and experimentally by Nakagawa and Frenzen (1955) and Rossby (1969). For this situation, Chandrasekhar (1961) alluded to the first consequence of rotation as being the inversion of the role of viscosity, which results from the Taylor-Proudmann and the Helmholtz-Kelvin theorems on vorticity.

At the outset, introducing rotation effects means that, the governing equations must be three-dimensional. So for inviscid fluids the system is expected to remain stable. However, when viscosity is taken into consideration, then thermal instability occurs. Nakagawa and Frenzen (1955) mentioned that it was Jeffreys in 1982 who first pointed out that "the effect of rotation is to maintain stability". They noted that high viscosities could actually aid

instability by preventing the high stabilizing effect of rotation.

In addition, in his study using linear stability analysis, Chandrasekhar (1961) found that rotation inhibits the onset of both stationary convection and oscillatory convection. The extent of the inhibition for stationary convection depends mainly on the Taylor number given by

$$Ta = \frac{\Omega^2}{\nu^2} d^4.$$

For the case of oscillatory convection instability depends on both the Taylor number and the Prandtl number

$$Pr = \frac{\nu}{\kappa_T}.$$

It has been found experimentally and theoretically that rotation inhibits instability for all adverse temperature gradients (Nakagawa and Frenzen, 1955). Furthermore, the onset of instability will be oscillatory as long as the Prandtl number exceeds a certain critical value (Nakagawa and Frenzen, 1955). Veronis (1968) studied large-amplitude Bènard convection in a rotating fluid. He found that fluids with large ($\gg 1$) Prandtl number exhibit behavior that is markedly different from that of fluids with $Pr \ll 1$. In addition the diameters of the convection cells vary inversely with the rate of rotation. In our discussions later will also involve analysis of convection using different nondimensional parameters such as the Prandtl number that arise from the equations of motion.

The equations governing the system under rotation are given by

$$\rho = \rho_0[1 - \alpha_T(T - T_0)], \tag{5.10}$$

$$\frac{\partial \mathbf{u}}{\partial t} + \mathbf{u} \cdot \nabla \mathbf{u} + 2\mathbf{\Omega_z} \times \mathbf{u} = -\frac{1}{\rho_0}\nabla p + \alpha_T \mathbf{g} + \nu \nabla^2 \mathbf{u}, \tag{5.11}$$

$$\nabla \cdot \mathbf{u} = 0, \tag{5.12}$$

$$\frac{\partial T}{\partial t} + \mathbf{u} \cdot \nabla T = \kappa_T \nabla^2 T, \tag{5.13}$$

where $\mathbf{u}$, p and T are velocity, pressure and temperature, whereas ρ_0 is the mean density, ν and κ_T are viscosity and thermal diffusion. $\mathbf{\Omega_z}$ is the rotation.

For the onset of stationary convection the Rayleigh number is given by

$$R = \frac{1}{a^2}\left[(\pi^2 + a^2)^3 + \pi^2 Ta\right]. \tag{5.14}$$

Here R attains its minimum when

$$2x^3 + 3x^2 = 1 + Ta/\pi^4$$

where $a^2 = \pi^2 x$. The critical Rayleigh number R_c will be determined for varying Ta. Chandrasekhar (1961) showed by the variational principle that for Ta/π^4 sufficiently large,

$$x_{min} \to \left(\frac{Ta}{2\pi^4}\right)^{1/3},$$

$$R_c \to 3\pi^4 \left(\frac{Ta}{2\pi^4}\right)^{2/3} = 8.6956 T^{1/2},$$

$$a_{min} \to \left(\frac{1}{2}\pi^2 T\right)^{1/6} = 1.3048 T^{1/6}.$$

The onset of oscillatory convection, manifesting as oscillations of increasing amplitude, is given by the condition

$$R = \frac{1}{x}\left[(1+x)^3 + Ta - (1+x)(1+2Pr)\sigma^2\right]. \tag{5.15}$$

Thus instability depends on the rotation number, Ta, and the Prandtl number Pr. Since both the rotation number and the Prandtl number depend on viscosity, it is can actually act as a stabilizing factor as noted by Nakagawa and Frenzen (1955). Studying fluid motions under high viscosity may yield useful results.

5.3 Double Diffusive Convection

When there are two quantities with vertical gradients, each affecting the density in an opposite fashion, and so causing different rates of diffusion, the ensuing process is called double-diffusive convection.

Double-diffusive convection in fluid layers, has been studied extensively for different contexts, both in theory and experiment. We note, in particular the publications by Turner (1973, 1974, 1985) and Huppert and Turner (1981) which review both aspects. The study of double-diffusive convection was extended to a Maxwell fluid by Awad *et al.* (2010). Caldwell (1974) also summarized experimental studies on the onset of thermohaline convection. As already mentioned, when one of the gradients is temperature, and the other is the concentration of a solute, this phenomenon is termed thermosolutal convection, and where the solute is salt, thermohaline convection. In the thermohaline case, heat diffuses 100 times faster than salt, resulting in instability. A common example in oceanography occurs when heating (or cooling) and salination (or refreshing) at the sea surface become further distributed in the oceanic boundary layer. The resulting thermohaline circulation

is important in ocean mixing and climate change. This shall be the focus of our attention in the next chapter.

The thermohaline convecting systems were first studied by Stommel *et al.* (1956). They discovered the salt fountain, which occurs when hot salty water lies above cold fresh water. Two fundamental cases were studied, firstly by Stern (1960) and then by Veronis (1965). Stern's study concentrated on the case when the temperature gradient was stabilizing and the salt gradient destabilizing, in other words, when salty warm water lies above cold and salty waters, a bottom-heavy configuration. Stern also confirmed the general properties of the motion known as 'salt fingers'. These structures appear as a closed-packed array of up and down flowing convection cells which exchange heat laterally but diffuse little salt. The result is a transport of salt and heat in the vertical. Typical cell widths in the ocean are 2-3 cm (Schmitt, 2001). Veronis (1965) studied the opposite, when the temperature gradient is destabilizing and salinity is stabilizing, the top-heavy configuration. The physics is different from the salt finger case. In this case elevated when cold fresh water become cold salty water then it becomes heavier than when it started upward. Instead of rising as in the salt finger case it sinks with greater force than it took to initially displace it (Schmitt, 2001). This is termed 'over-stability' or oscillatory convection and leads to growing oscillation. Thermohaline convection shall be the focus of our attention in the next chapter.

For thermohaline double diffusion, the equation of state is now

$$\rho = \rho_0[\alpha_T(T - T_0) - \alpha_S(S - S_0)], \tag{5.16}$$

where T is the temperature (measured in degree Celsius or Kelvin) and S is the salinity measured in parts per thousand. Here ρ_0 is the reference density measured at reference temperature T_0, and reference salinity S_0, also measured in degree Celsius or Kelvin and parts per thousand, respectively. Together with the equation of state, the governing equations are

$$\frac{\partial \mathbf{u}}{\partial t} + \mathbf{u} \cdot \nabla \mathbf{u} + 2\boldsymbol{\Omega} \times \mathbf{u} = -\frac{1}{\rho_0}\nabla p + (\alpha_T - \alpha_S)\mathbf{g} + \nu \nabla^2 \mathbf{u} \tag{5.17}$$

$$\nabla \cdot \mathbf{u} = 0, \tag{5.18}$$

$$\frac{\partial T}{\partial t} + \mathbf{u} \cdot \nabla T = \kappa_T \nabla^2 T, \tag{5.19}$$

$$\frac{\partial S}{\partial t} + \mathbf{u} \cdot \nabla S = \kappa_S \nabla^2 S, \tag{5.20}$$

where $\mathbf{u}$, ρ and T are velocity, pressure and temperature, whereas ρ_0 is the mean pressure,

ν, κ_T and κ_S are viscosity, thermal diffusion and haline contraction coefficient. $\mathbf{\Omega_z}$ is the rotation. These are the Boussinesq equations.

Using the method of normal modes, we arrive at equations when no rotation is present as

$$(D^2 - a^2)^3 W = -(R_T + R_S)a^2 W, \tag{5.21}$$

with the corresponding characteristic equation at $n = 1$ is

$$R_T = \frac{1}{a^2}(\pi^2 + a^2)^3 - R_S. \tag{5.22}$$

This shows that the salinity Rayleigh number

$$R_S = \frac{g\alpha_S \beta_S d^4}{\kappa_S \nu}, \tag{5.23}$$

will be a stabilizing effect.

For oscillatory convection Gupta *et al.* (2001) went on further, and prescribed upper limits for oscillatory motions of neutral or growing amplitude in the two types of configuration (Stern's and Veronis's configurations). This was carried out in such a way that it also resulted in sufficient conditions of stability in terms of the thermal Rayleigh number R_T and the salinity Rayleigh number R_S. It is important to note that Veronis's (1965) work was restricted to dynamically free boundaries, whereas Stern's (1960) work assumed the "principle of exchange of instabilities" (Barnejee *et al.*, 1993). This principle may be explained as follows.

If $p = p_r + ip_i$ is the growth rate, then the system is stable, neutral or unstable depending on whether p_r is negative, positive or zero. If $p_r \geq 0$ implies $p_i \neq 0$ then we have oscillatory motions of neutral or growing amplitude. If however, $p_r \geq 0$ implies $p_i = 0$ then for $p_r = 0$, we have $p = 0$. This is called the principle of exchange of instabilities, without it we will have over-stability. If, however, instability occurs, however, then it order to assess instability, it is not enough to know what mode of instability will occur, but also the characteristic frequency of the oscillations.

In a dimensionless formulation four parameters are required for the description of oscillatory motion, the thermal and salinity Rayleigh numbers, R_T and R_S, the thermal Prandtl number, Pr, and the Lewis number,

$$Le = \frac{\kappa_T}{\kappa_S}. \tag{5.24}$$

All of these are assumed to be constant, for simplicity. We will show in the next chapter how these nondimensional parameters enter the equations of motion. For given Prandtl number and Lewis number, results may be presented as contours in a Rayleigh number (R_T, R_S)-plane, each point on this plane representing a system with given temperature and salinity stratification. The line $R_T = R_S$ represents an equilibrium state of constant density, and if $R_T > R_S$, the density increases upwards (Baines and Gill, 1969). As we will see later, as more factors are added to the model, then the number of parameters increases correspondingly, and consequently, the analysis becomes more involved.

There are fundamentally two types of convection patterns that have been described in this type of convection; specifically, salt-fingers and layers. Salt-fingers were first described by Stommel *et al.* (1956) where they termed them 'salt fountain'. Further observations of salt fingering were conducted by Stern (1960) when he studied convection when hot salty water lies above cold fresh water. Veronis (1965) studied the opposite, when the temperature gradient is destabilizing and salinity is stabilizing. In this case the elevation of cold fresh water causes it to become cold salty water, and thus heavier. Instead of accelerating upward as in the salt finger case, it is actually driven back down with greater force than it took to initially displace it (Schmitt, 2001), thereby becoming layered structures. In some cases it is possible to observe thermohaline staircases as mentioned in Schmitt (2001), Pyolakov *et al.* (2012), Radko *et al.* (2014) and Zhou *et al.* (2014). Radko *et al* (2014) mentioned that thermohaline staircases are still surrounded by controversy. When temperature and salt vary in the horizontal, Schmitt (2001) observed "intrusions" which he likened to horizontal salt fingers.

The effect of rotation on double-diffusive convection has been extensively studied (Barnejee *et al.* (1983), (1988), (1995)). It has been found that in linear stability analysis, rotation inhibits the onset of convective instability. Sharma *et al.* (2001) studied thermosolutal convection in Rivlin-Eriksen rotating fluid in porous medium and found that solute and rotation has a stabilizing effect on stationary convection, but rotation also induce oscillatory modes in the system. Similar results were recently obtained by Dhiman and Goyal (2015) found on the study of Soret driven double-diffusion stationary convection. These results are important as we will evaluate them against our investigations in the next chapter.

5.4 Cross Diffusive Effects

Soret and Dufour effects are two important heat and mass transport properties. The thermal energy flux resulting from concentration gradients is referred to as the Dufour or diffusion-thermal effect. Similarly, the Soret or thermo-diffusion effect is the contribution to the mass fluxes due to the temperature gradient. Therefore Soret and Dufour effects are two important heat and mass transport properties. Typically, the energy transport is described adequately by Fourier diffusion and the mass transport by Fickian diffusion alone. Motjabi and Charrier-Motjabi (2005) showed that in many of the previous studies that they cited, the Soret and Dufour effects were neglected on the basis that their magnitudes are of smaller order than the effects described by Fourier's and Fick's laws. On the contrary, Eckert and Drake (1972) showed in their study on isotope separation that the Soret effect cannot be ignored. Likewise, Alloui *et al.* (2010) examined the Soret induced convection in a shallow cavity filled with a binary mixture where they found that both thermal and solutal contributions are destabilizing. Together, both effects were found to be significant in studies by Awad and Sibanda (2010) and by Awad *et al.* (2010),(2011). Similarly, Narayana *et al.* (2013) investigated the effect of cross diffusive parameters on the heat and mass transports of a binary viscoelastic fluid. Therefore, we contend that there is a large body of work to show that cross-diffusive factors cannot be ignored. In all cases, it has been shown that cross-diffusive factors cannot be ignored.

In view of the importance of these two effects, Alam and Rahman (2006) studied Dufour and Soret effects on mixed convection flow past a vertical porous flat plate. In their study of cross diffusive effects in coupled stress fluid system, Gaikwad *et al.* (2007), found that the Dufour parameter enhances the stability of the system in case of both stationary and oscillatory modes. A positive Soret parameter destabilizes the case in stationary mode and stabilizes the system in the oscillatory mode. The negative Soret parameter, however, enhances stability in both the stationary and oscillatory modes. The Dufour parameter increases the heat transfer whereas the Soret effect has negligible influence on heat transfer. The increase in both Dufour and Soret parameters causes an increase in mass transfer. Gbadeyan *et al.* (2011) investigated heat and mass transfer for Soret and Dufour effects in the presence of a magnetic field. In their study, an increase in the Dufour parameter led to an increase in both the velocity and temperature profiles and a decrease in the concentration boundary layer thickness. The Soret effect however increase the concentration boundary layer and has little effect on the temperature of the fluid.

Maleque (2010) investigated Dufour and Soret effects on unsteady MHD convective heat and mass transfer flow due to a rotating disk. In this case it was found that the Dufour

parameter had marked effects on temperature profiles but no apparent effect on velocity and mass profiles. The Soret parameter on the other hand was found to have a marked effect on the concentration profile and no apparent effect on velocity and temperature profiles. Basu and Layek (2013) considered the influences of these cross-diffusive effects on the double diffusive convection without due regard to rotation. Furthermore, they studied these effects in a layer of fluid heated and salted from above. In this case the analysis revealed that instability depends strongly on the cross-diffusive terms, and that stationary convection is followed by oscillatory convection provided that the Dufour parameter is always less than the reciprocal of the Lewis number for certain typical values of the cross diffusive parameters. Mohan (1996) studied the Soret effect on rotatory thermosolutal convection of the Veronis type. Mohan extended the work of Barnejee *et al.* (1995) by adding the Soret effect to the thermosolutal problem of the Veronis type and concluded that the Soret effect inhibits oscillatory motion of growing amplitude for a specific ratio of the salinity Rayleigh number, the Lewis number, and the Prandtl number. What is missing in Mohan's theorem is that it does not refer to the interaction of rotation and the Soret effect and instead make conclusions on the assumption that the Taylor number Ta is zero. Hayat *et al.* (2014) studied Soret and Dufour effects on MHD rotating fluid of a viscoelastic fluid and concluded that an increase in Soret number, Schmidt number and Dufour number increases heat transfer but decreases mass transfer. Goyal and Garg (2015) also showed that Soret and Dufour effects cannot be ignored.

5.5 Conclusion

In this chapter, we have provided a background to the study of double-diffusion and in particular, thermohaline convection. In the next chapter, we show how we conduct a study of thermohaline convection in rotating fluids under the influence of cross diffusive factors for dynamically free boundaries. As we have seen, when additional forces are added to the equation, the number of parameters also increases. So to address these we employ both linear and nonlinear stability analysis. The next chapter, consists of a research paper, submitted for peer review, which will thus extend the literature.

Chapter 6

Soret and Dufour Effects on Thermohaline Convection in Rotational Fluids

In the previous chapter we discussed double diffusive convection as it occurs in stratified fluids. We first revisited stability in Rayleigh-Bénard convection and how it is influenced by rotation. Double diffusive systems are subject to both the Dufour and Soret effects simultaneously. The Dufour, or diffusion-thermo, effect is the energy flux caused by a concentration gradient. The Soret, or thermo-diffusive, effect arise from mass fluxes created by temperature gradients. Instability is also possible in double-diffusive systems. Furthermore, as was noted in the previous chapter, in previous studiesthe Soret and Dufour effects have often been considered small enough to be neglected. Nevertheless, the literature cited indicated that rotation has a stabilizing effect by forcing fluid particles into a vertically rigid structure. In view of the aforementioned, it is clear that a system that combines rotation and stratification with the Soret and Dufour effects is complex and yet fascinating. To the best of my knowledge I have not as yet seen work in the literature that covers all four aspects of such a system; mass flux due to temperature gradients, energy flux due to salt migration, rotation and double-diffusive convection. In the paper that follows we consider the case that occurs when cross-diffusive factors, given by the Soret and Dufour parameters, together with rotation and density stratification all interact on a horizontal fluid layer.

In this case we employ both linear and nonlinear stability analysis. The linear stability analysis involves first the linearised equations of motion and the derivation of the stability parameter, given by the Rayleigh number. Due to the number of parameters, the system

is complex and involves six parameters. In the analysis of stationary convection, there are five parameters involved, the Dufour parameter, Soret parameter, Taylor number also referred to as rotation parameter, Lewis number which is the ratio of diffusivities, and the salinity Rayleigh number. We analysed the effect of each of these parameters on the Rayleigh number. In the analysis of oscillatory convection, the Prandtl number enters the fold. The results for both stationary convection and oscillatory convection are graphically represented.

For nonlinear stability analysis a minimum truncated representation of a Fourier series consisting of two terms is applied to the system. We obtained a dissipative system of six coupled first-order equations. Fixed point analysis was complex as it depended on which parameter is varied, a few examples have been given as the analysis could not be exhaustive. In some cases we obtained stable nodes, and in others we obtained strange attractors. Stability analysis corresponding to each of the parameters are represented and they yield bifurcation diagrams some which have been seen in literature before like Lorenzo's "butterfly effect". Some of the novel ones we obtained resemble the "beetle", the "woven fruit basket", "tornado-like effect" and others.

Furthermore, we consider heat and mass transport when cross-diffusive factors are also taken into account. We analyse heat and mass transport using the Nusselt and Sherwood numbers. It is shown here that the Dufour parameter and the Lewis number enhance heat transport whereas Soret parameter reduce the mass transport.

The remainder of this chapter consists of a paper which has been submitted for publication in a peer reviewed journal.

Submitted to Journal of Astrophysical and Geophysical Fluid Dynamics

Soret and Dufour effects on the Thermohaline Convection in Rotating fluids

C T DUBA* †, M SHEKAR‡, M NARAYANA‡ and P SIBANDA†

* *Department of Mathematics, Durban University of Technology, P O Box 1334, Durban, South Africa*

‡*Department of Mathematics, M S Ramaiah University of Applied Sciences, Bangalore 560 054, India*

†*School of Mathematics, Statistics and Computer Science, University of Kwazulu-Natal, Private Bag X01, Scottsville, 3209 Pietermaritzburg, South Africa*

March 31, 2016

Abstract

Using linear stability theory and weakly nonlinear stability theory, the effects of Soret and Dufour parameters are investigated on thermohaline convection of a horizontal layer of rotating fluid specifically the ocean. Thermohaline circulation is important in mixing processes and contributes to the earth's climate and to heat and mass transports. It is a general conception that due to the smallness of Soret and Dufour their effect is negligible. However, it is shown here that the Soret parameter, salinity and rotation stabilize the system whereas temperature destabilizes and the Dufour parameter has minimal effect on stationary convection. For oscillatory convection, the analysis is difficult as it shows that the Rayleigh number depends on six parameters, Soret and Dufour parameters, salinity Rayleigh number, Lewis number, Prandtl number, and Taylor number. We demonstrate the interplay between these parameters and their effects on oscillatory convection in a graphical manner. Furthermore, we find that the Soret parameter enhances oscillatory convection whereas the Dufour parameter, salinity Rayleigh number, the Lewis number, and rotation delay instability. We believe that these results have not been elucidated in this way before for large-scale fluids. Furthermore, we investigate weakly nonlinear stability and the effect of cross diffusive terms on heat and mass transports. We show the existence of new solution bifurcations not previously shown in literature.

Keywords: Thermohaline Convection; Soret number; Dufour number; Heat and mass transfer

1 Introduction

The phenomenon of thermal convection in fluids was described by Rumford in 1870, followed by the first quantitative experimental work by Bénard in the 1900's. Bénard studied the onset of thermal instability and the role of viscosity in thermal convection. In 1961, Lord Rayleigh conducted a theoretical study and developed a mathematical theory for this phenomenon. Instability is found to be due to the buoyancy effect arising when heating is from below. Convection due to buoyancy and the attendant modes of instability are important in many of the physical systems, notably in oceanography. The instability theory has been discussed in the classical book by Chandrasekhar (1961) and more recently by Drazin and Reid (2004), from which we draw the description below.

In the case when fluid is heated from below, the fluid at the bottom becomes lighter than the fluid at the top. As a result, the fluid begins to redistribute itself, but its viscosity will also begin to inhibit this rearrangement. Thus for a certain temperature distribution the system may be stably maintained until it reaches a certain critical temperature value at which the system becomes unstable. The fluid motions will result in an arrangement as cellular cells. Rayleigh laid the theoretical foundations and showed that the system remains stable provided that the thermal Rayleigh number, R_T, remains less than the critical value $R_c = 27\pi^4/4$. This Rayleigh number is a measure of strength of the buoyancy forcing relative to the viscous term. When $R_T \geq R_c$ the system becomes unstable and thermal convection (also known as Rayleigh- Bénard convection) sets in the form of a cellular pattern (Chandrasekhar 1961) thereby distorting the mean temperature profile. The critical value R_c depends on the boundary conditions which may be free on both surfaces, free on the one end and rigid on the other, or having both surfaces rigid.

When there are two vertical gradients involved and affecting the density in opposing directions, and having different rates of diffusion the process is called double-diffusive convection. The study thereof is of practical importance in many fields involving convective heat and mass transfer, including oceanography, astrophysics, geophysics, geology, atmospheric physics and chemical engineering. If the two gradients involved are temperature and concentration of solute,

the process is generally called thermosolutal convection: when the solute is salt (haline) the convection is specifically described as thermohaline. In this case, heat diffuses 100 times faster than salt, and as a result instability occurs. This process leads to thermohaline convection, which is important in ocean mixing. A common oceanographic example occurs when heating (or cooling) and salting (or refreshing) at the sea surface become distributed in the oceanic boundary layer. This process is called thermohaline circulation and is important in ocean mixing and climate change.

Thermohaline convecting systems were first studied by Stommel *et al.* (1956). In their study of hot salty water lying above cold fresh water, they described the formation of 'salt fountain'. Two fundamental cases were then studied, which we describe next. In the first study, Stern (1960) investigated a case that occurs when the temperature gradient was stabilizing and the salt concentration gradient destabilizing. In other words, when warm salty water lies above cold and less/more salty water, which is a bottom-heavy configuration. Stern confirmed the general properties of motion for 'salt fingers'. To elaborate, these structures appear as a close-packed array of convection cells flowing both upwards and downwards. The result is vertical transport of salt and heat. Laterally, only heat may be exchanged, but not salt. In the ocean, typical cell widths are 2-3 cm (Schmitt 2001).

Veronis (1965) studied the opposite case of a top-heavy configuration, in other words the situation when the temperature is destabilizing and salinity is stabilizing. The physics thereof is different from the salt finger case. In this case elevated cold fresh water become cold salty water, then it becomes heavier than when it started upward. Instead of rising as in the salt finger case it sinks with greater force than it took to initially displace it (Schmitt 2001). This is termed 'overstability' and leads to growing oscillation.

Following from Stern's and Veronis's studies on oscillatory motion, Gupta *et al.* (2001) went on further to prescribe upper limits for these oscillatory motions in both these configurations. Furthermore, they showed sufficient conditions for stability using the thermal Rayleigh number, R_T and the salinity Rayleigh number, R_S. There are essential differences in the way Stern and Veronis modelled the two cases. Veronis focuses his work on free boundaries, whereas Stern's work uses the "principle of exchange of instabilities" (Barnejee *et al.* 1993). This principle

can be explained as follows. For the growth rate $\sigma = \sigma_r + i\sigma_i$, the system is stable, neutral or unstable depending on whether σ_r is negative, positive or zero. If $\sigma_r \geq 0$ and $\sigma_i \neq 0$ then we have oscillatory motions of neutral or growing amplitude. If however, $\sigma_r \geq 0$ and $\sigma_i = 0$ then for $\sigma_r = 0$, we have $\sigma = 0$. This is called the principle of exchange of instabilities, otherwise we will have over-stability. If instability occurs, however, then it is not enough to know what mode of instability will occur, but also the characteristic frequency of the oscillations (Barnejee *et al.* 1993).

Four dimensionless parameters are required to describe the oscillatory fluid motion, thermal Rayleigh number R_T, salinity Rayleigh number, R_S, the Prandtl number, Pr, and the Lewis number, Le. All of these are assumed to be constant. For given Prandtl and Lewis numbers, Baines and Gill (1969) present the results as contours in the (R_T, R_S)-plane; each of the points on representing a system with given temperature and salinity stratification. They interpreted the line $R_T = R_S$ as representing equilibrium density, and when $R_T > R_S$, the density increased upwards.

The main interest in thermohaline convective problems is in the regions showing deviations from normal thermal convective motions. In this regard, two regions have been observed; the salt-fingering region and the overstable region characterized by layering. This difference in deviations is due to the varying diffusive rates in heat and salt. If these were equal, the system would be characterized by one Rayleigh number, R_T. Baines and Gill (1969) found a region of the R_S and R_T plane where the system is unstable and shows the "salt-finger" mechanism. They also showed that at the verge of instability, these structures become very tall and thin, a property first indicated by Stern (1960). Furthermore, they also showed that for the case $R_T > R_S$, the unstable modes do not grow at the same rate as those for stable modes.

Veronis (1965) explained the second major phenomenon of interest, oscillatory convection which results in layering. It arises when temperature gradient is destabilizing and salt concentration gradient is stabilizing, that is, when cold dilute water lies above warm salty water. Layered structures are rare in the oceans but are found mainly in the polar regions where temperature and salinity frequently increase downward. Salt fingering occurs in regimes where warm salty water lies above cold dilute water. Large regions of the subtropical and tropical oceans are

favorable for salt-fingering processes. Zhou *et al.* (2014), studied double-diffusive convection in the deep Arctic Ocean in so far as it affects thermohaline staircases. There are usually two parameters that are used to decide if fluid motion will result in diffusion convection (DC) staircases; namely, the density ratio R_ρ and the buoyancy frequency N. The density ratio, R_ρ, describes the ratio of R_S to R_T. The buoyancy frequency shows the stability of the stratification of the water column. Thermohaline staircases occur only when the density ratio $R_\rho < 1.7$ (Schmitt 2001). Radko *et al.* (2014) report that no salt-finger staircases have been reported for $R_\rho > 2$. Pyolakov *et al.* (2012) also investigated diffusion convection staircases over the Laptev Sea slope. The dynamics of thermohaline staircases are still surrounded by controversy and are a topic of much debate in the literature (Radko *et al.* 2014). Double-diffusive convection in a layer of fluid in different contexts has received extensive theoretical and experimental study. The studies by Turner (1973, 1974, 1985) and Huppert and Turner (1981) give the review of both theoretical and experimental works on double-diffusive convection. Caldwell (1974) gave a summary of experimental studies on the onset of thermohaline convection.

When temperature and salinity gradients vary in the horizontal, the unstable structures that occur are called 'intrusions' and are likened by Schmitt (2001) to horizontal salt fingers. They displace water-mass anomalies and maintain the tightness of the mean temperature-salinity relationship. According to Schmitt (2001), they can occur anywhere, and they are a major lateral mixing agents in both polar and equatorial latitudes.

Rotational effects on the onset of thermal instability were theoretically studied by Chandrasekhar (1961) and observed experimentally by Nakagawa and Frenzen (1955) and Rossby (1969). Nakagawa and Frenzen (1955) pointed out that it was Jeffreys in 1982 who first noted that rotation has the effect of preserving stability. They also conceded that high viscosities could actually aid instability by preventing the high stabilizing effect of rotation. Veronis (1965) confirmed the work of Chandrasekhar (1961) in which he applied linear stability analysis to conclude that rotational effects indeed inhibit the onset of instability. The extend of the inhibition depends on the Taylor number, Ta, and the Prandtl number Pr. Furthermore, it is generally agreed that the onset of instability will be oscillatory as long as the Prandtl number exceeds a certain critical value. Veronis (1968) studied large-amplitude Bènard convection in

a rotating fluid. He found that fluids with large ($\gg 1$) Prandtl number exhibit behavior that differs from those of fluids with $Pr \ll 1$. In addition, Nakagawa and Frenzen (1955) found that the diameter of the convection cells vary inversely with the rate of rotation. The effect of rotation on double-diffusive convection has been extensively studied (Barnejee *et al.* 1983, 1988, 1995). The study by Zhou *et al.* (2014), shows that convection occurs when buoyancy due to heat is larger than the resistance of salt stratification and rotation. The study of rotational effects is important in geophysical, astrophysical and cosmical fluid dynamics.

The effect of rotation on double-diffusive convection, specifically, thermohaline convection, finds its importance in geophysical fluids, particularly large-scale fluids like the ocean and atmosphere. In oceanography for example, thermohaline circulation is regarded as important in mixing processes and hence weather and climate change. For the most part, it can be described as an 'overturning' circulation as it causes warm water to flow upward near the surface and converts it into cold water (Burroughs 2007). Then the cooler water sinks and flows equatorward in the interior. Hence thermohaline circulation contributes to the earth's climate as it transports heat polewards into high latitudes. It also brings deep water filled with rich nutrients to the surface. Hence it is essential in heat and mass transport systems. In consideration of global warming, it has been discussed in many reports of the risk of a shutdown of thermohaline circulation. Studies by Wood *et al.* (2003) and Schmittner and Stocker (1999), and literature therein, for example, grappled with the question of whether or not thermohaline circulation will be weakened or remain stable under the influence of global warming.

Heat and mass transports depends primarily on Dufour and Soret effects. The Dufour effect or diffusion-thermal effect concerns the thermal energy flux that results from concentration gradients. Similarly, the Soret or thermo-diffusion effect contributes to mass fluxes due to temperature gradients. In general, energy transport is modelled to Fourier diffusion whereas mass transport is by means of the Fickian diffusion. Motjhabi and Charrier-Motjabi (2005) showed that in many of the previous studies they cited the Soret and Dufour effects have been neglected due to their smallness in magnitude compared to effects due to Fourier's and Fick's laws. However, many studies show that these cross-diffusive effects are significant and should be included, as we discuss next. The Soret effect is large enough to be useful for isotope separation

(Eckert and Drake 1972). In addition, for Soret induced convection in a shallow cavity filled with a binary mixture, Alloui *et al.* (2010), found that both thermal and solutal contributions are destabilizing. Furthermore, Chand and Rana (2015) also showed that Soret parameter has a destabilizing effect in double-diffusive convection in a horizontal layer of nanofluid when uniform vertical magnetic field is present. Similarly, the Dufour effect could not be ignored by Eckert and Drake (1972) in their study on a mixture of gases with different molecular weights. Together, both effects were found to be significant in studies by Awad and Sibanda (2010), Awad *et al.* (2010),(2011) and Chand and Rana (2012, 2014) . Similarly, Narayana *et al.* (2013) investigated the effect of cross diffusive parameters on the heat and mass transports of a binary viscoelastic fluid.

The Soret and Dufour effects can influence the stability or otherwise of convection systems. In this regards, Alam and Rahman (2006) considered the possibility that the effect of Soret and Dufour parameters in stability analysis for mixed convection flows past a vertical flat porous plate. Furthermore, in their study of cross-diffusive effects in a coupled stress fluid system, Gaikwad *et al.* (2007), showed a number of influences due to the parameters. Notably a positive Soret parameter destabilizes the system in stationary mode, with opposite effect in the oscillatory mode; a negative Soret parameter, however, enhances stability in both the stationary and oscillatory modes. The Dufour parameter was shown to delay instability of the system, for both stationary and oscillatory modes. Heat transfer increased with Dufour parameter increases whereas the Soret effect has negligible influence on heat transfer.

In the presence of a magnetic field Gbadeyan *et al.* (2011) found that increasing the Dufour parameter led to an increase in both the velocity and temperature profiles with a decrease in the concentration boundary layer thickness. The Soret effect however increases the concentration boundary layer and has little effect on the temperature of the fluid. It is thus evident that the Dufour and Soret effects have significant effects on diffusive systems. In the case of unsteady magnetohydrodynamics (MHD) convective heat and mass transfer flow due to a rotating disk, Maleque (2010) found that the Dufour parameter has a marked effect on temperature profiles but no apparent effect on velocity and mass profiles. The Soret parameter on the other hand was found to have a marked effect on the concentration profile and no apparent effect on velocity

and temperature profiles.

We further note studies on these cross-diffusive effects in the context of double diffusive convection. For example, Basu and Layek (2013) found that in a layer of fluid heated and salted from above in the absence of rotation, stability depends strongly on the cross-diffusive Soret-Dufour terms. Mohan (1996) extended the work of Barnejee *et al.* (1995) and studied the Soret effect on rotatory thermosolutal convection of the Veronis type. He concluded that, for a specific ratio of the salinity Rayleigh number, the Lewis number, and the Prandtl number, the Soret effect inhibits oscillatory motion of growing amplitude. What is missing in Mohan's theorem is that it does not include the interaction between rotation and the Soret effect. Instead, Mohan based the conclusions on the assumption that the Taylor number, Ta, is zero. Hayat *et al.* (2014) studied Soret and Dufour effects on MHD rotating fluid of a visco-elastic fluid and concluded that an increase in Soret number and Dufour number increase heat transfer but decrease mass transfer. Finally, in a recent study of Soret and Dufour effects in a horizontal layer, Goyal and Garg (2015) showed that the Soret parameter has both a stabilizing and destabilizing effect on the stationary modes, whereas the Dufour coefficient has a stabilizing effect. However, the study concentrated only on linear stability analysis.

Based on the aforementioned studies, it is clear that there is an overwhelming body of evidence to indicate that the Soret and Dufour effects should not be neglected. Instead, their influence on stability of double-diffusive systems is of great importance. Furthermore, due to the increasing complexity of the model as one adds more parameters, using only linear stability analysis does not provide enough information. Consequently, in this paper, we employ linear and weakly nonlinear stability theory and normal modes analysis to study the effects of the Soret and Dufour parameters on thermohaline convection for a fluid heated from below. Such would be the case when oceans experience geothermal heating from below. We study the onset of both stationary and oscillatory instability by examining the Rayleigh number. In this case the resulting Rayleigh number depends on salinity Rayleigh number, the Lewis number and the Taylor number. In Section 2, we develop a mathematical model for the system of a rotating fluid, heated and salted from below and subject to cross-diffusive factors. In Section 3, we discuss linear stability theory and study both stationary and oscillatory convection in the system. In

Section 4, we study weakly nonlinear stability theory using Fourier mode analysis. Heat and mass transfer are then investigated in Section 5. In Section 6, the results are discussed in detail and we make conclusions in Section 7.

2 Mathematical Formulation

We consider a horizontal layer of fluid rotating at a constant angular velocity Ω and also heated from below as would be the case in the ocean when there is geothermal heating. We use a Cartesian system of coordinates (x, y, z) where x and y are horizontal coordinates and z is the vertical coordinate:- The governing equations for the rotating fluid in the presence of cross diffusive effects are taken in such a way that the Oberbeck-Boussinesq approximation is valid. While the validity of the Oberbeck-Boussinesq approximation for the Navier-Stokes equations within geophysical fluid dynamics, has been under much debate (see Rajagopaul *et al.* 2009 and the arguments by Barnejee *et al.* 1983), it is not our intention here to enter the debate. We also assume that there is coupling between the two diffusing components. The governing equations are therefore:

$$\nabla \cdot \vec{q} = 0 \tag{1}$$

$$\frac{\partial \vec{q}}{\partial t} + (\vec{q} \cdot \nabla)\vec{q} = -\frac{1}{\rho_0}\nabla P + \left(1 + \frac{\delta\rho}{\rho_0}\right)\vec{X} + \nu\nabla^2\vec{q} - (2\vec{\Omega} \times \vec{q}) \tag{2}$$

$$\frac{\partial T}{\partial t} + (\vec{q} \cdot \nabla)T = \kappa_T \nabla^2 T + D_{TS}\nabla^2 S \tag{3}$$

$$\frac{\partial S}{\partial t} + (\vec{q} \cdot \nabla)S = \kappa_S \nabla^2 S + D_{ST}\nabla^2 T \tag{4}$$

where $\vec{q} = (u, v, w)$ is the velocity vector; $P = p - \frac{1}{2}|\vec{\Omega} \times \vec{\zeta}|^2$ is the effective hydrostatic pressure; $\vec{X} = (0, 0, -g)$ is the gravitational vector; $\vec{\Omega} = (0, 0, \Omega_z)$ is the angular velocity, $\nu = \mu/\rho_0$ is the kinematic viscosity which has different values at different temperatures; $\nu = 1.83 \times 10^{-6}$ m^{2}s^{-1} at 0° Celsius and $\nu = 1.05 \times 10^{-6}$ m$^2 s^{-1}$ at 20° Celsius. The angular velocity of the Earth $\Omega = 7.2921159 \times 10^{-5}$ rad.sec^{-1}. D_{TS} and D_{ST} are respectively, parameters quantifying the contribution to the heat flux due to solutal gradients and to the mass flux due to temperature

gradient; κ_T and κ_S are the thermal and solutal diffusivities. In the ocean, $\kappa_T \sim 1.5 \times 10^{-7}$ $\mathrm{m^2 s^{-1}}$ and $\kappa_S \sim 1.5 \times 10^{-5}$ $\mathrm{m^2 s^{-1}}$ (Basu & Layek, 2013). The values in literature are varied as they depend on molecular values, but what is consistent is that heat diffuses 100 times faster than salt). The density ρ, of the fluid depends linearly on both the temperature, T measured in degrees Celsius or Kelvin; and salinity, S measured in parts per thousand, or by the practical salinity unit "psu", derived from measurements of conductivity and having no units. For small variations at a constant pressure (Boussinesq approximation), the density variations are given by the equation

$$\delta\rho = -\rho_0[\alpha_T(T - T_0) + \alpha_S(S - S_0)], \tag{5}$$

where α_T and α_S are respectively, the thermal expansion coefficient and the haline contraction coefficient, and they are both positive ($\alpha_T = 2 \times 10^{-4}$ $\mathrm{K^{-1}}$ with an error of ± 1.5 and $\alpha_S = 7.6 \times 10^{-4}$ $\mathrm{ppt^{-1}}$ with error of ± 0.2 (Vallis, 2006)); $\rho_0 = 1.027 \times 10^3$ kg $\mathrm{m^{-3}}$ is the reference density at reference temperature $T_0 = 283$ K and reference salinity $S_0 = 35$ $\mathrm{ppt^{-1}}$.

The basic state of the fluid can be described by Malashetty (2008) as

$$\vec{q_b} = (0, 0, 0), \quad T_b = T_b(z) = T_0 + \Delta T\left(1 - \frac{z}{d}\right), \quad S_b = S_b(z) = S_0 + \Delta\left(1 - \frac{z}{d}\right) \tag{6}$$

$$\rho_b = \rho_b(z) = \rho_0[1 - \alpha_T(T_b - T_0) + \alpha_S(S_b - S_0)], \quad P_b = P_b(z) = -\rho_b g + \text{constant}, \tag{7}$$

where the subscipt b denotes basic state.

2.1 Perturbation of Basic State

We consider small perturbations to the physical quantities as follows:

$$\vec{q} = \vec{q_b} + \vec{q}\,', \quad T = T_b(z) + T', \quad S = S_b(z) + S', \quad P = P_b(z) + P', \quad \rho = \rho_b(z) + \rho'. \tag{8}$$

Substituting the above in (1)-(4) we get

$$\nabla \cdot \vec{q}\,' = 0, \tag{9}$$

$$\frac{\partial \vec{q}\,'}{\partial t} + (\vec{q}\,' \cdot \nabla)\vec{q}\,' = -\frac{1}{\rho_0}\nabla P' + (\alpha_T T' - \alpha_S S')g\hat{k} + \nu\nabla^2\vec{q}\,' - (2\vec{\Omega} \times \vec{q}\,'), \tag{10}$$

$$\frac{\partial T'}{\partial t} + (\vec{q}\,' \cdot \nabla)T' + w'\frac{dT_b}{dz} = \kappa_T\nabla^2 T' + D_{TS}\nabla^2 S', \tag{11}$$

$$\frac{\partial S'}{\partial t} + (\vec{q}\,' \cdot \nabla)S' + w'\frac{dS_b}{dz} = \kappa_S\nabla^2 S' + D_{ST}\nabla^2 T'. \tag{12}$$

We non-dimensionalise the above equations using the following new variables:

$$(x,y,z) = d(x^*,y^*,z^*), \quad t = \frac{d^2}{\kappa_T}t^*, \quad P' = \frac{\mu\kappa_T}{d^2}p^*, \quad (u',y',w') = \frac{\kappa_T}{d}(u^*,v^*,w^*)$$
$$T' = \Delta T\theta, \quad S' = \Delta S\phi, \quad \nabla = \frac{\partial}{\partial x}\hat{i} + \frac{\partial}{\partial y}\hat{j} + \frac{\partial}{\partial z}\hat{k} = \frac{1}{d}\left(\frac{\partial}{\partial x^*}\hat{i} + \frac{\partial}{\partial y^*}\hat{j} + \frac{\partial}{\partial z^*}\hat{k}\right) = \frac{1}{d}\nabla^* \quad (13)$$

and dropping asterisks for simplicity we get

$$\nabla\cdot\vec{q} = 0 \quad (14)$$
$$\frac{1}{Pr}\left\{\frac{\partial\vec{q}}{\partial t} + (\vec{q}\cdot\nabla)\vec{q}\right\} = -\nabla p + (R_T\theta - R_S\phi)\hat{k} + \nabla^2\vec{q} - \sqrt{Ta}\ \hat{k}\times\vec{q}. \quad (15)$$
$$\frac{\partial\theta}{\partial t} + (\vec{q}\cdot\nabla)\theta - w = \nabla^2\theta + Du\nabla^2\phi, \quad (16)$$
$$\frac{\partial\phi}{\partial t} + (\vec{q}\cdot\nabla)\phi - w = Le^{-1}(\nabla^2\phi + Sr\nabla^2\theta), \quad (17)$$

where $P_r = \nu/\kappa_T$, is the Prandtl number, $R_T = g\alpha_T\Delta T d^3/\nu\kappa_T$, is the thermal Rayleigh number, $R_S = g\alpha_S\Delta S d^3/\nu\kappa_T$, is the salinity Rayleigh number, $Ta = 4\Omega^2 d^4/\nu^2$, is the Taylor number, $Du = (D_{TS}/\kappa_T) * (\Delta S/\Delta T)$, is the Dufour number, $Sr = (D_{ST}/\kappa_S)(\Delta T/\Delta S)$ is the Soret number and $Le = \kappa_T/\kappa_S$, the Lewis number. For the ocean, the Lewis number is 0.0125. The Prandtl number has the value 13.4 at 0° Celsius and 7.2 at 20° Celsius. The boundary conditions are taken as

$$w = 0, \quad \frac{\partial^2 w}{\partial z^2} = 0, \quad \theta = 0, \quad \phi = 0, \quad \text{at} \quad z = 0 \quad (18a)$$
$$w = 0, \quad \frac{\partial^2 w}{\partial z^2} = 0, \quad \theta = 0, \quad \phi = 0, \quad \text{at} \quad z = 1. \quad (18b)$$

We derive vorticity-transport equation by taking the curl of (15) twice. Thus we obtain

$$\begin{aligned}\frac{1}{Pr}\frac{\partial}{\partial t}(\nabla^2\vec{q}) &= \frac{\partial^2}{\partial x\partial z}(R_T\theta - R_S\phi)\hat{i} - \frac{\partial^2}{\partial y\partial z}(R_T\theta - R_S\phi)\hat{j} \\ &+ \nabla_H^2(R_T\theta - R_S\phi)\hat{k} + \nabla^4\vec{q} - \sqrt{Ta}\ \frac{\partial\zeta}{\partial z}, \quad (19)\\ \frac{1}{Pr}\frac{\partial\zeta}{\partial t} &= \frac{\partial}{\partial y}(R_T\theta - R_S\phi)\hat{i} - \frac{\partial}{\partial x}(R_T\theta - R_S\phi)\hat{j} + \nabla^2\zeta + \sqrt{Ta}\ \frac{\partial\vec{q}}{\partial z}, \quad (20)\end{aligned}$$

where the vorticity vector is given by $\zeta = \nabla\times\vec{q} = (0,0,\zeta_z)$, and $\nabla_H^2 = \frac{\partial^2}{\partial x^2} + \frac{\partial^2}{\partial y^2}$.

3 Normal Mode Analysis

In this section, we conduct both linear and nonlinear stability analysis. The z component of the system of equations (19) and (20) are given by

$$\frac{1}{Pr}\frac{\partial}{\partial t}(\nabla^2 w) = \nabla^4 w + \nabla_H^2(R_T\theta - R_S\phi) - \sqrt{Ta}\ \frac{\partial \zeta_z}{\partial z}, \tag{21}$$

$$\frac{1}{Pr}\frac{\partial \zeta_z}{\partial t} = \nabla^2 \zeta_z + \sqrt{Ta}\ \frac{\partial w}{\partial z}. \tag{22}$$

The linearised versions of equations (16) and (17) are given by

$$\frac{\partial \theta}{\partial t} - w = \nabla^2\theta + Du\nabla^2\phi, \tag{23}$$

$$\frac{\partial \phi}{\partial t} - w = Le^{-1}(\nabla^2\phi + Sr\nabla^2\theta). \tag{24}$$

The perturbations are assumed to be wave-like, of the form

$$(w, \theta, \phi, \zeta_z) = (W(z), \Theta(z), \Phi(z), Z(z)) \exp\{\sigma t + i(k_x x + k_y y)\}, \nabla^2 = \frac{\partial^2}{\partial x^2} + \frac{\partial^2}{\partial y^2} + \frac{\partial^2}{\partial z^2} = \frac{d^2}{dz^2} - a^2, \tag{25}$$

where $W(z)$, $\Theta(z)$, $\Phi(z)$ and $Z(z)$ are amplitudes, where k_x, ky are horizontal wavenumbers and σ is the growth rate. Infinitesimal perturbations of the rest state may either reduce or grow depending on the value of the parameter σ.

The quantity $\sigma = \sigma_r + i\sigma_i$ is a complex quantity where σ_r is the growth rate and $\sigma_i = \omega$ is the frequency of oscillations. Substituting (25) into (21)-(24) we get

$$\frac{\sigma}{Pr}(D^2 - a^2)W(z) = (D^2 - a^2)^2 W(z) - a^2(R_T\Theta(z) - R_S\Phi(z)) - \sqrt{Ta}\ DZ, \tag{26}$$

$$\frac{\sigma}{Pr}Z(z) = (D^2 - a^2)Z(z) + \sqrt{Ta}\ DW, \tag{27}$$

$$\sigma\Theta(z) - W(z) = (D^2 - a^2)(\Theta(z) + Du\ \Phi(z)), \tag{28}$$

$$\sigma\Phi(z) - W(z) = (D^2 - a^2)Le^{-1}(\Phi(z) + Sr\ \Theta(z)), \tag{29}$$

where

$$D(\cdot) = d/dz(\cdot),$$

and $a^2 = k_x^2 + k_y^2$ is the dimensionless wavenumber. We assume stress-free, isothermal and isohaline boundary conditions in the form:

$$W = D^2W = \Theta = \Phi = 0 \quad \text{at} \quad z = 0, \quad \text{and} \quad z = 1, \tag{30}$$

as we are not interested in the interference of topography on the circulation. A rigid bottom in the ocean may be uneven and convection there may generate ocean waves. Equation (27) can be written as

$$(D^2 - a^2 - \frac{\sigma}{Pr})Z = -\sqrt{Ta}\ DW. \tag{31}$$

Applying the operator $(D^2 - a^2 - \frac{\sigma}{Pr})$ to equation (22) and using the above relation we get

$$\begin{aligned} \frac{\sigma}{Pr}(D^2 - a^2)\left(D^2 - a^2 - \frac{\sigma}{Pr}\right)W &= (D^2 - a^2)^2\left(D^2 - a^2 - \frac{\sigma}{Pr}\right)W \\ &- a^2\left(D^2 - a^2 - \frac{\sigma}{Pr}\right)(R_T\Theta - R_S\Phi) + Ta\ D^2W. \end{aligned} \tag{32}$$

The solutions of equations (28), (29) and (32) subject to the boundary conditions can be assumed as periodic wave solutions with sinusoidal variations in (W, Θ, Φ), namely

$$W(z) = W_0 \sin(\pi z) \quad \Theta(z) = \Theta_0 \sin(\pi z) \quad \Phi(z) = \Phi_0 \sin(\pi z). \tag{33}$$

Here (W_0, Θ_0, Φ_0) are the amplitudes of the velocity, temperature and salinity perturbations. Clearly these satisfy the boundary conditions (18). Using (33) in (28), (29) and (32) we get

$$\begin{aligned} \frac{\sigma}{Pr}J^2\left(J^2 + \frac{\sigma}{Pr}\right)W_0 &= -J^4\left(J^2 + \frac{\sigma}{Pr}\right)W_0 + a^2\left(J^2 + \frac{\sigma}{Pr}\right)(R_T\Theta_0 - R_S\Phi_0) \\ &- Ta\ \pi^2 W_0, \end{aligned} \tag{34}$$

$$\sigma\Theta_0 - W_0 = (-J^2)(\Theta_0 + Du\Phi_0), \tag{35}$$

$$\sigma\Phi_0 - W_0 = (-J^2)Le^{-1}(\Phi_0 + Sr\Theta_0), \tag{36}$$

where $(D^2 - a^2) = -(\pi^2 + a^2) = -J^2$ is the total wave number. Thus equations (34)-(36) form a homogeneous system in W_0, Θ_0, Φ_0. In matrix form, we have

$$\begin{bmatrix} J^2\left(J^2 + \frac{\sigma}{Pr}\right)^2 + Ta\ \pi^2 & -R_T\ a^2\left(J^2 + \frac{\sigma}{Pr}\right) & R_S\ a^2\left(J^2 + \frac{\sigma}{Pr}\right) \\ -1 & \sigma + J^2 & J^2Du \\ -1 & J^2Sr\ Le^{-1} & \sigma + J^2Le^{-1} \end{bmatrix} \begin{bmatrix} W_0 \\ \Theta_0 \\ \Phi_0 \end{bmatrix} = \begin{bmatrix} 0 \\ 0 \\ 0 \end{bmatrix} \tag{37}$$

For non-trivial solutions of the above homogenous system we require the determinant to vanish:

$$\begin{vmatrix} J^2\left(J^2 + \frac{\sigma}{Pr}\right)^2 + Ta\ \pi^2 & -R_T\ a^2\left(J^2 + \frac{\sigma}{Pr}\right) & R_S\ a^2\left(J^2 + \frac{\sigma}{Pr}\right) \\ -1 & \sigma + J^2 & J^2Du \\ -1 & J^2Sr\ Le^{-1} & \sigma + J^2Le^{-1} \end{vmatrix} = 0, \tag{38}$$

which gives

$$\left\{J^2\left(J^2+\frac{\sigma}{Pr}\right)^2+Ta\ \pi^2\right\}\left\{(\sigma+J^2)(\sigma+J^2Le^{-1})-J^4Sr\ Du\ Le^{-1}\right\}$$
$$+R_T\ a^2\left(J^2+\frac{\sigma}{Pr}\right)\left\{J^2Du-(\sigma+J^2Le^{-1})\right\}+R_S\ a^2\left(J^2+\frac{\sigma}{Pr}\right)\left\{(\sigma+J^2)-J^2Sr\ Le^{-1}\right\}=0.$$

Solving for R_T we get

$$\begin{aligned} R_T &= \frac{\left\{J^2\left(J^2+\frac{\sigma}{Pr}\right)^2+Ta\ \pi^2\right\}\left\{J^4Du\ Sr\ Le^{-1}-(\sigma+J^2)(\sigma+J^2Le^{-1})\right\}}{a^2\left(J^2+\frac{\sigma}{Pr}\right)\left\{J^2Du-(\sigma+J^2Le^{-1})\right\}} \\ &+ R_S\left\{\frac{J^2Sr\ Le^{-1}-(\sigma+J^2)}{J^2Du-(\sigma+J^2Le^{-1})}\right\}, \end{aligned} \tag{39}$$

which clearly depends on six other parameters.

3.1 Stationary convection

We observe the onset of stationary convection (exchange of instabilities) when we set $\sigma=0$ in (39), and we get

$$R_T^{st}=\frac{\{(\pi^2+a^2)^3+Ta\ \pi^2\}}{a^2}\left(\frac{1-Du\ Sr}{1-Du\ Le}\right)+R_S\left(\frac{Le-Sr}{1-Du\ Le}\right) \tag{40}$$

where R_T^{st} is the Rayleigh number for exchange of instabilities. This holds provided $Du\neq Le^{-1}$. In the ocean, the Rayleigh number can be very large, up to 10^{24} if molecular values are used (Vallis, 2006).

The critical wavenumber a_c can be obtained by minimizing R_T^{st} with respect to a^2, that is, we set

$$\frac{\partial R_T^{st}}{\partial a^2}=0, \tag{41}$$

implying that

$$\frac{\partial}{\partial a^2}\left\{\frac{(\pi^2+a^2)^3+Ta\ \pi^2}{a^2}\left(\frac{1-Du\ Sr}{1-Du\ Le}\right)+R_S\left(\frac{Le-Sr}{1-Du\ Le}\right)\right\}=0, \tag{42}$$

giving

$$2a^6+3\pi^2a^4-\pi^2(\pi^4+Ta)=0. \tag{43}$$

This equation gives critical wavenumber a_c which only depends on the Taylor number, implying that the influence of rotation on the onset of convection will be significant. In the absence of rotation, $Ta = 0$, we get

$$2a^6 + 3\pi^2 a^4 - \pi^6 = 0 \tag{44}$$

yielding

$$a_c = \frac{\pi}{\sqrt{2}}, \tag{45}$$

and the corresponding critical Rayleigh number R_c is

$$R_c = \frac{27}{4}\pi^4 = 657.5,$$

which confirms the result in literature (e.g. Chandrasekhar, 1961).

Goyal & Garg (2015) showed that in the limit $Ta = 0$ the Soret parameter has both the stabilizing and destabilizing effects on stationary modes according to $Le < Du$ or $Le > Du$. The condition for the Soret parameter to be stabilizing arises when

$$\frac{\partial R_T^{st}}{\partial Sr} > 0.$$

That is when

$$\begin{aligned} \frac{\partial R_T^{st}}{\partial Sr} &= \frac{(\pi^2 + a^2)^3 + Ta\pi^2}{a^2}\left(\frac{Du}{DuLe - 1}\right) + R_s\left(\frac{1}{DuLe - 1}\right) \\ &> 0. \end{aligned} \tag{46}$$

This gives the condition $Du > 1/Le$, with $Ta = 0$ for the Soret parameter to be stabilizing.

Furthermore, Goyal & Garg (2015) found that the Dufour parameter has stabilizing effect for $Le \neq Du$. In a similar manner the Dufour parameter stabilizes if and only if

$$\begin{aligned} \frac{\partial R_T^{st}}{\partial Du} &= \left[\frac{(\pi^2 + a^2)^3 + Ta\pi^2}{a^2} + LeR_S\right]\left[\frac{Le - Sr}{(1 - DuLe)^2}\right] \\ &> 0 \end{aligned} \tag{47}$$

meaning $Le > R_S$, with $Ta = 0$, for the Dufour parameter to be stabilizing.

The question that arises is why are we getting completely different results. The answer lies in their equation (17) and our equation (13). We scaled our equations with κ_T whereas they

used κ_S for scaling. We are convinced that if the nondimensional parameters were the same, we would get the same results.

We show graphically the effect of cross diffusive parameters Sr and Du as well as that of rotation in Figures 1 and 2.

3.2 Oscillatory convection

It is well known that the oscillatory motions are possible only if some additional constraints like rotation, salinity gradient and magnetic field are present. Consider the oscillatory mode, $\sigma_i = i\omega$. Substituting $\sigma_i = i\omega$ into (39) and imposing the condition $\omega^2 > 0$, which is the requirement for ω to be real in order to get overstability possible at all, yields two algebraic equations by requiring the imaginary and the real part of (39) to vanish separately. This provides the solution for the characteristic values of the Rayleigh number and the frequency ω of the oscillations at the margin of stability, so that (39) becomes

$$\begin{aligned} R_T^{osc} &= \frac{\left\{J^2\left(J^2-\frac{\omega^2}{Pr^2}\right)+Ta\ \pi^2+i\frac{2J^4}{Pr}\omega\right\}\left\{J^4Le^{-1}(Du\ Sr-1)+\omega^2-iJ^2(1+Le^{-1})\omega\right\}}{a^2\left\{J^4(Du-Le^{-1})+\frac{\omega^2}{Pr}+i\left(\frac{Du-Le^{-1}}{Pr}-1\right)J^2\omega\right\}} \\ &+ \frac{R_S\ a^2\left\{J^4(Sr\ Le^{-1}-1)+\frac{\omega^2}{Pr}+i\left(\frac{Sr\ Le^{-1}-1}{Pr}-1\right)J^2\omega\right\}}{a^2\left\{J^4(Du-Le^{-1})+\frac{\omega^2}{Pr}+i\left(\frac{Du-Le^{-1}}{Pr}-1\right)J^2\omega\right\}}, \end{aligned} \tag{48}$$

which is of the form

$$R_T^{osc} = \frac{(a_1+ib_1\omega)(a_2-ib_2\omega)+(a_3+ib_3\omega)}{(a_0+ib_0\omega)}, \tag{49}$$

where

$$\begin{aligned} a_0 &= a^2\left\{J^4(Du-Le^{-1})+\frac{\omega^2}{Pr}\right\}, \qquad b_0 = a^2\left\{\frac{Du-Le^{-1}}{Pr}-1\right\}J^2, \\ a_1 &= J^2\left(J^2-\frac{\omega^2}{Pr^2}\right)+Ta\ \pi^2, \qquad b_1 = \frac{2J^4}{Pr}, \\ a_2 &= J^4Le^{-1}(Du\ Sr-1)+\omega^2, \qquad b_2 = J^2(1+Le^{-1}), \\ a_3 &= R_S\ a^2\left\{J^4(Sr\ Le^{-1}-1)+\frac{\omega^2}{Pr}\right\}, \qquad b_3 = R_S\ a^2\left(\frac{Sr\ Le^{-1}-1}{Pr}-1\right)J^2, \end{aligned} \tag{50}$$

where R_T^{osc} is the Rayleigh number for the oscillatory convection. Equation (49) can further be reduced to the form

$$R_T = \Delta_1 + i\omega\Delta_2,$$

where

$$\begin{aligned}\Delta_1 &= \frac{a_0(a_1a_2 + b_1b_2\omega^2 + a_3) + b_0(b_1a_2 - a_1b_2 + b_3)\omega^2}{a_0^2 + b_0^2\omega^2} \\ \Delta_2 &= \frac{a_0(b_1a_2 - a_1b_2 + b_3) - b_0(a_1a_2 + b_1b_2\omega^2 + a_3)}{a_0^2 + b_0^2\omega^2}.\end{aligned} \tag{51}$$

Since R_T is always real, this implies $\mathrm{Im}(R_T) = 0$, or simply that $\Delta_2 = 0$. That is,

$$a_0(b_1a_2 - a_1b_2 + b_3) - b_0(a_1a_2 + b_1b_2\omega^2 + a_3) = 0. \tag{52}$$

Thus we have

$$c_0(\omega^2)^2 + c_1(\omega^2) + c_2 = 0, \tag{53}$$

where

$$\begin{aligned}c_0 &= J^4(3 + Du - Pr), \\ c_1 &= PrJ^8(Du - Le^{-1})(3 + Le^{-1}) + 2J^8Le^{-1}(Du\ Sr - 1) - PrJ^2(1 + Le^{-1})(J^4 + Ta\ \pi^2), \\ &- J^2(Du - Le^{-1} - Pr)\{Pr(J^4 + Ta\ \pi^2) - J^6Le^{-1}(Du\ Sr - 1) + 2J^6(1 + Le^{-1}) + R_S\ a^2\} \\ &+ R_S\ a^2J^2(Sr\ Le^{-1} - Pr - 1), \\ c_2 &= PrJ^4(Du - Le^{-1})\left\{2J^8Le^{-1}(DuSr - 1) - PrJ^2(1 + Le^{-1})(J^4 + Ta\pi^2)\right\} \\ &+ R_Sa^2J^6Pr\left\{(Du - Le^{-1})(SrLe^{-1} - Pr - 1) - (Du - Le^{-1} - Pr)(SrLe^{-1} - 1)\right\} \\ &- J^2(Du - Le^{-1} - Pr)\left\{Pr(J^4 + Ta\ \pi^2)J^2Le^{-1}(Du\ Sr - 1)\right\}.\end{aligned} \tag{54}$$

Now the expression for R_T^{osc} is given by

$$R_T^{osc} = \frac{a_0(a_1a_2 + a_3) + \{a_0b_1b_2 + b_0(b_1a_2 - a_1b_2 + b_3)\}\omega^2}{a_0^2 + b_0^2\omega^2}, \tag{55}$$

where ω^2 is the minimum positive root of the dispersion relation (53). Figures 4-8 demonstrate the effect of each of the parameters Sr, Du, Ta, R_S, Pr and Le on oscillatory convection.

4 Weakly Nonlinear Stability Analysis

In this section we study nonlinear stability analysis using a minimal truncated representation of a Fourier series consisting of two terms. As the linear stability analysis fails to provide

insight about the convection amplitudes and the rate of heat and mass transfer we revert to the nonlinear stability analysis. We return to equation (15)

$$\frac{1}{Pr}\left\{\frac{\partial \vec{q}}{\partial t}+(\vec{q}\cdot\nabla)\vec{q}\right\}=-\nabla p+(R_T\theta-R_S\phi)\hat{k}+\nabla^2\vec{q}-\sqrt{Ta}\;\hat{k}\times\vec{q}$$

since $\vec{q}=(u,v,w)$ we have $\hat{k}\times\vec{q}=-v\hat{i}+u\hat{j}$, thus (15) becomes

$$\frac{1}{Pr}\left\{\frac{\partial \vec{q}}{\partial t}+(\vec{q}\cdot\nabla)\vec{q}\right\}=-\nabla p+(R_T\theta-R_S\phi)\hat{k}+\nabla^2\vec{q}+\sqrt{Ta}\;(v\hat{i}-u\hat{j}). \tag{56}$$

We restrict the analysis to the case of 2D rolls so that all the physical quantities are independent of y and the equations in component form reduce to

$$\frac{1}{Pr}\left\{\frac{\partial u}{\partial t}+u\frac{\partial u}{\partial x}+w\frac{\partial u}{\partial z}\right\}=-\frac{\partial p}{\partial x}+\frac{\partial^2 u}{\partial x^2}+\frac{\partial^2 u}{\partial z^2}+Ta^{1/2}v, \tag{57}$$

$$\frac{1}{Pr}\left\{\frac{\partial v}{\partial t}+u\frac{\partial v}{\partial x}+w\frac{\partial v}{\partial z}\right\}=\frac{\partial^2 v}{\partial x^2}+\frac{\partial^2 v}{\partial z^2}-Ta^{1/2}u, \tag{58}$$

$$\frac{1}{Pr}\left\{\frac{\partial w}{\partial t}+u\frac{\partial w}{\partial x}+w\frac{\partial w}{\partial z}\right\}=-\frac{\partial p}{\partial z}+\frac{\partial^2 w}{\partial x^2}+\frac{\partial^2 w}{\partial z^2}+R_T\theta-R_S\phi, \tag{59}$$

and the continuity equation becomes

$$\frac{\partial u}{\partial x}+\frac{\partial w}{\partial z}=0.$$

Differentiating (57) with respect to z and (59) with respect to x and subtracting we get

$$\begin{aligned}&\frac{1}{Pr}\left\{\frac{\partial}{\partial t}\left(\frac{\partial u}{\partial z}-\frac{\partial w}{\partial x}\right)+\left(u\frac{\partial}{\partial x}+w\frac{\partial}{\partial z}\right)\left(\frac{\partial u}{\partial z}-\frac{\partial w}{\partial x}\right)\right\}\\ =\;&\left(\frac{\partial^2}{\partial x^2}+\frac{\partial^2}{\partial z^2}\right)\left(\frac{\partial u}{\partial z}-\frac{\partial w}{\partial x}\right)+Ta^{1/2}\frac{\partial v}{\partial z}-R_T\frac{\partial \theta}{\partial z}+R_S\frac{\partial \phi}{\partial x}.\end{aligned} \tag{60}$$

We now introduce the two-dimensional stream function $\psi(x,z)$ such that

$$u=\frac{\partial \psi}{\partial z}\quad w=-\frac{\partial \psi}{\partial x},$$

then the continuity equation is trivially satisfied and further

$$\frac{\partial u}{\partial z}-\frac{\partial w}{\partial x}=\frac{\partial^2\psi}{\partial z^2}+\frac{\partial^2\psi}{\partial x^2}=\nabla^2\psi.$$

Thus equation (60) takes the form

$$\frac{1}{Pr}\left\{\frac{\partial}{\partial t}(\nabla^2\psi)-\frac{\partial(\psi,\nabla^2\psi)}{\partial(x,z)}\right\}=\nabla^4\psi+Ta^{1/2}\frac{\partial v}{\partial z}-R_T\frac{\partial \theta}{\partial x}+R_S\frac{\partial \phi}{\partial x}, \tag{61}$$

and equation (57) becomes

$$\frac{1}{Pr}\left\{\frac{\partial v}{\partial t}-\frac{\partial(\psi,v)}{\partial(x,z)}\right\}=\nabla^2 v-Ta^{1/2}\frac{\partial\psi}{\partial z}. \tag{62}$$

Similarly, by expressing $\theta=\theta(x,z)$ and $\phi=\phi(x,z)$ and using the stream function we obtain from (16) and (17), respectively,

$$\frac{\partial\theta}{\partial t}-\frac{\partial(\psi,\theta)}{\partial(x,z)}+\frac{\partial\psi}{\partial x}=\nabla^2\theta+Du\ \nabla^2\phi, \tag{63}$$

and

$$\frac{\partial\phi}{\partial t}-\frac{\partial(\psi,\phi)}{\partial(x,z)}+\frac{\partial\psi}{\partial x}=Le^{-1}(\nabla^2\phi+Sr\nabla^2\theta). \tag{64}$$

A minimal double Fourier series describing the finite amplitude convection is given by

$$\psi(x,z,t)=A(t)\sin(ax)\sin(\pi z), \tag{65}$$

$$\theta(x,z,t)=B(t)\cos(ax)\sin(\pi z)+C(t)\sin(2\pi z), \tag{66}$$

$$\phi(x,z,t)=D(t)\cos(ax)\sin(\pi z)+E(t)\sin(2\pi z), \tag{67}$$

$$v(x,z,t)=F(t)\sin(ax)\cos(\pi z)+G(t)\sin(2\pi z), \tag{68}$$

where $A(t), B(t), D(t), E(t), F(t)$ and $G(t)$ are time dependent amplitudes. Substituting in (62) to (64), the following set of equations is obtained:

$$\frac{dA}{dt}=\frac{Pr}{J^2}\{-J^4A+\pi Ta^{1/2}F-aR_TB+aR_SD\}, \tag{69}$$

$$\frac{dF}{dt}=Pr\{-J^2F-\pi Ta^{1/2}A\}, \tag{70}$$

$$\frac{dB}{dt}=-aA-J^2B-J^2Du\ D-\pi aAC, \tag{71}$$

$$\frac{dC}{dt}=\pi a\frac{AB}{2}-4\pi^2C-4\pi^2Du\ E, \tag{72}$$

$$\frac{dD}{dt}=-aA-Le^{-1}J^2D-Le^{-1}Sr\ J^2B-\pi aAE, \tag{73}$$

$$\frac{dE}{dt}=\pi a\frac{AD}{2}-4\pi^2Le^{-1}E-4\pi^2Le^{-1}SrC. \tag{74}$$

Let us define the following new variables

$$X_1=\frac{\pi a}{J^2}A,\quad X_2=-\pi RB,\quad X_3=-\pi RC,\quad X_4=-\pi RD,$$

$$X_5 = -\pi RE, \quad X_6 = \frac{\pi^2 a Ta^{1/2}}{J^6} F, \quad R = \frac{a^2}{J^6} R_T, \quad b = \frac{4\pi^2}{J^2}, \quad \tau = J^2 t.$$

Then we arrive at the following system of coupled nonlinear equations

$$\begin{aligned}
\frac{dX_1}{d\tau} &= Pr(-X_1 + X_2 - NX_4 + X_6), \\
\frac{dX_2}{d\tau} &= RX_1 - X_2 - Du\ X_4 - X_1 X_3, \\
\frac{dX_3}{d\tau} &= \frac{X_1 X_2}{2} - b(X_3 + Du\ X_5), \\
\frac{dX_4}{d\tau} &= RX_1 - Le^{-1} Sr X_2 - Le^{-1} X_4 - X_1 X_5, \\
\frac{dX_5}{d\tau} &= \frac{X_1 X_4}{2} - b\ Le^{-1}(Sr\ X_3 + X_5), \\
\frac{dX_6}{d\tau} &= -Pr(Ta^* X_1 + X_6),
\end{aligned} \tag{75}$$

where $N = \frac{R_S}{R_T} = \frac{\alpha_S \Delta S}{\alpha_T \Delta T}$ is the buoyancy ratio, $Ta^* = \frac{\pi^2}{J^6} Ta$.

The solution of equations (75) are uniformly bounded in time and have many characteristics of the initial problem. Also, the system (75) is dissipative with the volume in phase-space contracting at a uniform rate given by

$$\begin{aligned}
&\frac{\partial}{\partial X_1}\left(\frac{dX_1}{d\tau}\right) + \frac{\partial}{\partial X_2}\left(\frac{dX_2}{d\tau}\right) + \frac{\partial}{\partial X_3}\left(\frac{dX_3}{d\tau}\right) + \frac{\partial}{\partial X_4}\left(\frac{dX_4}{d\tau}\right) + \frac{\partial}{\partial X_5}\left(\frac{dX_5}{d\tau}\right) + \frac{\partial}{\partial X_6}\left(\frac{dX_6}{d\tau}\right) \\
= \ & -[2Pr + (1 + Le^{-1})(1 + b)],
\end{aligned} \tag{76}$$

which is always negative, and therefore the system is bounded and dissipative. As a result, the trajectories are attracted to a set of measure zero in the phase space; in particular, they may be attracted to a fixed point, a limit cycle or perhaps a strange attractor. From equation (76) we conclude that if a set of initial points in phase space occupies a region $V(0)$ at time $\tau = 0$, then after some time τ, the end points of the corresponding trajectories will fill the volume (Gaikwad *et al.*, 2007)

$$V(\tau) = V(0) \exp\left[-(2Pr + (1 + Le^{-1})(1 + b))\tau\right]. \tag{77}$$

This expression indicates that the volume decreases exponentially with time. We can also infer that the Prandtl number, Pr, enhances dissipation.

Figures 11-18 depict the different bifurcation diagrams we obtain for different of set of parameters.

5 Fixed Point Analysis

Setting $\dot{X}_1 = \dot{X}_2 = \dot{X}_3 = \dot{X}_4 = \dot{X}_5 = \dot{X}_6 = 0$, we have six possible solutions. One solution which is always present is $X_1 = X_2 = X_3 = X_4 = X_5 = X_6 = 0$. If we linearize about this solution we obtain

$$\frac{d}{d\tau}\begin{bmatrix}\delta X_1\\ \delta X_2\\ \delta X_3\\ \delta X_4\\ \delta X_5\\ \delta X_6\end{bmatrix} = \begin{bmatrix} -Pr & Pr & 0 & -N*Pr & 0 & Pr \\ R & -1 & 0 & -Du & 0 & 0 \\ 0 & 0 & -b & 0 & -b*Du & 0 \\ R*-Le^{-1}*Sr & 0 & -Le^{-1} & 0 & 0 & 0 \\ 0 & 0 & -b*Le^{-1}Sr & 0 & -b*Le^{-1} & 0 \\ -Pr*Ta^* & 0 & 0 & 0 & 0 & -Pr \end{bmatrix}\begin{bmatrix}X_1\\ X_2\\ X_3\\ X_4\\ X_5\\ X_6\end{bmatrix} \tag{78}$$

The Jacobian matrix of our system is given by

$$J = \begin{bmatrix} -Pr & Pr & 0 & -N*Pr & 0 & Pr \\ R & -1 & 0 & -Du & 0 & 0 \\ 0 & 0 & -b & 0 & -b*Du & 0 \\ R*-Le^{-1}*Sr & 0 & -Le^{-1} & 0 & 0 & 0 \\ 0 & 0 & -b*Le^{-1}Sr & 0 & -b*Le^{-1} & 0 \\ -Pr*Ta^* & 0 & 0 & 0 & 0 & -Pr \end{bmatrix} \tag{79}$$

To find the fixed points we determine $\det[J] \neq 0$ for different values of the parameters.

Due to the variation of many parameters, depending on the combination we get different eigenvalues and thus different reaction of the system towards these small variations. For the parameters $R = 100$, $Du = 0.03$, $Sr = 2$, $Le = 0.0125$, $Ta = 0.48$, $Pr = 13.4$, the eigenvalues of the system are given by $\lambda_1 = -213.762, \lambda_2 = -14.4517 + 90.205i, \lambda_3 = -14.4517 - 90.205i, \lambda_4 = 80.3187, \lambda_5 = -2.5079, \lambda_6 = 0.78472$. In this case the system is oscillatory and unstable. For the parameters, $R = 10^4, Le = 2.59, Pr = 13.4, Du = 12, Sr = 0.005$ and $Ta = 0.48$ the eigenvalues are given by $\lambda_1 = -372.779, \lambda_2 = 345.856, \lambda_3 = -13.4003, \lambda_4 = 12.9095, \lambda_5 = -2.76522$ and $\lambda_6 = -0.935665$, system is unstable and the fixed point is a saddle node. As it can been seen here that it is not straightforward to make any conclusions about the nonlinear stability of the system as a set of parameters, yield a different result from a previous set of parameters.

Furthermore, we let $p = \text{trace}[J]$ and $q = \det[J]$. For $p > 0$ and $q > 0$, we expect to obtain the repellors; saddle points when $p > 0$ and $q < 0$ and also when $p < 0$ and $q < 0$. Attractors are obtained for $p < 0$ and $q > 0$. In the analysis of fixed points related to Figure 11 and Figure 12, we obtain $p < 0$ and $q < 0$ which gives us saddle points. Figure 14 shows the first three diagrams as saddle point whereas the figure corresponding to $Ta = 10^3$ depicts an attractor. For Figure 14 representing the effect of Rayleigh number on nonlinear stability, when all parameters are considered the system has $q > 0$ and $p < 0$ implying that we have attractors. The variation of the Lewis number yields saddle points and attractors for the values considered in Figure 16, whereas the parameter values considered to reproduce Figure 17, give $q < 0$ and $p < 0$ thus yielding saddle points.

In Figures, 11 and 12, we show various phase portraits generated from (X_i, X_i')-plane of some of the solution sets corresponding to different sets of parameters.

6 Heat and Mass Transports

The rate of heat and mass transport per unit area, respectively, denoted by H and J are given by

$$H = -\kappa_T \langle \frac{\partial T_{total}}{\partial z} \rangle_{z=0} - D_{TS} \langle \frac{\partial S_{total}}{\partial z} \rangle_{z=0}, \tag{80}$$

$$J = -\kappa_S \langle \frac{\partial S_{total}}{\partial z} \rangle_{z} - D_{ST} \langle \frac{\partial T_{total}}{\partial z} \rangle_{z=0}, \tag{81}$$

where the angular bracket corresponds to a horizontal average and z is the dimensionless space variable. The total temperature and salinity, T_{total} and S_{total} are given by

$$T_{total} = T_0 - (\Delta T)z + (\Delta T)\theta(t, x, z), \tag{82}$$

$$S_{total} = S_0 - (\Delta S)z + (\Delta S)\phi(t, x, z). \tag{83}$$

Substituting equations (66) and (67) we obtain

$$T_{total} = T_0 - (\Delta T)z + \Delta T[B(t)\cos(ax)\sin(\pi z) + C(t)\sin 2\pi z], \tag{84}$$

$$S_{total} = S_0 - (\Delta S)z + \Delta S[D(t)\cos(ax)\sin(\pi z) + E(t)\sin 2\pi z], \tag{85}$$

and using equations (80) and (81) we arrive at

$$H = \Delta T[\kappa_T(1 - 2\pi C) + D_{TS}(1 - 2\pi E)], \tag{86}$$

$$J = \Delta S[\kappa_S(1 - 2\pi E) + D_{ST}(1 - 2\pi C)]. \tag{87}$$

The Nusselt and Sherwood numbers are respectively defined by

$$Nu = \frac{H}{\kappa_T \Delta T} = (1 - 2\pi C) + Du(1 - 2\pi E), \tag{88}$$

$$Sh = \frac{J}{\kappa_S \Delta S} = (1 - 2\pi E) + Sr(1 - 2\pi C). \tag{89}$$

Using on the scaled variable $(X_3, X_5) = -\pi R(C, E)$ we obtain

$$Nu = \left(1 + \frac{2}{R}X_3\right) + Du\left(1 + \frac{2}{R}X_5\right), \tag{90}$$

$$Sh = \left(1 + \frac{2}{R}X_5\right) + Sr\left(1 + \frac{2}{R}X_3\right). \tag{91}$$

It is to be noted here that the Nusselt and Sherwood numbers both depend on X_1 and X_5.

Figures 19a and 19b depict the effect of cross diffusive terms on heat and mass transport. Figures 20a-23b show the effects of the other parameters on the Nusselt and the Sherwood numbers.

7 Results and Discussion

The purpose of this investigation was to study thermohaline circulation which is important in mixing processes and it contributes to the earth's climate and heat and mass transports. In this study, the onset of thermohaline convection in a rotating fluid as affected by both Soret and Dufour parameters has been investigated using normal modes linear analysis and weakly nonlinear analysis. Analytical expressions for the critical Rayleigh number and the corresponding wavenumbers for the onset of stationary convection subject to cross diffusive effects were determined using linear stability theory. It is shown here that both salinity and rotational effects have significant stabilizing effect on stationary convection confirming the results found in literature. The effect of cross diffusive factors is here discussed and summarized.

Our study shows that the Soret parameter stabilizes stationary convection significantly whereas the Dufour parameter has minimal effect (as seen in Figures 20b and 21a).

In the analysis of oscillatory convection our study shows that the critical Rayleigh number for the onset of convection depends on six parameters, the Prandtl number Pr, Soret parameter Sr, Dufour parameter Du, Taylor number or rotation parameter Ta, Lewis number Le and the salinity Rayleigh number R_s. In the ocean, the Lewis number, Le is 0.0125, The Prandtl number $Pr = 13.4$ for 0° Celsius and $Pr = 7.2$ for water temperature 20° Celsius. The Rayleigh number R_T can reach up to 10^{24} depending on the molecular value (Vallis, 2006). In this analysis we used smaller values to validate the results as the use of big numbers create a computational difficulty. Since the system depends on such a big number of parameters, it thus requires some robustness to clearly understand the effect of cross diffusive factors.

The effect of rotation and Soret parameter on the oscillatory convection is shown in Figure 4. We find that when we increase Ta the critical value of the Rayleigh number and the corresponding wavenumber also increase implying that the rotation has a stabilizing effect on the thermohaline convection. This means that rotation acts so as to suppress vertical motion, and hence thermohaline convection, by restricting the motion to the horizontal plane (Malashetty, 2008). Furthermore, Figure 4 also indicates that for small Ta the instability manifests as stationary convection while as Ta is increased, the instability sets in as oscillatory convection. We also observe that Soret parameter stabilizes for both negative and positive Sr.

Figure 5 shows the effect of rotation and Dufour parameter on the oscillatory convection. We observed that an increase in the Dufour parameter shows an decrease in the critical Rayleigh number and hence delaying the oscillatory convection. The effect of rotation stabilizes for different values of Dufour parameter.

The variation of critical Rayleigh number for oscillatory modes with salinity Rayleigh number R_S for different values of rotation parameters is shown in Figure 6. We observe from Figure 1 that the critical Rayleigh number increases with increase in the value of the salinity Rayleigh number indicating that the salinity Rayleigh number delays the onset of convection.

The effect of Lewis number on the stability is shown in Figure 7. We find that Lewis number has

a more stabilizing effect for small values whereas for large values stabilizing effect is negligible. In the case of the ocean where the Lewis number is 0.0125. Thus the Lewis number is a stabilizing factor.

The variation of critical oscillatory Rayleigh number for different values of Prandtl number and Taylor number with all other parameters kept fixed is revealed in Figure 8. It is clear that the critical value of oscillatory Rayleigh number decreases with the increase in the values of Prandtl number indicating that it has a destabilizing effect on the system. One can also observe that the critical Rayleigh number of overstable mode almost levels off for large Prandtl number values meaning that after some stage increasing the Prandtl number will not have any significant effect in controlling the stability of the system. It is also observed through the computation that regime of overstable solutions bifurcating into the stationary solutions shifts towards larger wavenumber region, for increasing values of the Prandtl number. Therefore the Prandtl number increases the oscillatory convection region. However, the reverse effect has been observed with the Taylor number.

A minimal representation of Fourier series has been employed for a weakly nonlinear stability analysis that resulted in a sixth order generalised Lorenz model. The characterization of chaotic solutions is quite difficult and involves seven parameters- Lewis number, salinity Rayleigh number, Prandtl number, thermal Rayleigh number, Taylor number, Soret and Dufour parameters. Figures 11-18 show the evolution of the Lorenz equations when these parameters are varied at various planes. These equations exhibit very interesting diagrams some of which we have not seen anywhere in literature.

Figure 9 depicts the phase portraits mapped onto (X_i, X_i')-plane for X_1, X_2, X_3 and X_4 respectively. As we can se that for X_1 the system starts from the origin and ends at the origin, but for X_2 and X_4 the path followed stays at the origin for a while but then leaves the orgin from two exit points. For X_3 the solution starts from the origin and stabilizes at some point. Figure 10 depicts the amplitude solutions for X_1, X_2, X_3 and X_4 respectively at different values of the Rayleigh parameter. This shows that for any parameter that we vary, we are likely to get very interesting results and different amplitude behaviours.

The variation of the Dufour parameter on the (X_3, X_4)-plane yields Lorenz's "butterfly" effect as shown in Figures 11. This shows that the Dufour parameter has significant effect on the stability of the nonlinear system (75). It has also been shown in Figure 12 that the Lorenz equations when projected on the (X_1, X_2) and the Soret parameter is varied, exhibit chaotic solutions like a process of making "woven fruit bowl". When the Soret parameter is increased, the system stabilizes. An increase in the Taylor number, representing the rotational effect, causes the Lorenz equation to exhibit the spiral-like form for lower Ta values and a "tornado-like" motion as Ta is increased and dies down exhibiting a "woven fruit bowl" albeit different from that in the case of the Soret effect for very large values as demonstrated in Figure 13. The Rayleigh parameter R when varied shows that the Lorenz equations when projected on the (X_3, X_4)-plane initially displays a chaotic solution from whom a "Beetle"-like structure develops, and as if it opens its "mouth" it degenerates into a stable ellipse as R increases as shown in Figure 14. The system is chaotic at small values of the Rayleigh number, but stabilizes to an ellipse when the Rayleigh number is increased. In this Figure 14 however, the Lewis number is taken at $Le = 2.59$ which is higher than that of the seawater. When we consider the Lewis number for seawater $Le = 0.0125$ the system still exhibit very interesting bifurcations. At $R = 100$ Lorenz's butterfly evolves, but with the increase in R that butterfly disintegrates and at $R = 10^6$ a "bat-like" bifurcation is observed. At a further increase in R, the "bat" attractor disintegrates again and the system stabilizes into an ellipse.

Figures 16 and 17 show respectively, the sensitivity of the Lorenz equations to the Lewis number and the Prandtl number. It is shown here that the Lewis number destabilizes whereas the Prandtl number stabilizes. In all cases we have demonstrated that chaotic solutions exists when a two-phase space. However, in Figure 18 we observe similar chaotic structures in 3D phase space. Some of these bifurcations we have not seen in literature before.

Heat and mass transports were determined with the help of weakly nonlinear theory. The Figures (19a) and (19b) simplify the findings for the heat and mass transfer. Figure (19a) shows that the increase in the Dufour parameter enhances heat transport and Figure (19b) clearly demonstrates that the Soret parameter affects mass transport negatively. We also investigated the effect of other parameters the Prandtl, Taylor, Lewis and Rayleigh numbers

in Figures 20a-22b on heat and mass trasports. It is clear in Figure 20a and 20b that the increase in the rotational parameter, Ta reduces both the Nusselt and Sherwood numbers thus showing a negative contribution to heat and mass transports. The Lewis number on the other hand, enhances heat and mass trasports as shown in Figures 21a and 21b that an increase in Lewis number, increases both the Nusselt and Sherwood numbers. The Rayleigh number and the Prandtl number show no contribution to the Nusselt and Sherwood numbers as depicted in Figures 22a- 23b.

8 Conclusion

The effect of Soret and Dufour parameters on thermohaline convection in rotating fluids, which is heated and salted from below, is investigated analytically using the linear and nonlinear theories. We applied the usual normal mode technique to solve the linear problem. The minimal double Fourier series method is used to make the finite amplitude analysis. The following conclusions are drawn:

The effect of Dufour parameter is to stabilize in both stationary and oscillatory convection. The Soret parameter enhances oscillatory convection and delays stationary convection. The Lewis number advances oscillatory convection whereas the salinity Rayleigh number delays the onset of both stationary and oscillatory convection. The rotation parameter is always acting as a stabilizing factor.

Nonlinear analysis depends on six parameters, Soret, Dufour, Taylor, Rayleigh, Lewis and Prandtl numbers. The Lorenz system obtained exhibit various chaotic solutions when projected on various X_i planes showing that nonlinear dynamical systems can behave in complex ways. We have thus demonstrated here that the stability of the thermohaline convection is unpredictable under various parameters.

The results obtained show that chaotic motions occur in rotating diffusive flows. The Soret, Lewis and Taylor numbers have significant influence on both the existence and form of the chaotic responses.

The Dufour parameter and the Lewis number enhance heat transport whereas Soret parameter reduces the mass transport. The Rayleigh number, Taylor number and the Prandtl numbers have no influence to the heat and mass transports.

References

[1] Alam, M. S. and Rahman, M. M. Dufour and Soret effects on mixed convection flow past a vertical porous plate with variable suction. *Nonlinear Analysis: Modelling and Control*, 2006, **11(1)**, 3-12.

[2] Alloui, I., Benmoussa H., Vasseur, P. Soret and thermosolutal effects on natural convection in shallow cavity filled with a binary mixture. *Int. J. Heat and Fluid Flow*, 2010, **31**, 191-200.

[3] Awad, F.G. and Sibanda, P., Dufour and Soret Effects on heat and mass transfer in a micropolar fluid in a horizontal channel. *WSEAS Transactions on Heat and Mass Transfer*, 2010, **5** (3), 165-177.

[4] Awad, F.G., Sibanda, P. and Motsa, S.S., On the linear stability analysis of a Maxwell fluid with double-diffusive convection. *Appl. Math. Modelling*, 2010, **34**, 3509-3516.

[5] Awad, F.G., Sibanda, P., Motsa, S.S. and Makinde, O.D., Convection from an inverted cone in a porous medium with cross-diffusion effects. *Computers and Mathematics with Applications*, 2011, **61**, 1431-1441.

[6] Baines, P. G. and Gill, A. E. On Thermohaline convection with linear gradients. *J. Fluid Mech.*, 1969, **37 (2)**, 289-306.

[7] Barnejee, M. B., Gupta, J. R., Shandil, R. G., Sharma, K. C. and Katoch, D. C. A modified analysis of thermal and thermohaline instability of a liquid layer heated underside. *J. Math. Phys. Sci.*, 1983, **17 (6)**, 603-629.

[8] Barnejee, M. B., Gupta, J. R., Shandil, R. G., Sood, S. K., Sharma, K. C. and Katoch, D. C. A modified analysis of thermal and thermohaline instability of a liquid layer II. The effect of rotation. *J. Math. Phys. Sci.*, 1988, **22**, 457-474.

[9] Barnejee, M. B., Gupta, J. R. and Prakash, J. On thermohaline convection of the Veronis type. *J. Math. Anal and Appl.*, 1993, **179**, 327-334.

[10] Barnejee, M. B., Shandil R. G., Lal, P., and Kanwar, V. A mathematical theorem in rotatory thermohaline convection. *J. Math. Anal and Appl.*, 1995, **189**, 351-361.

[11] Basu, R. and Layek, G.C. Influences of cross-diffusive coefficients on the onset of double diffusive convection in a horizontal fluid layer. *Int. J. of Appl. Math and Mech.*, 2013, **9 (6)**, 86-107.

[12] Burroughs, W.J., *Climate Change: A multidisciplinary approach.* 2nd ed. 2007 (Cambridge, Cambridge Press).

[13] Caldwell, D. R. Experimental studies on the onset of thermohaline convection. *J. Fluid Mech.*, 1974, **64**, 347-367.

[14] Chand, R. and Rana, G.C., Dufour and Soret Effects on the Thermosolutal Instability of Rivlin-Ericksen Elastico-Viscous Fluid in Porous Medium. *Z. Naturforsch.* 2012, **69**a, 685-691. DOI:10.5560/ZNA.2012-0074

[15] Chand, R. and Rana, G.C., Double Diffusive Convection in a layer of Maxwell Viscoelastic Fluid in Porous Medium in the presence of Soret and Dufour Effects. *J. Fluids*, **2014**, Article ID 479107, 7 pages, DOI:10.1155/2014/479107

[16] Chand, R. and Rana, G.C., Magento Convection in a layer of nanofluid with Soret effect. *Acta Mechanica et Automatica*,2015, **9**(2), 63-69

[17] Chandrasekhar, S. Hydrodynamic and hydromagnetic stability, 1961 (Oxford Univ. Press, Oxford).

[18] Drazin, P. G. and Reid, W. H. Hydrodynamic stability, Second Edition, 2004. (Cambridge Univ. Press, London/New York).

[19] Eckert, E. R. G. and Drake, R. M. Analysis of heat and mass transfer, 1972. (McGraw-Hill, New York).

[20] Gaikwad, S. N., Malashetty, M. S., Rama Presad, K. An analytical study of linear and nonlinear double diffusive convection with Soret and Dufour effects in couple stress fluid. *Int. J. Nonlinear Mechanics*, 2007, **42**, 903-913.

[21] Gaikwad, S. N., Malashetty, M. S. Rama Prasad, K. Linear and nonlinear double diffusive convection in a fluid saturated anisotropic porous layer with cross diffusive effects. *Transp. Porous Med.*, 2009, **80**, 537-560.

[22] Gbadeyan, J. A., Idowu, A. S., Ogunsola, A. W., Agboola, O. O. and Olanrewaju, P. O. Heat and mass transfer for Soret and Dufour's effect on mixed convection boundary layer flow over a stretching vertical surface in a porous medium filled with viscoelastic fluid in the presence of magnetic field. *Global J. Sci. Frontier Res.*, 2011, **11 (8)**, 97-114.

[23] Goyal M. R. and Garg B. P. (2015). Influences of Soret and Dufour effects on double-diffusive convection in a horizontal fluid layer. *J. Rajastan Academy of Phys. Sci.*, ISSN: 0972-6306; URL:https://raops.org.in **14 (2)**, 127-144.

[24] Gupta, J. R., Dhiman, J. S. and Thakur, J. Thermohaline convection of Veronis and Stern type revisited. *J. Math. Anal. and Appl.*, 2001, **264**, 398-407.

[25] Hayat, T., Naz R., Asghar, S., Alsaedi A. Soret-Dufour effects on MHD rotating flow of a viscoelastic fluid. *Int. J. Num. Meth. Heat and Fluid Flow*, 2014, **24 (2)**, 498-520.

[26] Huppert, H. E. and Turner, J. S. Double-diffusive convection. *J. Fluid Mech.*, 1981, *106*, 299-329.

[27] Malashetty, M. S. The Effect of rotation on the onset of double-diffusive convection in a horizontal anisotropic porous layer. *Transp Porous Med.*, 2008, **74** 105-127.

[28] Maleque, Kh A. Dufour and Soret effects on unsteady MHD convective heat and mass transfer flow due to a rotating disk. *Latin American Applied Research*, 2010, **40**, 105-111.

[29] Mohan, H. The Soret effect on the rotatory thermosolutal convection of the Veronis type. *J. Pure Appl. Math.*, 1996, **27 (6)**, 609-619.

[30] Motjabi, A. and Charrier-Motjabi, M.C., *Double diffusive convection in porous media. Handbook of Porous media*. 2nd edition, 2005.

[31] Nakagawa, Y. and Frenzen, P. A theoretical and experimental study of cellular convection in rotating fluids. *Tellus*, 1955, **7 (1)**, 1-21.

[32] Narayana, M., Sibanda, P., Siddeshwar, P. G. and Jayalatha, G. Linear and nonlinear stability analysis of binary viscoelastic fluid convection. *Appl. Math. Modelling*, 2013, **37**, 8162-8178.

[33] Polyakov, I. V., Pnyushkov, A. A., Rember, R and Ivanov, V. V. Mooring-based observations of double-diffusive staircases over the Laptev sea slope. *J. Phys. Oceanogr.*, 2012, **42**, 95-109.

[34] Radko, T., Bulters A., Flanagan, J. D. and Campin, J. -M. Double-diffusive Recipes. Part I: Large-scale dynamics of thermohaline staircases. *J. Phys. Oceangr.*, 2014, **44**, 1269-1284.

[35] Rajagopal, K. R., Saccomandi, G. and Vergori, L. On the Oberbeck-Boussinesq approximation for fluids with pressure dependent viscosities. *Nonlinear Analysis: Real World Applications*, 2009, **10**, 1139-1150.

[36] Rossby, H. T. A Study of Bénard convection with and without rotation. *J. Fluid Mech.*, 1969, **36 (2)**, 309-335.

[37] Schmitt R. W. Double Diffusive Convection. In: Encyclopaedia of Ocean Sciences, John H. Steele, Steve A. Thorpe, and Karl K. Turekian, Editors,
Academic Press, San Diego; 2001, **2**, 757-766.

[38] Schmittner, A. and Stocker, T.F., The Stability of the Thermohaline Circulation in Global Warming Experiments. *J. Climate*, 1999, **12**, 1117-1133.

[39] Stern, M. E. The salt fountain and thermohaline convection. *Tellus*, 1960, **12**, 172-175.

[40] Stommel, H., Arons, A. B. and Blanchard, D. An oceanographical curiosity: the perpertual salt fountain. *Deep Sea Research*, 1956, **3**, 152.

[41] Tagare, S. G., Raman Murthy, M. V. and Rameshwar, Y. Nonlinear thermohaline convection in rotating fluids. *Int. J. Heat and Mass Transfer*, 2007, **50**, 3122-3140.

[42] Turner, J. S. Buoyancy Effects in Fluids, 1973, (Cambridge University Press, London).

[43] Turner, J. S. Double-diffusive phenomena. *Annu. Rev. Fluid Mech.*, 1974, **6**, 37-56.

[44] Turner, J. S. Multicomponent convection, *Annu. Rev. Fluid Mech.*, 1985, **17**, 11-44.

[45] Vallis, G. Atmospheric and Oceanic Fluid Dynamics: Fundamentals and Large-scale Circulation, 2006 (Cambridge Press, New York)

[46] Veronis, G. On finite amplitude instability in thermohaline convection. *J. Mar. Res.*, 1965, **23**, 1-17

[47] Veronis, G. Large-amplitude Bénard convection in a rotating fluid. *J. Fluid Mech.*, 1968, **31 (1)**, 113-139.

[48] Wood, R.A., Vellinga, M. and Thorpe, R., Global warming and thermohaline circulation stability. *Phil. Trans. R. Soc. Lond. A*, 2003, 1961-1975

[49] Zhou, S. -Q. Qu, L., Lu, Y. -Z, Song, X. -L. The instability of diffusive convection and its implication for the thermohaline staircases in the deep Arctic ocean. *Ocean Sci.*, 2014, **10**, 127-134.

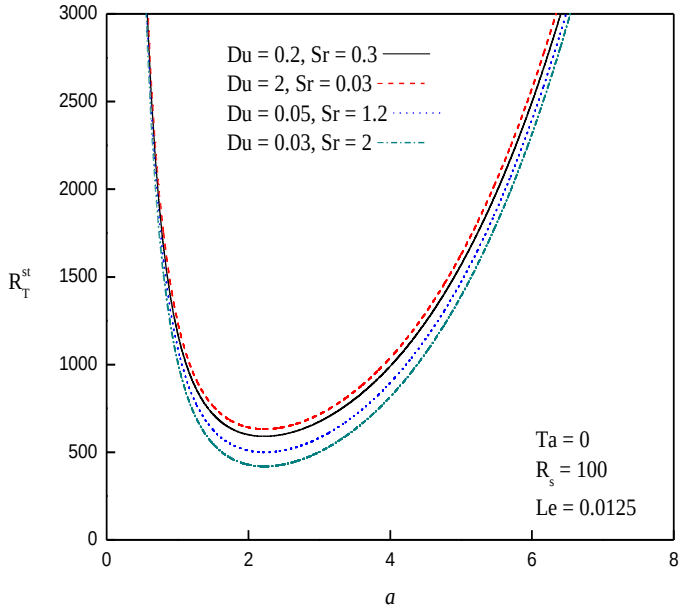

Figure 1: Effect of Dufour and Soret number on the stationary Rayleigh number R_T^{st}.

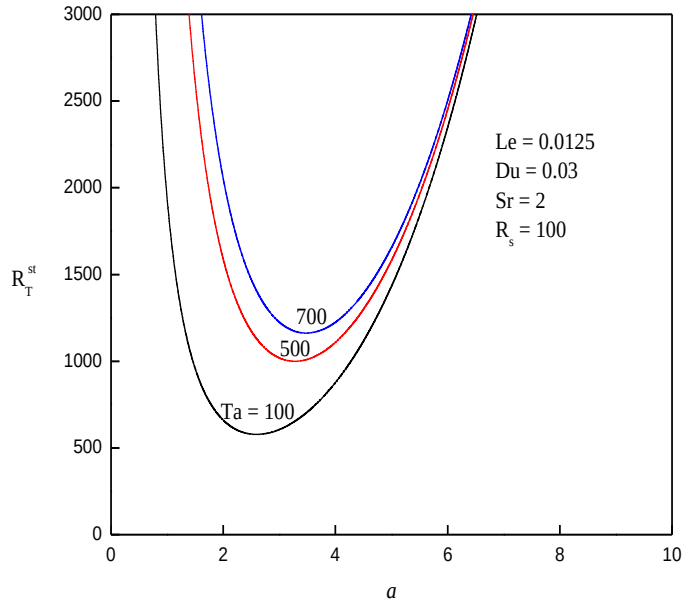

Figure 2: Effect of rotation on the stationary Rayleigh number R_T^{st}

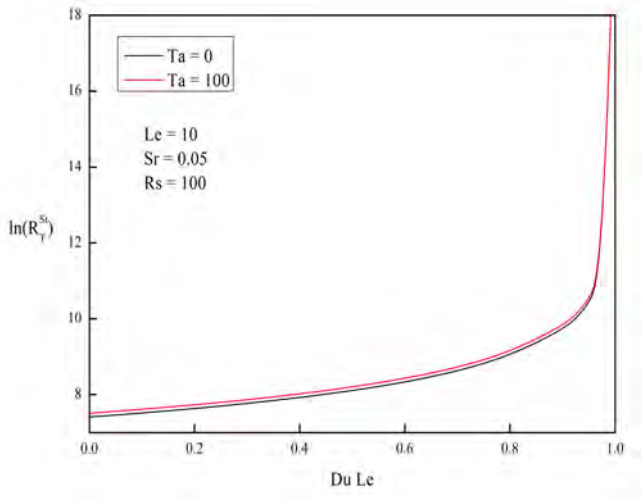

Figure 3: Effect of $Du\ Le$ and rotation on the critical R_T^{st}.

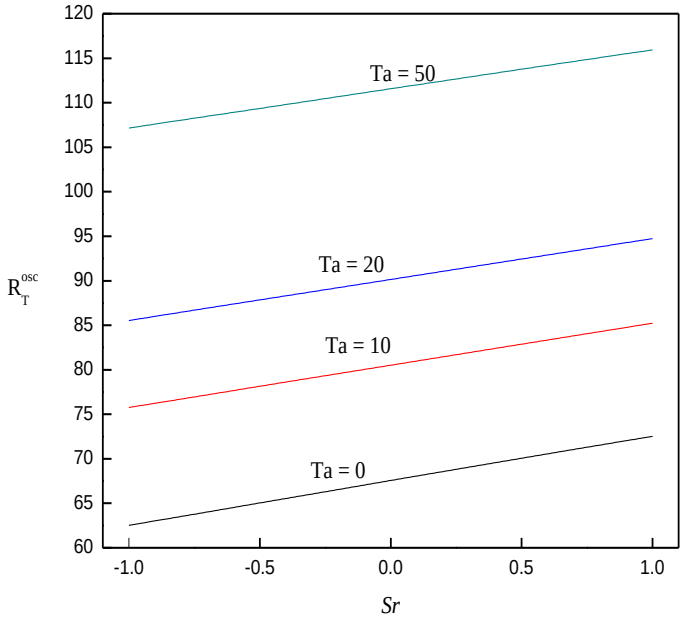

Figure 4: Effect of rotation and Soret number on the critical R_T^{osc}.

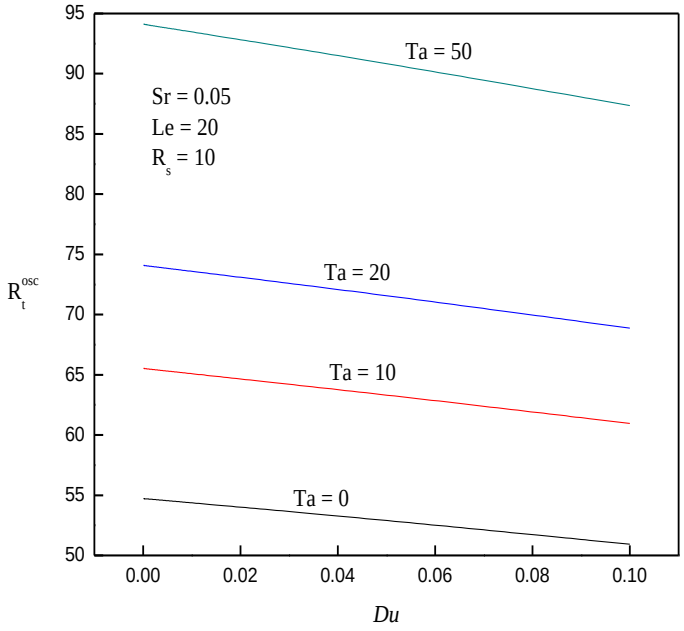

Figure 5: Effect of rotation and Dufour number on the critical R_T^{osc}.

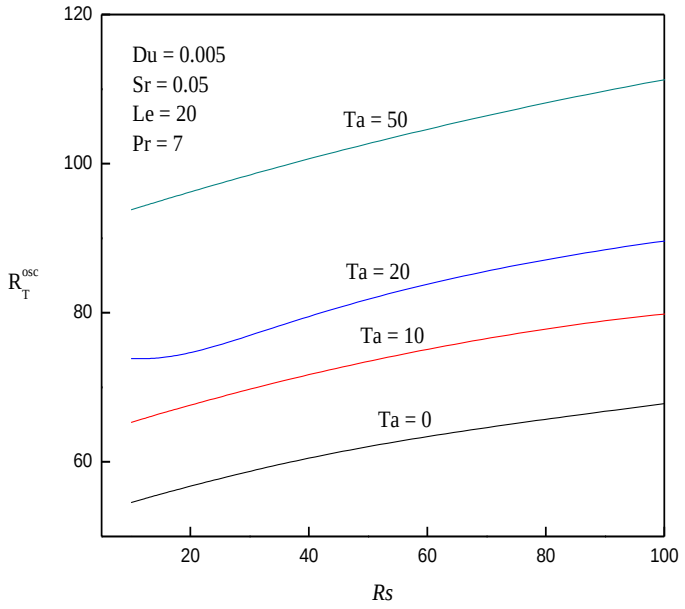

Figure 6: Effect of rotation and salinity Rayleigh number on the critical R_T^{osc}.

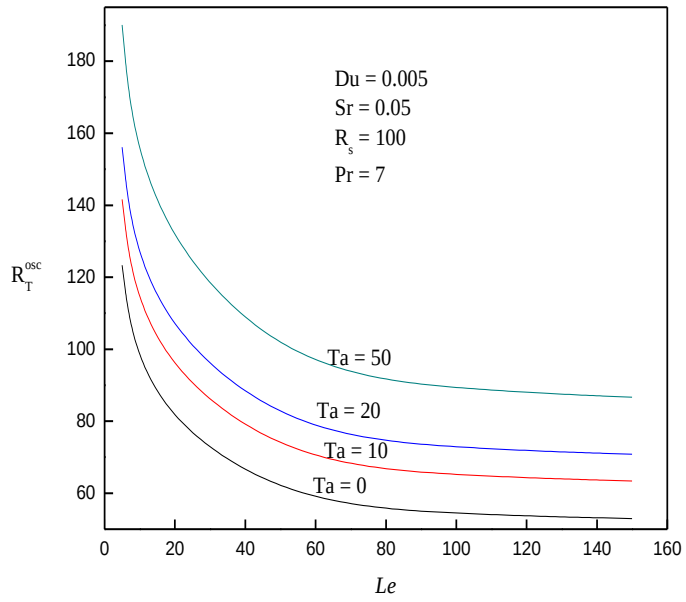

Figure 7: Effect of rotation and Lewis number on the critical R_T^{osc}.

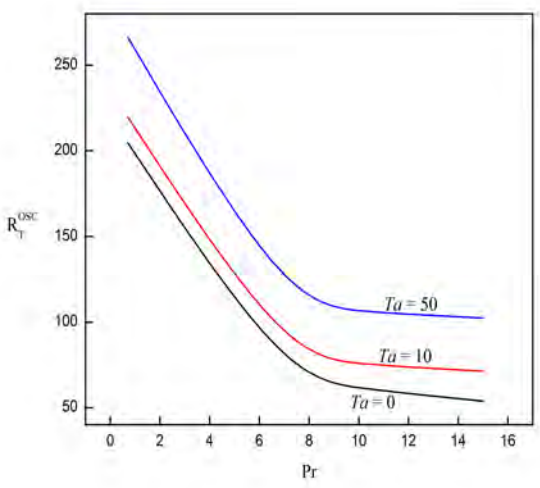

Figure 8: Effect of the Prandtl number and rotation on the critical R_T^{osc}.

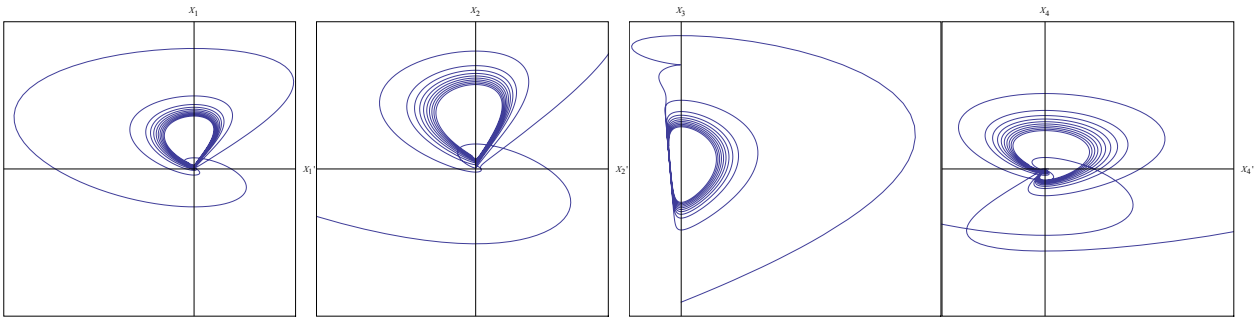

Figure 9: Phase portraits for X_1, X_2, X_3 and X_4 with values of the parameters given by $Pr = 13.4$, $Du = 0.03$, $Sr = 2$, $Le = 0.0125$, $R = 100$ and $Ta = 0.48$.

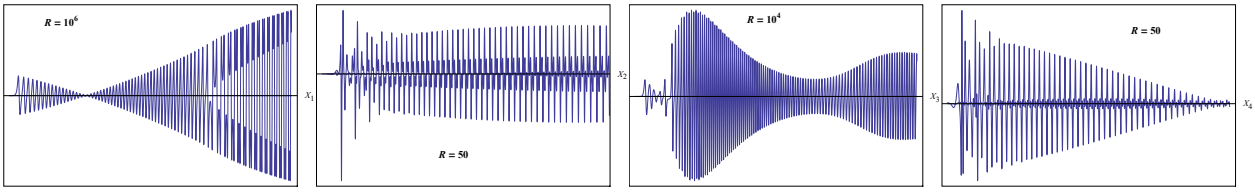

Figure 10: Phase portraits of the different solutions, X_1, X_2, X_3 and X_4 at different values of the Rayleigh number, with other parameters kept constant at $Le = 2.59$, $Pr = 13.4$, $Du = 12$, $Sr = 0.005$ and $Ta = 0.48$.

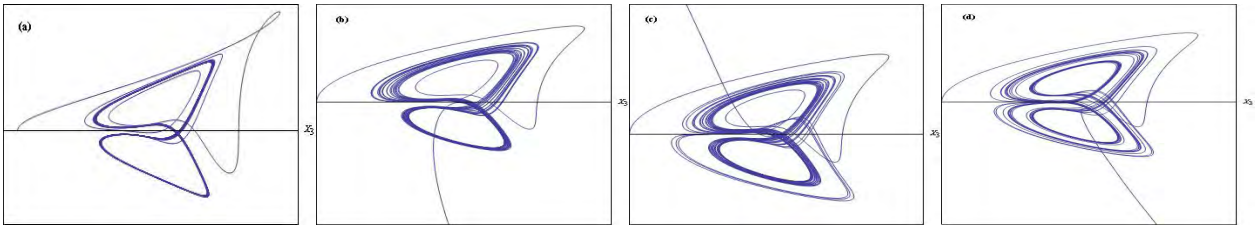

Figure 11: Evolution of the Lorenz equations showing sensitivity to the Dufour parameter. The evolution exhibits the "butterfly effect" when projected onto the (X_3, X_4) plane. The values of the Dufour parameter are (a) $Du = 0.3$, $Sr = 0.2$; (b) $Du = 1.2$, $Sr = 0.05$ (c) $Du = 2$, $Sr = 0.03$ and (d) $Du = 3$, $Sr = 0.02$.The other parameters are $R = 100$, $Le = 0.0125$, $Pr = 13.4$, $Ta = 0.48$.

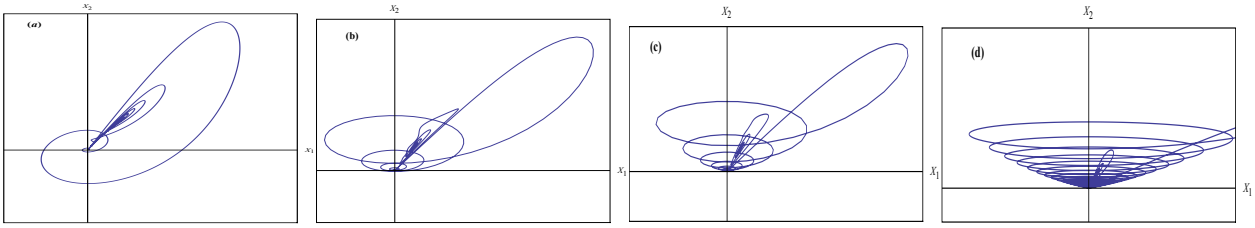

Figure 12: Evolution of Lorenz equations showing sensitive dependence on Soret Parameter. The evolution exhibits a "woven fruit bowl" effect when projected onto (X_1, X_2) plane. The various values considered here are, respectively, (a) $Sr = 1.5$, (b) $Sr = 40$, (c) $Sr = 100$ and (d) $Sr = 10^3$. The corresponding Dufour parameters are (a) $Du = 0.04$, (b) $Du = 0.0015$, (c) $Du = 0.0006$, and (d) $Du = 0.00006$. The other parameters are given by $R = 100$, $Le = 0.0125$, $Pr = 13.4$, and $Ta = 0.48$. These figures demonstrate the stabilizing effect of the Soret Parameter.

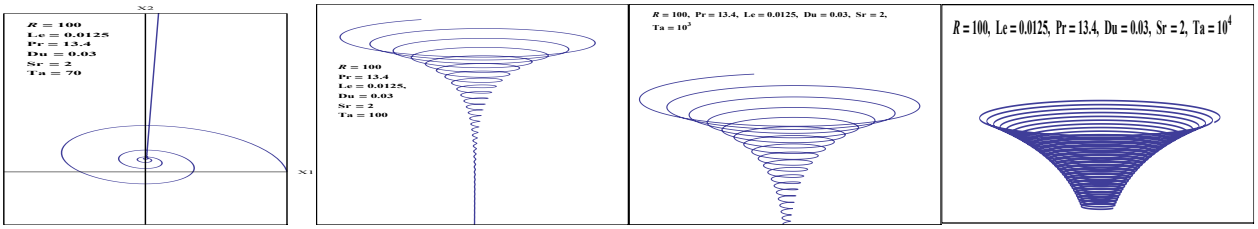

Figure 13: Lorenz Equations projected onto (X_1, X_2) plane responds in a tornado-like spiral. For smaller values of Ta we observe a limit cycle. But as Ta increases then a tornado-like spiral forms. However, for very large Ta the spiral dies down exhibiting a "woven fruit bowl", albeit with a different base than that of the Soret case.The values of the Taylor number are respectively, $Ta = 70$, $Ta = 100$, $Ta = 10^3$ and $Ta = 10^4$. The other parameters are $R = 100$, $Le = 0.0125$, $Pr = 13.4$, $Du = 0.03$ and $Sr = 2$.

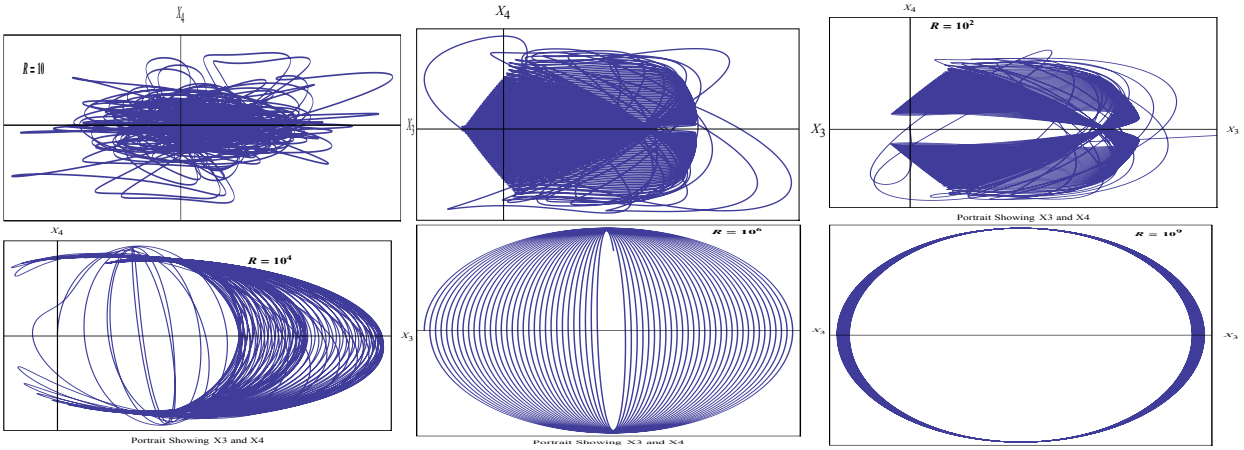

Figure 14: The change in dynamics as a fraction of the Rayleigh parameter R displays the evolution of a "Beetle" as the Lorenz equations are projected onto the (X_3, X_4)-plane. We call it the "Beetle Effect". The values of R considered here are respectively, $R = 50$, $R = 10^2$, $R = 10^4$, and $R = 10^6$. The other parameters are given by $Le = 2.59$, $Pr = 13.4$, $Du = 12$, $Sr = 0.005$ and $Ta = 0.48$. These diagrams demonstrate that the Rayleigh number is stabilizing the system.

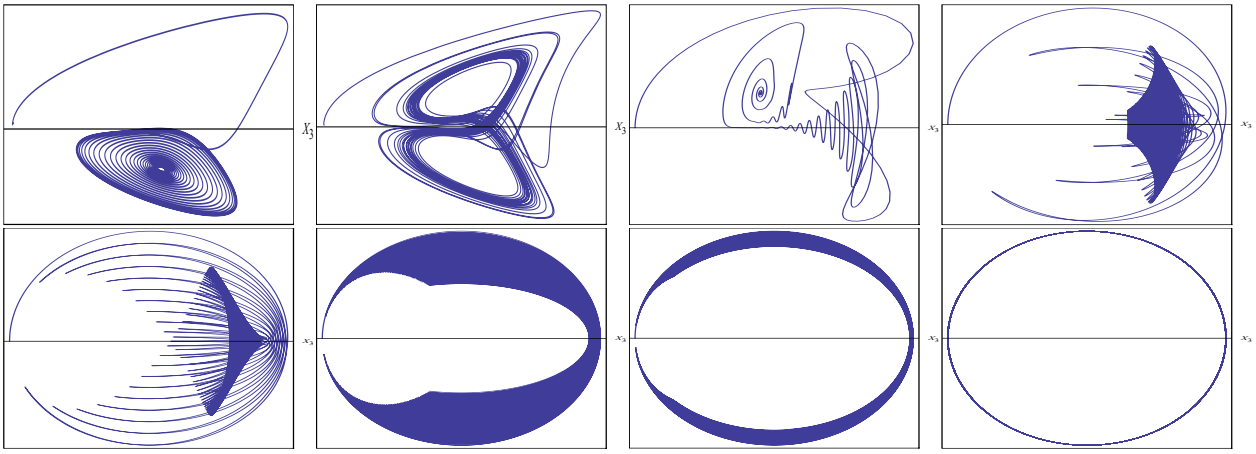

Figure 15: Rayleigh number stabilizes the system even with smaller value of the Lewis number $Le = 0.0125$. The figure demonstrates different bifurcations at different Rayleigh numbers which are, respectively, $R = 50$, $R = 100$, $R = 10^4$, $R = 10^6$, $R = 10^7$, $R = 10^9$, $R = 10^{10}$ and $R = 10^{24}$. The other values are kept constant and are given by $Pr = 13.4$, $Du = 12$, $Sr = 0.005$ and $Ta = 0.48$.

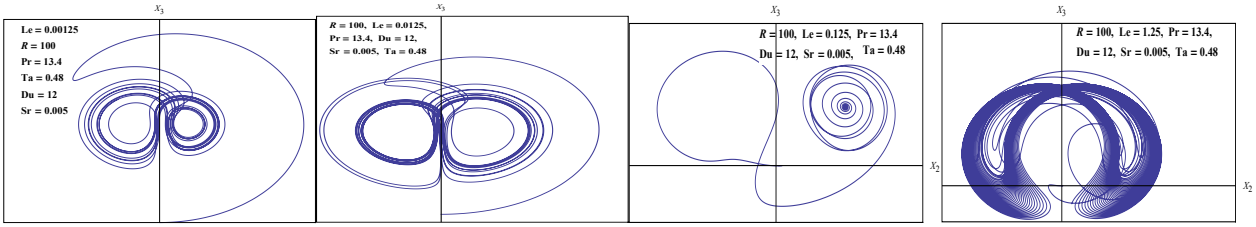

Figure 16: Lorenz equations showing sensitivity to the Lewis number projected on to the (X_2, X_3)-plane. From left to right, $Le = 0.00125$, $Le = 0.0125$, $Le = 0.125$ and $Le = 1.25$. The other parameters are $R = 100$, $Pr = 13.4$, $Ta = 0.48$, $Du = 12$ and $Sr = 0.005$.

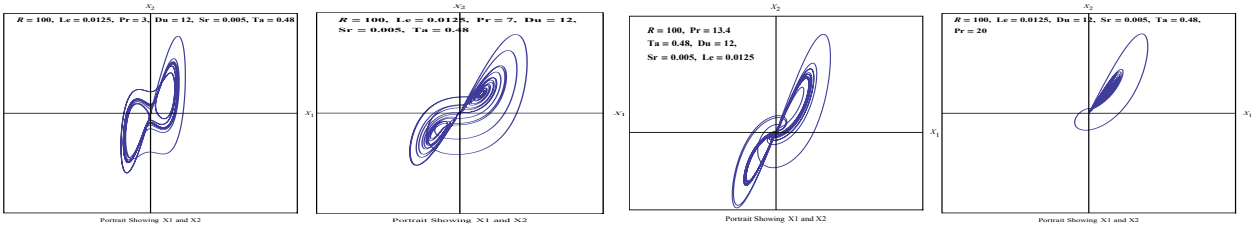

Figure 17: When projected onto the (X_2, X_3) plane, the Lorenz equations exhibit a "twist" effect when the Prandtl number is varied. These figures show, respectively, $Pr = 3$, $Pr = 7$, $Pr = 13.4$ and $Pr = 20$. Any figures more or less than these are not practical for the ocean as the Prandtl number for the ocean is between $Pr = 7$ and $Pr = 13.4$ at 0° Celsius and 20° Celsius, respectively. The other values are kept constant at $R = 100$, $Le = 0.0125$, $Du = 12$, $Sr = 0.005$ and $Ta = 0.48$.

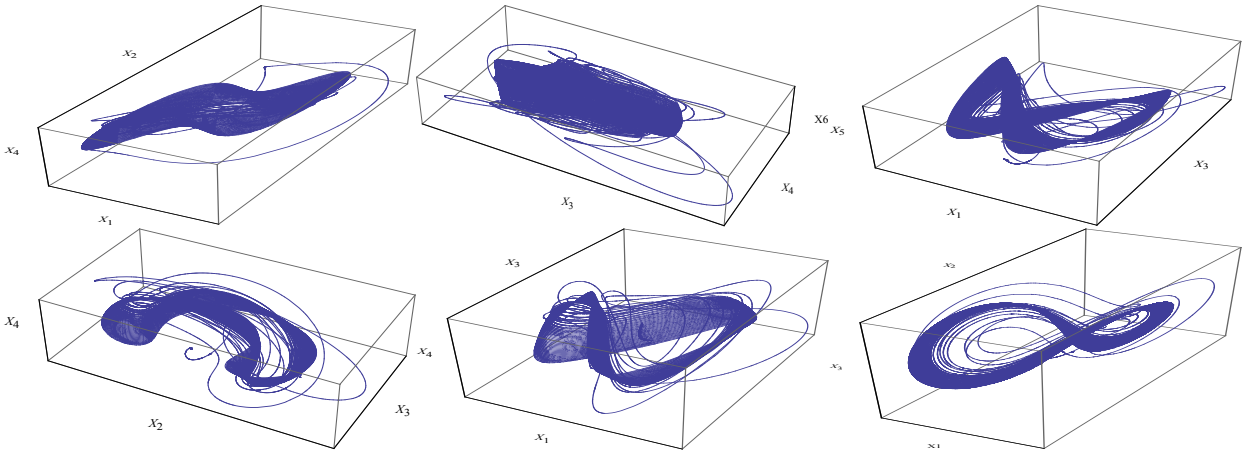

Figure 18: The figure shows the bifurcations in $3D$ form for different solution sets (X_1, X_2, X_3), (X_3, X_4, X_6) and (X_1, X_3, X_5) respectively, for the top figures, and solution sets (X_2, X_3, X_4), (X_1, X_3, X_4) and (X_1, X_2, X_3) for the bottom figures. The parameter values are given by $R = 50$, $Le = 2.59$, $Pr = 13.4$, $Du = 12$ and $Du = 0,005$. The last figure was constructed using the following parameter values $Le = 0.0125$, $R = 100$, $Pr = 13.4$, $Du = 12$, $Sr = 0.005$ and $Ta = 0.48$.

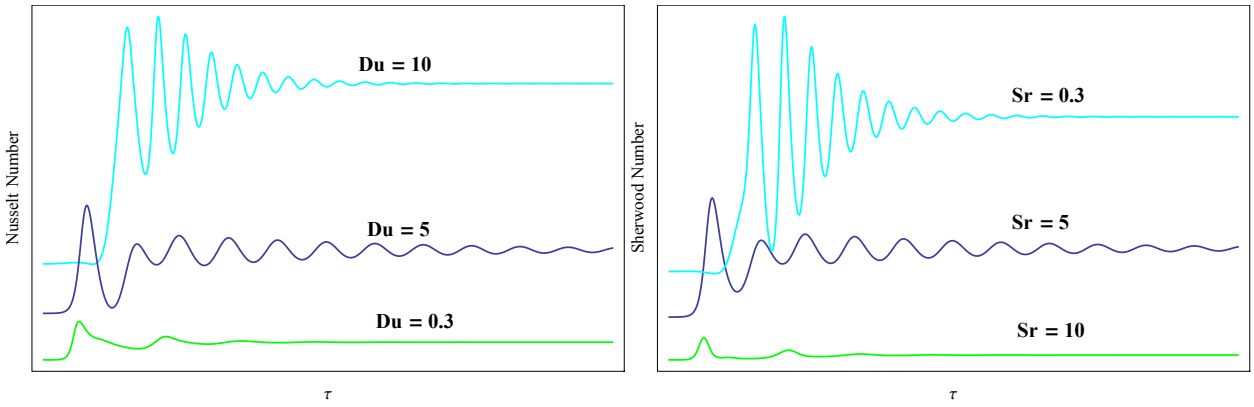

(a) Nusselt number for various values of the Dufour parameter.

(b) Sherwood number for various values of the Soret parameter.

Figure 19: Effect of cross diffusive parameters on heat and mass transports. The other parameters are kept constant at $R = 100$, $Pr = 13.4$, $Le = 0.0125$, and $Ta = 0.48$

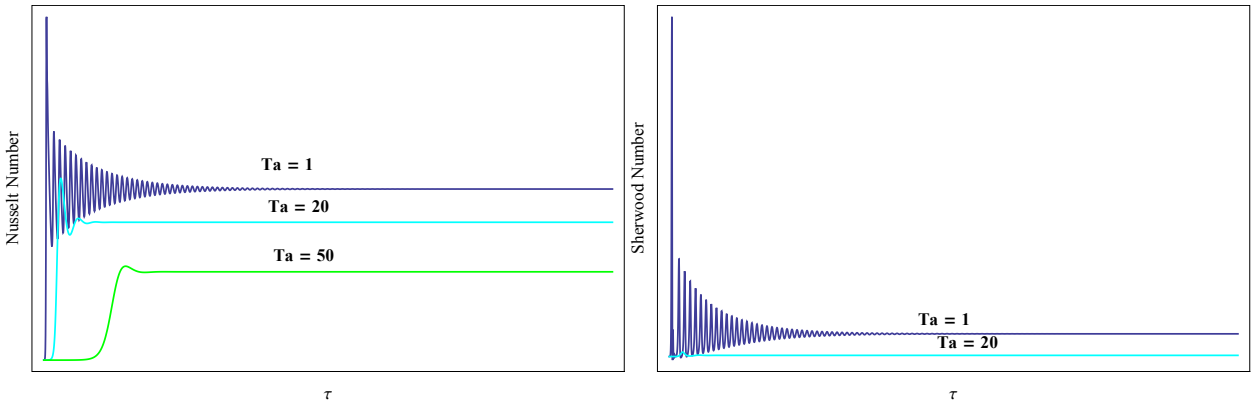

(a) Effect of Rotation on heat transport.

(b) Effect of Rotation on mass transport.

Figure 20: Effect of Rotation on heat and mass transports. The other values are given by $R = 100$, $Le = 0.0125$, $Pr = 13.4$, $Du = 2$ and $Sr = 0.03$.

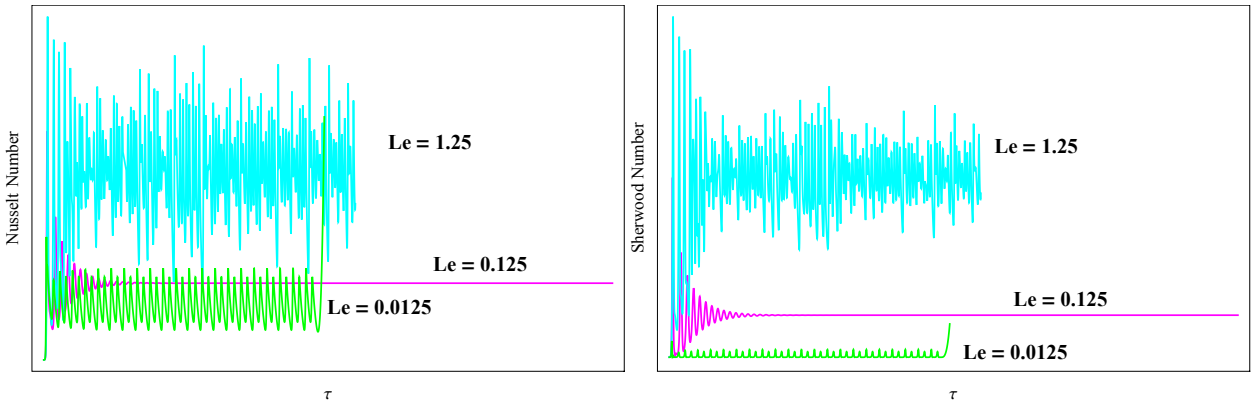

(a) Effect of Lewis number on heat transport. (b) Effect of Lewis number on mass transport.

Figure 21: Effect of Lewis number on heat and mass transports. The other values are given by $R = 100$, $Le = 0.0125$, $Pr = 13.4$, $Du = 2$ and $Sr = 0.03$.

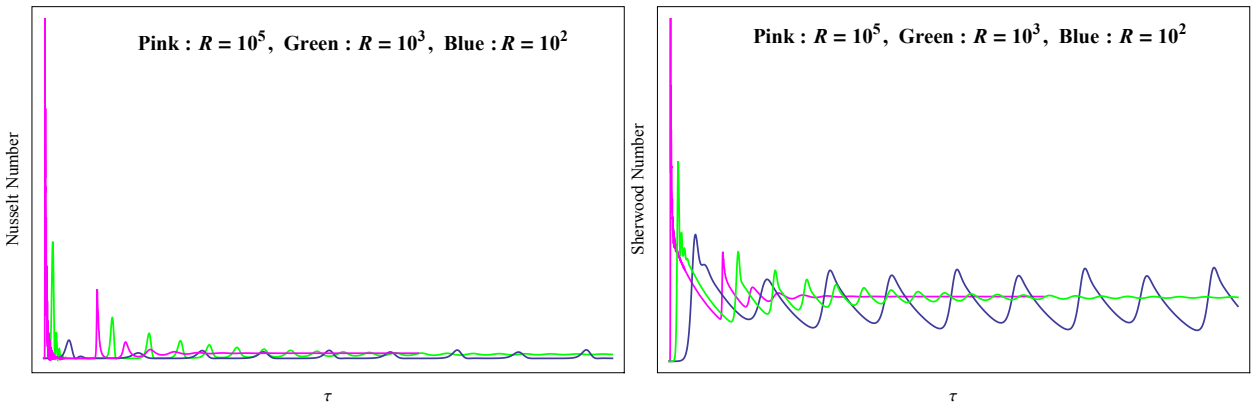

(a) Effect of Rayleigh number on the Nusselt number. (b) Effect of Rayleigh number on the Sherwood number.

Figure 22: The other values are given by $Le = 0.0125$, $Pr = 13.4$, $Ta = 0.48$, $Du = 12$ and $Sr = 0.03$.

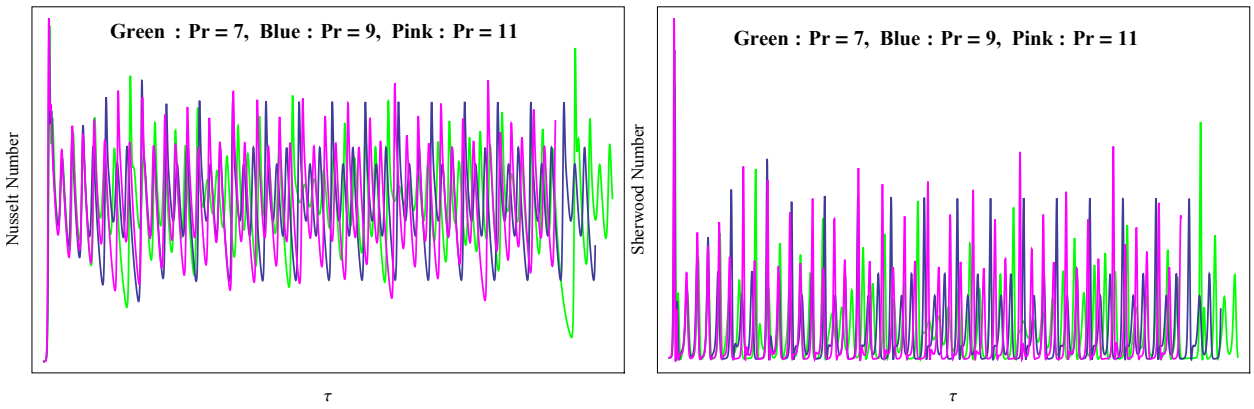

(a) Effect of Prandtl number on the heat transport. (b) Effect of Prandtl number on mass transfer.

Figure 23: The other parameters are given by $R = 100$, $Le = 0.0125$, $Du = 2$, $Sr = 0.03$ and $Ta = 0.48$.

Chapter 7

Conclusion

In this chapter we highlight and discuss the significance of our main findings, for each of the three papers, which were published in peer reviewed journals or submitted for review. We then make recommendations for further research.

7.1 Propagation Properties of Rossby waves

We studied the propagation properties of mid-latitude Rossby waves, for both shallow water and topographic waves. We started with the shallow water equations for a rotating layer of fluid, and developed the wave and dispersion equation for a Rossby wave on a beta plane. The local dispersion equation, as a wave normal form, highlights the dispersive and anisotropic nature of the wave. In particular, Longuet-Higgins (1964) used the wave normal diagrams to show that the phase velocity is a circle displaced westward. We have here used Longuet-Higgins's idea and now shown that the group velocity diagram is, in fact, an ellipse. In this way it differs from the phase velocity. The centre of this ellipse is displaced westward, and it has major and minor axes that yield both the maximum westward, eastward and northward (southward) group speeds. The speeds are a function of wave frequency and the parameter m of the planet, which we found to be $\beta_y c/f_0^2$, where $f_0 = 2\Omega \sin \phi_0$, Ω the angular frequency of the Earth, ϕ_0 the latitude. The parameter m is in fact the measure the ratio of the low frequency long wavelength Rossby wave zonal speed, to the shallow water speed, $c = \sqrt{gH}$, where g is the gravitational acceleration and H is the fluid depth.

For topographic waves, we have also further developed Longuet-Higgins's work with shallow water waves by investigating topographic wave propagation properties, using wave

normal diagrams in $k = (k_x, k_y)$-space. For these waves, like his results for shallow water waves, we found that the wave normal diagram for the phase velocity is a circle displaced positively along the k_y axis. This means that topographic wave phase propagation is always northward. As with shallow water waves, the group velocity diagram also gives us an ellipse with northward and southward components. The results here are as if we rotated the earlier results with shallow water waves by ninety degrees.

The results concerning first, the group velocity as an ellipse, and second, the phase and group velocity diagrams of topographic waves, had not been reported until we published them. These elegant features complement the Longuet-Higgins offset circle in revealing the propagation properties of Rossby waves which are important in weather and climate change. We have shown here the anisotropic properties group velocity which is responsible for energy propagation.

7.2 Rossby waves in winds

In the study of Rossby wave interaction with winds, we first derived the second-order partial differential equation describing the latitudinal structure of Rossby type wave perturbations on a beta-plane, in zonal and meridional winds. We followed Lighthill (1978) and were able to show how the local dispersion equation, when interpreted as a wave number diagram in k space at a given frequency ω, can be used to construct the radiation pattern generated by a time harmonic compact source in a laboratory frame relative to which the zonal and meridional winds flow. The effect of the Doppler shift frequency on the Longuet-Higgins offset circle is shown in a series of diagrams, Figures 3 to 8 of Chapter 4. The main effect is that the offset circle is now transformed into a closed ovoid. Furthermore, the ovoid shows an extension in a form of a blocking line or an indented line, at $k_x = \omega/U$, and a "hump". We then investigated radiation patterns associated with the blocking line and closed ovoid. The ovoid and blocking line, with corresponding radiation patterns, have different forms depending on whether winds blow in the same direction as, or opposite to, the Rossby wave. When zonal westerly winds are blowing in the direction of Rossby wave propagation, the hump and the blocking line are directed eastwards. The radiation patterns of the closed ovoid in this case are found to be a family of eastward-facing paraboloids, reminiscent of capillary waves generated by an object in a stream. These are similar to the hyperbolas in the case of no flow for which Rhines (2003) and McKenzie (2014) investigated. On the other hand, the radiation pattern for the blocking line is a family of deltoids, which resemble a reversed Kelvin ship wave.

When the zonal easterly winds are blown in the direction of Rossby waves, the hump and the indented line lie completely westward as shown in Figure 7 of Chapter 4. The corresponding radiation pattern corresponding to the ovoid yields parabolic curves that lie both eastward and westward. On the other hand, the radiation pattern corresponding to the hump and the indented line are deltoids which lie entirely westward.

In the case of the stationary wave, in which $\omega = 0$, we found entirely different forms. The wave normal diagram is a circle of radius $\sqrt{(\beta/U) - (f^2/c^2)}$. When $U > 0$, that is westerly, we obtain results similar to Lighthill's (1978) case for the two-dimensional internal gravity wave patterns generated in a horizontal flow as depicted in Figure 10(a). The corresponding radiation pattern consists of a semi-circle (taken twice), the double line $k_y = 0$ and the two lines extending westwards.

The case of meridional winds is even more interesting but complicated and these are depicted in Figures 11-17, of Chapter 4. They were unusual in that they showed a great variety in patterns that have not been reported before which may suggest a phenomena that may require further investigation.

What is significant about these results is that the study of radiation patterns is in fact equivalent to studying wave generation by travelling forcing effects (Lighthill, 1978) and thus the interaction of Rossby waves with these traveling winds is useful in the study of wave propagation in a moving medium and hence of weather and climate patterns. Some of these radiation patterns have not been reported before in literature.

7.3 Thermohaline Convection

In the third research paper, we reported on the onset of thermohaline convection in a rotating fluid, such as is found in the ocean, under the influence of Soret and Dufour effects. We investigated the case using normal modes, linear stability analysis and weakly, nonlinear stability analysis. Analytical expressions for the critical Rayleigh number and the wavenumbers corresponding to the onset of stationary convection subject to cross diffusion, were determined using linear stability theory. It was shown here that both salinity and rotational effects have significant stabilizing effects on stationary convection; thereby confirming the results found in literature. Our study shows that the Soret parameter has a stabilizing effect on stationary convection whereas the Dufour parameter has minimal effect.

In the analysis of oscillatory convection our study further shows that the Rayleigh number critical for the onset of convection depends on six parameters, the Prandtl number Pr,

Soret parameter Sr, Dufour parameter Du, Taylor number or rotation parameter Ta, Lewis number Le and the salinity Rayleigh number R_s. Such a complex system requires some robustness to fully understand the effect of each of the parameters on thermohaline convection. In this analysis we used smaller parameter values than those published, when validating the results. Nevertheless, we believe that our computations are still useful because the bigger parameter values create a computational difficulty.

We found that increasing the rotation parameter and the Soret parameter increase the Rayleigh number critical to oscillatory convection. This means that rotation and Soret parameter will contribute to an unstable system, and so generates oscillatory convection, in agreement with results by Sharma *et al.* (2001) in their study of Rivlin-Eriksen rotating fluids and that of Dhiman and Goyal (2015). In fact, the Soret parameter stabilizes for both positive and negative values. This result is in contrast to Gaikwad *et al.* (2007) in their study of coupled stress fluid who found that he positive Soret parameter destabilizes and the negative Soret parameter stabilizes. Conversely, an increase in the Dufour parameter resulted in a lower critical Rayleigh number. In other words, with greater thermal energy flux resulting from the concentration gradients, we can expect a delayed oscillatory convection, confirming the results by Gaikwad *et al.* (2007).

A minimal representation of Fourier series has been employed for a weakly nonlinear stability analysis that resulted in a sixth order generalised Lorenz model. The characterization of chaotic solutions was challenging and involved seven parameters - Lewis number, salinity Rayleigh number, Prandtl number, thermal Rayleigh number, Taylor number, Soret and Dufour parameters. Figures 10-17 show the evolution of the Lorenz equations when these parameters are varied at various planes. These equations exhibit very interesting bifurcation diagrams some of which we have not seen anywhere in literature. We found here that the Dufour parameter and the Lewis number have a destabilizing effect to the system, whereas the Soret parameter, the Rayleigh number, the Taylor number and the Prandtl number are stabilizing. In most literature, the nonlinear study was not constructed due to the many parameters that arise in rotating double diffusive convection under cross-diffusive effects. Whereas Lorenz in his study of weather patterns obtained a chaotic butterfly-effect whilst varying the initial conditions, our work here shows that it is also possible to find such chaotic solutions when the system is affected by cross diffusive effects. These results are important in the study of climate change. Due to global warming, there are currently studies on ocean dynamics particularly on the stability of thermohaline circulation. There are fears that the conveyor belt might be interrupted as the water heats up and the sea gets desalinitized.

Heat and mass transports were quantified with the help of weakly nonlinear theory. The Figures 18 to 20 summarizes the findings for the heat and mass transfer. The increase in the Dufour parameter enhance heat transport whereas the Soret parameter affects mass transport negatively. The Prandtl and the Rayleigh numbers have no contribution whatsoever to both heat and mass transports. However, rotation has a negative contribution towards both heat and mass transports, whereas the Lewis number enhances both heat and mass transports.

In a nutshell, we have in Chapters 3 and 4 investigated the propagation of Rossby waves and their interaction with the winds, respectively by means of two published papers in peer reviewed journals. In Chapter 6 we analysed further the effect of cross diffusion on thermohaline convection under the influence of rotation; the work which is summarized as a research paper under peer review.

7.4 Further Research

Propagation of Rossby waves have been considered in this thesis together with the interaction of Rossby waves with zonal and meridional winds. Using the method of stationary wave patterns, the study focuses on radiation patterns that arise from the interaction. Duba *et al.* (2014) showed that the Doppler shifted frequency $\omega' = \omega - k_x U$ has a profound effect on the geometry of the local wave normal curve in the (k_x, k_y) space. The effect of the zonal wind on the wave normal diagram has already been described by Duba *et al.* (2014) for westerly wind $U > 0$ and for easterly wind $U < 0$. This work could be extended by analysing the ray paths in both westerly and easterly jets using the geometry of the wave normal curves. In this regard, a ray path in a zonal wind shear $U_x(y)$ may be determined by constructing the wave normal curves in the (k_x, k_y) space at successive latitudes, and following the direction of the arrows (direction of rays) drawn normal to the wave normal curve where it is intersected by a line $k_x =$ constant at each latitude. This elegant construction has been used to examine the ray paths by Lighthill (1978) in the case of travelling forcing effects and by Mekki and McKenzie (1977) for Rossby waves. It may be useful to extend their work by examining ray paths for meridional waves to supplement work on Rossby waves. The ray tracing technique can give a full description of wave behaviour at critical latitude where the Doppler frequency equals the frequency of the Rossby wave, so as to determine whether it acts as absorber, reflector or emitter of Rossby waves. Although a ray path in a meridional wind may be challenging by looking at Figure 11 of Duba *et al.* (2014) it is nonetheless worth considering because such further

knowledge would give a full description of critical wave behaviour at critical latitude.

It is also possible to consider Rossby wave interactions with cyclonic winds. Indeed, McKenzie and Webb (2015) studied Rossby waves in azimuthal winds. It will be interesting to extend the study to radiation patterns using Green's functions as was done by Rhines (2003) and McKenzie (2014) for Rossby waves on a beta-plane. They studied the Green's function wherein the disturbance is generated by a given time source. In the other work elsewhere, Webb *et al.* (under review) discuss the Green's function in azimuthal wind. They extend the work by Veronis (1958) who obtained the Green's function for the case of no wind and investigated in detail the case when the Rossby deformation radius $R_d \gg L$, where L is the scale length of Rossby waves for which the effects of R_d can be neglected. Webb *et al.* (under review) consider the case when $1/R_d \neq 0$ and when $1/R_d = 0$.

For Part II of the thesis, we considered Soret and Dufour effects on thermohaline convection in rotating winds. In this case we considered our boundaries to be both free. As we have seen the cross diffusive terms have an effect on both linear and nonlinear stability analysis. The Soret effect together with rotation indeed having a stabilizing effect for the stationary convection and the Dufour parameter stabilizing for oscillatory convection. We can extend the work by considering the free-rigid boundaries and the rigid-rigid boundaries. It will be interesting to see what type of effects do Soret and Dufour effects have when the boundaries are changed. Such study would be useful for systems that are considered under these boundaries as may be the case for the bottom of the ocean studies.

References

Alam, M. S. and Rahman, M. M. Dufour and Soret effects on mixed convection flow past a vertical porous plate with variable suction. *Nonlinear Analysis: Modelling and Control*, 2006, **11 (1)**, 3-12.

Alloui, I., Benmoussa, H., Vasseur, P. Soret and thermosolutal effects on natural convection in shallow cavity filled with a binary mixture. *Int. J. Heat and Fluid Flow*, 2010, **31**, 191-200.

Awad, F. G. and Sibanda, P. Dufour and Soret Effects on heat and mass transfer in a micropolar fluid in a horizontal channel. *WSEAS Transactions on Heat and Mass Transfer*, 2010, **5 (3)**, 165-177.

Awad, F. G., Sibanda, P. and Motsa, S. S. On the linear stability analysis of a Maxwell fluid with double-diffusive convection. *Appl. Math. Modelling*, 2010, **34**, 3509-3516.

Awad, F. G., Sibanda, P., Motsa, S. S. and Makinde, O. D. Convection from an inverted cone in a porous medium with cross-diffusion effects. *Computers and Mathematics with Applications*, 2011, **61**, 1431-1441.

Baines, P. G. and Gill, A. E. On Thermohaline convection with linear gradients. *J. Fluid Mech.*, 1969, **37 (2)**, 289-306.

Barnejee, M. B., Gupta, J. R., Shandil, R. G., Sharma, K. C. and Katoch, D. C. A modified analysis of thermal and thermohaline instability of a liquid layer heated underside. *J. Math. Phys. Sci.*, 1983, **17 (6)**, 603-629.

Barnejee, M. B., Gupta, J. R., Shandil, R. G., Sood, S. K., Sharma, K. C. and Katoch,

D. C. A modified analysis of thermal and thermohaline instability of a liquid layer II. The effect of rotation. *J. Math. Phys. Sci.*, 1988, **22**, 457-474.

Barnejee, M. B., Gupta, J. R. and Prakash, J. On thermohaline convection of the Veronis type. *J. Math. Anal. and Appl.*, 1993, **179**, 327-334.

Barnejee, M. B., Shandil, R. G., Lal, P., and Kanwar, V. A mathematical theorem in rotatory thermohaline convection. *J. Math. Anal. and Appl.*, 1995, **189**, 351-361.

Basu, R. and Layek, G.C. Influences of cross-diffusive coefficients on the onset of double diffusive convection in a horizontal fluid layer. *Int. J. of Appl. Math. and Mech.*, 2013, **9 (6)**, 86-107.

Booker, J. R. and Bretherton, F. P. The critical layer for internal gravity waves in a shear flow. *J. Fluid Mech.*, 1967, **27**, 513-539.

Bretherton, F. P. and Garrett, C. J. R. Wave trains in inhomogeneous moving media. *Proc. Roy. Soc.* **A**, 1968, **302**, 529-554.

Burroughs, W. J. Climate Change: A multidisciplinary approach. 2nd ed. 2007, Cambridge Press, Cambridge.
Caldwell, D. R. Experimental studies on the onset of thermohaline convection. *J. Fluid Mech.*, 1974, **64**, 347-367.

Chandrasekhar, S. Hydrodynamic and hydromagnetic stability, 1961, (Oxford Univ. Press, Oxford).

Cushman-Roisin, B. and Beckers, J-M. *Introduction to Geophysical Fluid Dynamics.* 2nd Edition, 2011, (Elsevier, Amsterdam), 828.

Dhiman, J. S. and Goyal, M. R. On the effect of rotation on Soret driven double-diffusive stationary convection. *Advances in Applied Science Research*, 2015, **6 (9)**, 27-37.

Diamond, P. H., Gurcan, D. D., Hahn, T. S., Miki, K., and Grbet, X. Momentum theorems and the structure of atmospheric jets and zonal flows in plasmas. *Plasma Phys.*

Control. Fusion, 2008, **50**, 124018, doi:10.1088/0741-3335/50/12/124018.

Dickinson, R. E. Planetary Rossby Waves Propagating Vertically through Weak Westerly Wind Wave Guides. *J. Atmos. Sci.*, 1968, **25**, 984-1002.

Doyle, T.B. and McKenzie, J. F. Stationary wave patterns in deep water. *Questiones Mathematicae*, 2013, **36**, 1-14.

Drazin, P. G. and Reid, W. H. Hydrodynamic stability, Second Edition, 2004, (Cambridge Univ. Press, London/New York).

Duba, C. T. and McKenzie, J. F. Propagation properties of Rossby waves for latitudinal β-plane variations of f and zonal variations of the shallow water speed. *Ann. Geophys.*, 2012, **30**, 1-7.

Duba, C. T., Doyle, T. B. and McKenzie, J. F. Rossby wave patterns in zonal and meridional winds. *Geophys. and Astrophys. Fluid Dynamics*, 2014, **108 (3)**, 237-257.

Duba, C. T., Shekhar, M., Narayana, M., and Sibanda, P. Soret and Dufour Effects on the Thermohaline Convection in Rotating Winds. *Under review.*

Eckart, C. Hydrodynamics of oceans and atmospheres. 1960, (Pergamon Press).

Eckert, E. R. G. and Drake, R. M. Analysis of heat and mass transfer, 1972, (McGraw-Hill, New York).

Eltayeb, A. and McKenzie, J. F. Propagation of hydromagnetic planetary waves on a beta-plane through magnetic and velocity shear. *J. Fluid Mech.*, 1977, **81**, 1-12.

Gaikwad, S. N., Malashetty, M. S., Rama Presad, K. An analytical study of linear and nonlinear double diffusive convection with Soret and Dufour effects in couple stress fluid. *Int. J. Nonlinear Mechanics*, 2007, **42**, 903-913.

Gbadeyan, J. A., Idowu, A. S., Ogunsola, A. W., Agboola, O. O. and Olanrewaju, P. O. Heat and mass transfer for Soret and Dufour's effect on mixed convection boundary layer

flow over a stretching vertical surface in a porous medium filled with viscoelastic fluid in the presence of magnetic field. *Global J. Sci. Frontier Res.*, 2011, **11 (8)**, 97-114.

Gerkema T., Maas, L. R. M. and van Haren, H. A note on the role of mean flows in Doppler-shifted frequencies. *J. Phys. Oceanogr.*, 2013, **43 (2)**, 432-441.

Gill, A. E. *Atmosphere and Ocean Dynamics*. 1982, (London, Academic Press).

Goyal, M. R. and Garg, B. P. Influences of Soret and Dufour effects on double-diffusive convection in a horizontal fluid layer. *J. Rajastan Academy of Phys. Sci.*, ISSN: 0972-6306; URL:https://raops.org.in, 2015, **14 (2)**, 127-144.

Gupta, J. R., Dhiman, J. S. and Thakur, J. Thermohaline convection of Veronis and Stern type revisited. *J. Math. Anal and Appl.*, 2001, **264**, 398-407.

Hayat, T., Naz, R., Asghar, S., Alsaedi, A. Soret-Dufour effects on MHD rotating flow of a viscoelastic fluid. *Int. J. Num. Meth. Heat and Fluid Flow*, 2014, **24 (2)**, 498-520.

Holton, J. R. and Hakim, G. J. An Introduction to Dynamic Meteorology 5th Edition, 2013. (Academic Press, United States) 532.

Huppert, H. E. and Turner, J. S. Double-diffusive convection. *J. Fluid Mech.*, 1981, **106**, 299-329.

Killworth, P. D. and McIntyre, M. E. *Do Rossby Wave Critical Layers Absorb, Reflect or Over-reflect? J. Fluid Mech.*, 1985, **161**, 449-492.

Lighthill, J. Studies on magneto-hydrodynamical waves and their anisotropic wave motions. *Proc. Roy. Soc.* **A**, 1960, **252**, 397-430.

Lighthill, J. *Waves in Fluids*. 1978 (Cambridge, Cambridge University Press).

Longuet-Higgins, M. S. Planetary waves on a rotating sphere. *Proc. Royal Soc.* **A**, 1964, **279**, 446-473.

Malashetty, M. S. The effect of rotation on the onset of double-diffusive convection in a horizontal anisotropic porous layer. *Transp. Porous Med.*, 2008, **74**, 105-127

Malashetty, M. S. and Biradar, B. S. The onset of double-diffusive convection in a binary Maxwell fluid saturated porous layer with cross diffusion effects. *Phys. Fluids*, 2011, **23**,

Maleque, Kh. A. Dufour and Soret effects on unsteady MHD convective heat and mass transfer flow due to a rotating disk. *Latin American Applied Research*, 2010, **40**, 105-111.

McKenzie, J. F., Chandrasekhar: The all rounder. *PRAMANA -J. Phys.* September 2011, **77 (3)**, 509-517.

McKenzie, J. F., Instability of combined gravity-inertial-Rossby waves in atmospheres and oceans. *Ann. Geophys.*, 2011, **29**, 997-1003.

McKenzie, J. F. The group velocity and radiation patterns of Rossby waves. *Geophys. and Astrophys. Fluid Dynamics*, 2014, **108**, 225-268 doi:10.1080/03091929.2014-896459.

McKenzie, J. F. and Webb, G. M. Rossby Waves in an azimuthal wind. *Geophys. and Astrophys. Fluid Dynamics*, 2015, **109 (1)**, 21-38 doi:10.1080/03091929.2014.986473.

McWilliams, J. C. Fundamentals of Geophysical Fluid Dynamics. 2006 (Cambridge University Press, Cambridge) 249.

Mekki, O. M. and McKenzie, J. F. The propagation of atmospheric Rossby-gravity waves in latitudinally sheared zonal flows. *Phil. Trans. Roy. Soc.*, 1977, **287**, 115-143.

Mohan, H. The Soret effect on the rotatory thermosolutal convection of the Veronis type. *J. Pure Appl. Math.*, 1996, **27 (6)**, 609-619.

Motjabi, A. Charrier-Motjabi, M. C. Double diffusive convection in porous media. *Handbook of Porous media*. 2nd edition, 2005.

Nakagawa, Y. and Frenzen, P. A theoretical and experimental study of cellular convection in rotating fluids. *Tellus*, 1955, **7 (1)**, 1-21.

Narayana, M., Sibanda, P., Siddeshwar, P. G. and Jayalatha, G. Linear and nonlinear stability analysis of binary viscoelastic fluid convection. *Appl. Math. Modelling*, 2013, **37**, 8162-8178.

Paldor, N., Rubin S., and Mariano, A. J. A Consistent theory for linear waves of the shallow water equations on a rotating plane in mid-latitudes. *J. Phys. Oceanogr.*, 2007, **37**, 115-128

Pedlosky, J. *Geophysical Fluid Dynamics*. 1987 (New York, Springer-Verlag), 710

Pedlosky, J. *Waves in the Ocean and Atmosphere. Introduction to Wave Dynamics*, 2010 (Springer, New York), 260.

Philander, S. G. El Niño, La Niña, and the Southern Oscillation. 1990 (Academic Press, United States of America). 293

Pokhotev, O. A., McKenzie, J. F., Shukla, P. K. and Stenflo, L. Nonlinearly coupled inertial and Rossby waves. *Phys. Fluids*, 1995, **7**, 1785

Polyakov, I. V., Pnyushkov, A. A., Rember, R and Ivanov, V. V. Mooring-based observations of double-diffusive staircases over the Laptev sea slope. *J. Phys. Oceanogr.*, 2012, **42**, 95-109.

Radko, T., Bulters, A., Flanagan, J. D. and Campin, J. -M. Double-diffusive Recipes. Part I: Large-scale dynamics of thermohaline staircases. *J. Phys. Oceangr.*, 2014, **44**, 1269-1284.

Rajagopal, K. R., Saccomandi, G. and Vergori, L. On the Oberbeck-Boussinesq approximation for fluids with pressure dependent viscosities. *Nonlinear Analysis: Real World Applications*, 2009, **10**, 1139-1150.

Ratcliffe, C. An introduction to the ionosphere and magnetosphere. 1972 (Cambridge University Press, Cambridge).

Rhines, P.B. Rossby waves in *Encyclopaedia of Atmospheric Sciences. E. in 2003 Chief James R. Holton, J. A. Curry and J. A. Pyle*, 1-37 (Academic Press, Oxford).

Rossby, C. G. Relation between variations in the intensity of the zonal circulation of the atmosphere and the displacements of semi-permanent centers of action. *J. Mar. Res.*, 1939, **2**, 38-55

Rossby, H. T. A Study of Bénard convection with and without rotation. *J. Fluid Mech.*, 1969, **36 (2)**, 309-335.

Rudraiah, N. and Siddeshwar, P. G. A weak nonlinear stability analysis of double diffusive convection with cross-diffusion in a fluid-saturated porous medium. *Heat Mass Transf.*, 1998, **33**, 287-293

Schmitt, R. W. Double Diffusive Convection. In. Encyclopaedia of Ocean Sciences, John H. Steele, Steve A. Thorpe, and Karl K. Turekian, editors 2001, Academic Press, San Diego, **2**, 757-766.

Sharma, R. C., Sunil, Pal, M. Thermosolutal Convection in Rivlin-Eriksen Rotating Fluid in porous medium in hydromagnetics. *Indian J. Pure Appl. Math.*, 2001, **32 (1)**, 143-156.

Stern, M. E. The salt fountain and thermohaline convection. *Tellus*, 1960, **12**, 172-175.

Stommel, H., Arons, A. B. and Blanchard, D. An oceanographical curiosity: the perpetual salt fountain. *Deep Sea Research*, 1956, **3**, 152.

Tagare, S. G., Raman Murthy, M. V. and Rameshwar, Y. Nonlinear thermohaline convection in rotating fluids. *Int. J. Heat and Mass Transfer*, 2007, **50**, 3122-3140.

Turner, J. S. Buoyancy Effects in Fluids, 1973 (Cambridge University Press, London).

Turner, J. S. Double-diffusive phenomena. *Annu. Rev. Fluid Mech.*, 1974, **6**, 37-56.

Turner, J. S. Multicomponent convection, *Annu. Rev. Fluid Mech.*, 1985, **17**, 11-44.

Vallis, G. Atmospheric and Oceanic Fluid Dynamics: Fundamentals and Large-scale Circulation, 2006 (Cambridge Press, New York).

Veronis, G. On the transient response of a beta-plane ocean. *Jour. Oceanogr. Soc. Japan*, 1958, **14 (1)**, 1-5.

Veronis, G. On finite amplitude instability in thermohaline convection. *J. Mar. Res.*, 1965, **23**, 1-17.

Veronis, G. Large-amplitude Bénard convection in a rotating fluid. *J. Fluid Mech.*, 1968, **31 (1)**, 113-139.

Wang, B. Kelvin Waves. *Encyclopaedia of Meteorology.* Ed. J. Holton *et al.*, 2003, Academic Press, 1062-1067.

Webb, G., Duba, C. T., and Hu, Q. Rossby Wave Green's Functions in an Azimuthal Wind. *Under review.*

Yagamata, T. On trajectories of Rossby wave-packets released in a lateral shear flow. *J. Oceanogr. Soc. Japan*, 1976, **32**, 162-168.

Zhou, S. -Q. Qu, L., Lu, Y. -Z, Song, X. -L. The instability of diffusive convection and its implication for the thermohaline staircases in the deep Arctic ocean. *Ocean Sci.*, 2014, **10**, 127-134.